Universität Potsdam

Institut für Ernährungswissenschaft

Molecular and Experimental Nutritional Medicine

Investigating metabolic consequences of an HSP60 reduction during diet-induced obesity

---

Autor:
Robert Hauffe

1. Gutachter:
Prof. Dr. André Kleinridders

2. Gutachterin:
Prof. Dr. Annette Schürmann

Dissertation

zur Erlangung des akademischen Grades

"Doctor rerum naturalium"

(Dr. rer. nat.)

in der Wissenschaftsdisziplin “Physiologie und Pathophysiologie”

eingereicht an der Mathematisch-Naturwissenschaftlichen Fakultät der Universität Potsdam

Berlin, den 18. Februar 2021

Published online on the
Publication Server of the University of Potsdam:
https://doi.org/10.25932/publishup-50929
https://nbn-resolving.org/urn:nbn:de:kobv:517-opus4-509294

Abstract

Investigating metabolic consequences of an HSP60 reduction during diet-induced obesity

Robert Hauffe

The mitochondrial chaperone complex HSP60/HSP10 facilitates mitochondrial protein homeostasis by folding more than 300 mitochondrial matrix proteins. It has been shown previously that HSP60 is downregulated in brains of type 2 diabetic (T2D) mice and patients, causing mitochondrial dysfunction and insulin resistance. As HSP60 is also decreased in peripheral tissues in T2D animals, this thesis investigated the effect of overall reduced HSP60 in the development of obesity and associated co-morbidities.

To this end, both female and male C57Bl/6N control (*i.e.* without further alterations in their genome, Ctrl) and heterozygous whole-body Hsp60 knock-out ($Hsp60^{+/-}$) mice, which exhibit a 50 % reduction of HSP60 in all tissues, were fed a normal chow diet (NCD) or a high-fat diet (HFD, 60 % calories from fat) for 16 weeks and were subjected to extensive metabolic phenotyping including indirect calorimetry, NMR spectroscopy, insulin, glucose and pyruvate tolerance tests, *vena cava* insulin injections, as well as histological and molecular analysis.

Interestingly, NCD feeding did not result in any striking phenotype, only a mild increase in energy expenditure in $Hsp60^{+/-}$ mice. Exposing mice to a HFD however revealed an increased body weight due to higher muscle mass in female $Hsp60^{+/-}$ mice, with a simultaneous decrease in energy expenditure. Additionally, these mice displayed decreased fasting glycemia. Opposingly, male $Hsp60^{+/-}$ compared to control mice showed lower body weight gain due to decreased fat mass and an increased energy expenditure, strikingly independent of lean mass. Further, only male $Hsp60^{+/-}$ mice display improved HOMA-IR and Matsuda insulin sensitivity indices.

Despite the opposite phenotype in regards to body weight development, $Hsp60^{+/-}$ mice of both sexes show a significantly higher cell number, as well as a reduction in adipocyte size in the subcutaneous and gonadal white adipose tissue (sc/gWAT). Curiously, this adipocyte hyperplasia – usually associated with positive aspects of WAT function – is disconnected from metabolic improvements, as the gWAT of male $Hsp60^{+/-}$ mice shows mitochondrial dysfunction, oxidative stress, and insulin resistance. Transcriptomic analysis of gWAT shows an up

regulation of genes involved in macroautophagy. Confirmatory, expression of microtubule-associated protein 1A/1B light chain 3B (LC3), as a protein marker of autophagy, and direct measurement of lysosomal activity is increased in the gWAT of male Hsp60$^{+/-}$ mice.

In summary, this thesis revealed a novel gene-nutrient interaction. The reduction of the crucial chaperone HSP60 did not have large effects in mice fed a NCD, but impacted metabolism during DIO in a sex-specific manner, where, despite opposing body weight and body composition phenotypes, both female and male Hsp60$^{+/-}$ mice show signs of protection from high fat diet-induced systemic insulin resistance.

Zusammenfassung

Metabolische Folgen einer HSP60 Reduktion während des Diät-induzierten Übergewichts

Robert Hauffe

Der mitochondriale Chaperonkomplex HSP60/10 ist für die korrekte Faltung von über 300 mitochondrialen Matrixproteinen verantwortlich. Es wurde bereits gezeigt, dass HSP60 in Gehirnen von Patienten sowie Mäusen mit Typ 2 Diabetes (T2D) reduziert ist, was zu mitochondrialer Dysfunktion und Insulinresistenz führt. HSP60 ist darüber hinaus auch in peripheren Organen von T2D Mäusen reduziert. Die hier vorliegende Arbeit hat daher den Einfluss einer generellen Reduktion von HSP60 auf die Entwicklung von Übergewicht und die damit assoziierten Komorbiditäten untersucht.

Hierfür wurden weibliche und männliche C57Bl/6N Kontroll Mäuse (d.h. ohne wietere Veränderung ihres Genoms, Ctrl), sowie C57Bl/6N Mäuse mit einer heterozygoten Deletion von HSP60 ($Hsp60^{+/-}$) genutzt. Die $Hsp60^{+/-}$ Maus zeigt eine 50 % Reduktion von HSP60 in allen Geweben. Allen Tieren wurde in der Folge entweder eine normale Haltungsdiät (NCD) oder eine 60 % Hochfettdiät (HFD) gefüttert und einer intensiven metabolischen Charakterisierung unterzogen. Dies beinhaltete indirekte Kalorimetrie, NMR Spektroskopie, Insulin, Glukose und Pyruvat Toleranztests, direkte *vena cava* Insulinapplikation, sowie eingehende histologische und molekulare Untersuchungen.

Interessanterweise zeigte die Fütterung mit der NCD keine stark ausgeprägten Phänotypen, lediglich ein leichter Anstieg im Energieverbrauch war zu beobachten. Die Fütterung mit der HFD dagegen führte auf Grund von größerer Muskelmasse zu einem erhöhten Körpergewicht in weiblichen $Hsp60^{+/-}$ Mäusen, was mit gleichzeitig verringertem Energieverbrauch einherging. Zusätzlich war bei diesen Mäusen der gefastete Bluzuckerspiegel verringert. Im Gegensatz dazu zeigten männliche $Hsp60^{+/-}$ Mäuse ein verringertes Körpergewicht, bedingt durch eine geringere Fettmasse sowie erhöhtem Energieverbrauch. Darüber hinaus war bei männlichen $Hsp60^{+/-}$ Mäusen eine Verbesserung der Insulin Sensitivitätsindizes HOMA-IR und Matsuda Index zu verzeichnen.

Trotz dieses gegenteiligen Phänotyps zeigten beide Geschlechter eine erhöhte Zellzahl, sowie eine verringerte Zellgröße der Adipozyten im subkutanen und gonadalen weißen Fettgewebe (sc/gWAT (*engl: white adipose tissue*)). Überraschenderweise ist diese Adipozytenhyperplasie – normalerweise assoziiert mit verbesserter Fettgewebsfunktion – losgelöst von verbesserter WAT Funktion, da das gWAT männlicher Hsp60$^{+/-}$ Mäuse mitochondriale Dysfunktion, oxidativen Stress und Insulinresistenz zeigt. Eine folgende Transkriptomanalyse gab Hinweise auf eine Induktion der Makroautophagie. Bestätigend hierfür ist im gWAT der heterozygoten Mäuse die Expression des Autophagie Markers microtubule-associated protein 1A/1B light chain 3B (LC3), sowie die direkt gemessene lysosomale Aktivität erhöht.

Zusammenfassend konnte in dieser Arbeit eine neuartige Gen-Nährstoff Interaktion gezeigt werden. So zeigte die Reduktion des wichtigen Chaperons HSP60 unter NCD Fütterung nur schwache Effekte, während unter Hochfettdiätfütterung der Stoffwechsel geschlechtsspezifisch beinflusst wurde. Obwohl die beiden Geschlechter der Hsp60$^{+/-}$ Mäuse gegenteilige Phänotypen im Bezug auf Körpergewicht und Körperzusammensetzung aufwiesen, zeigen beide Anzeichen eines Schutzes vor Hochfettdiät-induzierter Insulinresistenz.

Danksagung

Nach einer intensiven Zeit des Lernens und Forschens möchte ich allen Personen danken, die mich während dieser Zeit unterstützt haben.

An erster Stelle gilt mein Dank Herrn Prof. Dr. André Kleinridders für die Bereitstellung meines spannenden Projektes. Noch größerer Dank allerdings für die konstante hervorragende Betreuung und offene Tür in allen theoretischen und praktischen Fragen, die eine Forschungsarbeit mit sich bringt. Darüber hinaus möchte ich ihm für die Möglichkeit danken, meine Arbeit auf internationalen Kongressen vorstellen zu können.

Ich möchte Frau Prof. Dr. Annette Schürmann danken meine Arbeit als Zweitgutachterin zu beurteilen, sowie für die konstruktiven Anregungen und Gespräche im Rahmen der Doktorandenseminare und der spannenden internen Datengruppen. Für seine Bereitschaft das externe Gutachten meiner Arbeit zu übernehmen, bedanke ich mich herzlich bei Herrn Prof. Dr. Michael Schupp.

Für die gute Kooperation innerhalb dieses Projektes, sowie meines Nebenprojektes und der daraus entstandenen Publikation, gilt mein Dank Prof. Dr. Kai Kappert, Dr. Karin Müller, Dr. Christiane Ott, Prof. Dr. Tanja Schwerdtle, Prof. Dr. Anna Kipp und Prof. Dr. Matthias Blüher. Vielen Dank an Markus Jähnert für die Unterstützung bei bioinformatischen Auswertungen, an Dr. Wenke Jonas für die Aufarbeitung der indirekten Kalorimetrie Daten.

Ohne die großartige Unterstützung meiner derzeitigen und ehemaligen Kollegen aus der Nachwuchsforschungsgruppe „Zentralen Regulation des Stoffwechsels“ wäre diese Arbeit nicht in dieser Form entstanden: Vielen Dank Kristina Wardelmann, Eugenia Alfine, Chantal Chudoba, Mareike Schell, Vanessa Stein und Antoine Leboucher. Danke Michaela Rath für Deine Hilfe in allen Dingen „Maus“ sowie Laborорganisation. Großer Dank an alle Mitarbeiter des MRL für die tolle Zusammenarbeit, insbesondere Dr. Anja Voigt für die Leitung, sowie Ines Grüner, Tanita Blum, Elisabeth Meyer und Carola Gehrmann.

Ein besonderer Dank gilt meinen Freunden und meiner Familie für die mentale Unterstützung während dieser Zeit. Besonders meine Eltern tragen maßgebliche Veranwortung für meinen Werdegang, vielen Dank für die fortwährende Unterstützung durch alle Lebenslagen.

Zu Guter Letzt: Vielen Dank an meine Frau Franziska Hauffe, Licht meines Lebens. Ohne Dich wäre ich nicht hier.

Contents

List of Figures

List of Tables

List of Abbreviations

Throughout this work gene and protein names are written following the NCBI gene nomenclature:

Gene	*Mus musculus* gene name
GENE	*Mus musculus* protein product of *Gene*
GENE	*Homo Sapiens* gene name
GENE	*Homo Sapiens* protein product of *GENE*

ABHD5	1-acylglycerol-3-phosphate O-acyltransferase
ACC1	acetyl-CoA carboxylase 1
ACLY	ATP-citrate lyase
AGPAT	y 1-acyl-sn-glycerol-3-phosphate acyltransferase
AKT	protein kinase B
aP2	adipocyte protein 2
APS	ammonium persulfate
AMP	adenosine monophosphate
ADP	adenosine diphosphate
ATP	adenosine triphosphate
ATG	autophagy related protein
ATGL	adipose triglyceride lipase
AMPK	AMP-activated protein kinase
ANOVA	analysis of variance
BAT	brown adipose tissue
BMI	body mass index
bp	base pairs
BSA	bovine serum albumin
CCL2	chemokine (C-C motif) ligand 2
ClpP	caseinolytic peptidase
CoA	coenzyme A
CYCS	cytochrome c
DAG	diacylglyceride
DIO	diet-induced obesity
DMEM	Dulbecco's Modified Eagle's Medium
DMSO	dimethyl sulfoxide
DNA	deoxyribonucleic acid
DNAJA3	DnaJ homolog subfamily A member 3, mitochondrial
DOG	2-deoxy-d-glucose
e.g.	*exempli gratia*, for example
EDTA	ethylenediaminetetraacetic acid
EE	energy expenditure
ELISA	enzyme-linked immunosorbent assay
ER	endoplasmic reticulum

ERK	mitogen-activated protein kinase
ETC	electron transport chain
FA	fatty acid
FASN	fatty acid synthase
FBS	fetal bovine serum
FFA	free fatty acids
FCCP	carbonyl cyanide-4-(trifluoromethoxy)phenylhydrazone
FOXO1	forkhead box protein O1
GLUT	glucose transporter
GPAT	glycerol-3-phosphate acyltransferase
GPx	glutathione peroxidase
GRB2	growth factor receptor-bound protein 2
GSIS	glucose-dependent insulin secretion
GSK	glycogen synthase kinase
HBSS	Hank's buffered salt solution
HFD	high fat diet
HSL	hormone-sensitive lipase
HSP	heat shock protein
HSPD1	heat shock protein family D (gene coding for HSP60)
HSPE1	heat shock protein family E (gene coding for HSP10)
IBMX	3-isobutyl1-methylxanthine
i.e.	*id est*, that is
IGF-1	insulin-like growth factor-1
IKK	inhibitor of nuclear factor kB kinase
IL	interleukin
InsR	insulin receptor
i.p.	intraperitoneal
IRS	insulin receptor substrate
ITT	insulin tolerance test
JNK	c-Jun N-terminal kinase
KD	knockdown
K_m	Michaelis constant
KO	knockout
LC3	microtubule-associated protein 1A/1B-light chain 3
LonP	lon protease
LPA	lysophosphatic acid
MAG	monoacylglyceride
MAPK	mitogen activated protein kinase
MGL	monoacylglycerol lipase
MHCα	myosin heavy chain, α isoform
mitoNEET	CDGSH iron sulfur domain 1 protein
M-MLV RT	Moloney murine leukemia virus reverse transcriptase
MPC	mitochondrial pyruvate carrier
MSR	mitochondrial stress response
mTOR	mammalian target of rapamycin
MTT	3-(4,5-dimethylthiazol-2-yl)-2,5-diphenyltetrazolium bromide
NAC	N-acetylcysteine
NAD	nicotinamide adenine dinucleotide
NCD	normal chow diet
NfκB	nuclear factor 'κ-light-chain-enhancer' of activated B-cells
NMR	nuclear magnetic resonance

Nnt	NAD(P) transhydrogenase, mitochondrial
oGTT	oral glucose tolerance test
OVX	ovariectomized
OXA1L	Mitochondrial inner membrane protein OXA1L
OXPHOS	oxidative phosphorylation system
PBS	phosphate buffered saline
PCR	polymerase chain reaction
PDE	phosphodiesterase
PDK1	phosphatidylinositol dependent protein kinase
PGC1α	peroxisome proliferator-activated receptor γ coactivator 1α
PI3K	phosphoinositide 3-kinase
PINK1	PTEN-induced kinase 1
PIP_2	phosphatidylinositol 4,5-bisphosphate
PIP_3	phosphatidylinositol 3,4,5-trisphosphate
PKA	protein kinase A
PKC	protein kinase C
PTPN1	tyrosine-protein phosphatase non-receptor type 1
PTT	pyruvate tolerance test
PVDF	polyvinylidene difluoride
qPCR	quantitative real-time PCR
RCF	relative centrifugal force
RER	respiratory exchange ratio
RNA	ribonucleic acid
ROS	reactive oxygen species
RPM	revolutions per minute
RT	room temperature
RT-PCR	reverse transcription polymerase chain reaction
SDS-PAGE	sodium dodecyl sulfate–polyacrylamide gel electrophoresis
SEM	standard error of the mean
SIRT3	sirtuin 3
SOD2	superoxide dismutase 2
SOS	son of sevenless homolog
SPG13	hereditary spastic paraplegia
SREBP-1	sterol regulatory element-binding protein 1
SVF	stromal vascular fraction
T2D	type-2 diabetes
TAG	triacylglyceride
TBC1D4	tubulin-specific chaperone domain 1 family member 4
TBS	Tris-buffered saline
TEMED	tetramethylethylendiamin
TFAM	mitochondrial transcription factor A
TLR	toll-like receptors
TNFα	tumor necrosis factor alpha
TOMM6	mitochondrial import receptor subunit TOM6 homolog
ULK	Unc-51 like autophagy activating kinase
UPR^{mt}	mitochondrial unfolded protein response
gWAT	gonadal white adipose tissue
scWAT	subcutaneous white adipose tissue

Introduction

1.1 Obesity and its effect on adipose tissue physiology

Past decades have seen an unprecedented rise in obesity rates across both developing and developed nations. As of 2016, the world's obesity prevalence has nearly tripled since 1975. World-wide, 40 % (39 % of men and 40 % of women) of adults are classified as overweight, and 13 % (11 % of men and 15 % of women) as obese (WHO, 2017). The reasons for the sharp increase in obesity rates are multifaceted, involving both genetic and environmental factors. However, the imbalance between energy intake and expenditure is seen as the major driver for the development of overweight and obesity (Delgado, 2003; Popkin *et al.*, 2012). Major contributors to this imbalance are the availability of affordable and energy-dense (*i.e.* rich in sugar and fats) food, paired with a continued trend to more sedentary lifestyles. For optimal usage of available nutrition, excess energy needs to be stored in order to survive periods where food is not readily available. Specifically, glucose is taken up by the liver and skeletal muscle and processed to glycogen for short-term storage. For long-term storage, glucose and fatty acids are taken up by the white adipose tissue (WAT), converted to triglycerides *via* lipogenesis, and stored in lipid droplets within the adipocytes. This stored energy can be recovered through lipolysis to meet energy demands when external food sources are scarce. Beyond its energy storing function however, in the previous decades the WAT has been recognized as a vital endocrine organ. By secreting peptide hormones called adipokines, such as leptin or adiponectin, the WAT contributes to the control of hunger and thereby food intake, as well as glucose utilization and energy expenditure (Badman *et al.*, 2007). The loss of either hormone leads to severe metabolic alterations, including obesity, insulin resistance, type 2 diabetes (T2D) and cardiovascular complications (Ingalls *et al.*, 1950; Zhang *et al.*, 1994; Lindström, 2006; Xia *et al.*, 2018).

In healthy states, energy intake and expenditure are in an equilibrium. However, in a continuous state of over-nutrition, the adipose tissue expands to be able to cope with the influx of nutrients. Adipose tissue expansion can occur *via* two processes, either an increase in the number of adipocytes, or the increase in size of existing adipocytes. This is called adipocyte hyperplasia and hypertrophy, respectively. Hyperplasia as a mechanism for WAT expansion is viewed as "healthy" WAT expansion. Whereas these cells are usually still fully functional in terms of metabolic activity, adipokine release and insulin sensitivity, hypertrophic adipocytes are often insulin resistant and exhibit deteriorated metabolic and endocrine functions, as well. Excess glucose and lipid availability can lead to mitochondrial stress and thus an increase on reactive oxygen species (ROS) generation. ROS are known to induce the activation of stress kinases and subsequently insulin resistance. Moreover, WAT rich in hypertrophic cells is more prone to show signs of inflammation, a known risk factor for further metabolic complications and both cause and consequence of mitochondrial stress and subsequent ROS generation (Hotamisligil, 2006). Thus, this cascade of increasing cellular and mitochondrial stress, ROS generation, WAT inflammation and insulin resistance can turn into a vicious self-sustaining cycle (Fig. 1.1). As adipocytes expand and reach maximum capacity for lipid storage, "lipid-spillover" can occur. Here, free fatty acids are released from the WAT and are stored in ectopical fat-depots in *e.g.* skeletal muscle and the liver, leading to decreased muscle function and non-alcoholic fatty liver disease (NAFLD), the latter being a strong predictor for the development of T2D (Tokita *et al.*, 2017). On the other hand, a lack of functional white adipose tissue is equally detrimental to metabolism. Lipodystrophic diseases are characterized with the inability to properly process or store lipids, leading to a similar ectopic accumulation of fat (Phan *et al.*, 2005; Ajluni *et al.*, 2017; Polyzos *et al.*, 2019; Bruder-Nascimento *et al.*, 2019).

As a consequence of the rise in obesity prevalence, pathologies associated with obesity have equally increased in the past decades. Most notably, the incidence of cardiovascular diseases, as well as metabolic disorders, such as insulin resistance and T2D, is in sharp incline (O'Neill *et al.*, 2015). As such, they are on the forefront of obesity-related health risks. One of the most common early co-morbidities in obesity is the development of insulin resistance, *i.e.* the lack of an appropriate cellular response to an insulin stimulus.

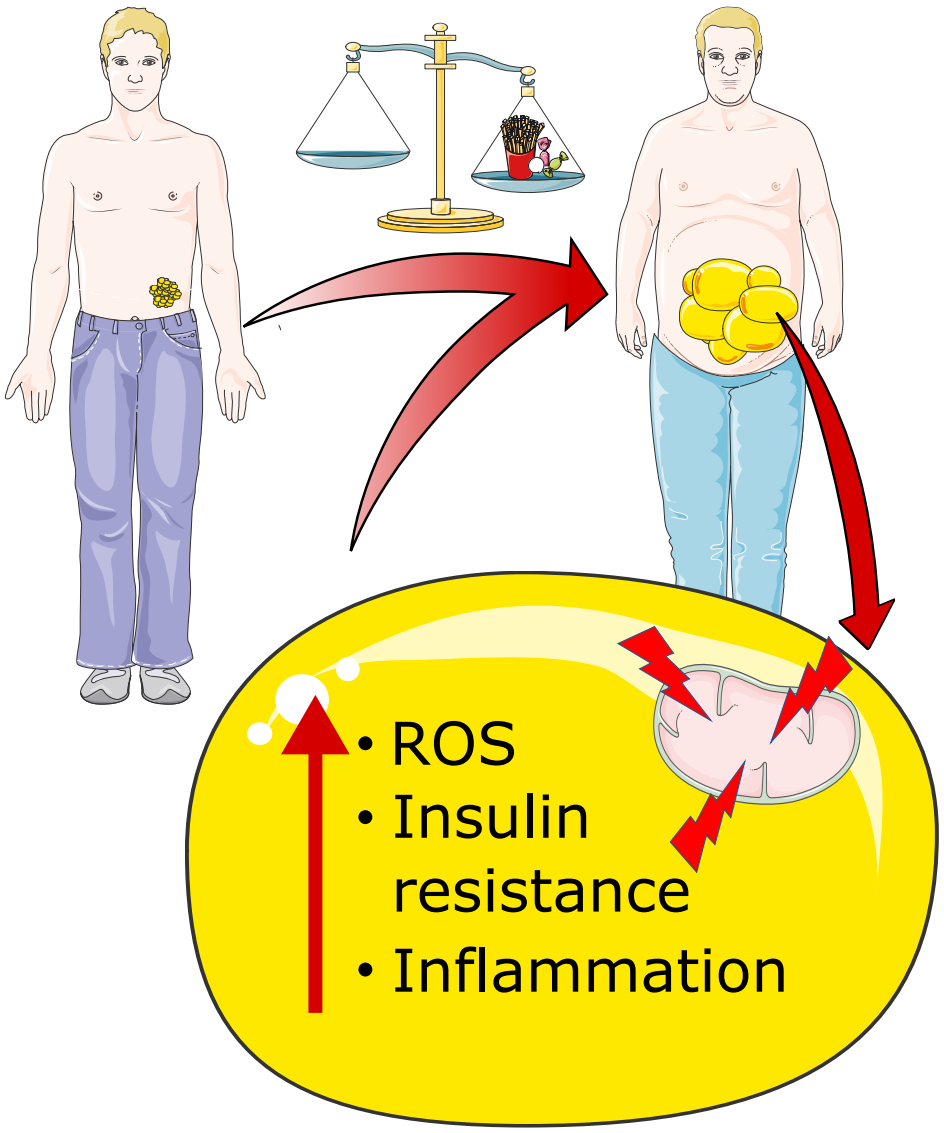

Figure 1.1: Interaction between obesity and mitochondrial function creates a vicious cycle.
Obesity leads to adipocyte hypertrophy and subsequent elevated reactive oxygen species (ROS), inflammation, and insulin resistance. This in turn contributes to the development of obesity, creating a vicious cycle of self propagating obese phenotypes.

1.2 Healthy insulin action

After digestion of food in the gastrointestinal tract, carbohydrates, mainly in form of glucose, are released into the blood stream, leading to an increase in blood glucose levels and subsequently to insulin release. Insulin then stimulates glucose uptake and utilization, suppresses hepatic gluconeogenesis, and induces lipogenesis in the adipose tissue.

In the pancreatic β-cell insulin is stored in granules. Glucose from the blood stream is taken up via the glucose transporter 2 (GLUT2) and enters the classical ATP generating pathway of the mitochondrial oxidative phosphorylation. Here, conversion of ADP to ATP decreases the ADP/ATP ratio, which deactivates the ATP-dependent potassium channel K_{ATP}, leading to the depolarization of the β-cell membrane. Following, voltage gated calcium channels ($Ca_v1.2/1.3$) are opened and the resulting calcium influx triggers exocytosis of insulin into the circulation. Released insulin then circulates in the bloodstream and binds the insulin receptor (InsR), a tyrosine kinase receptor, on the cell surface of target tissues. The InsR is a dimeric transmembrane receptor, with each monomer consisting of one α-chain (containing the extracellular domains), and one β-chain (intracellular domains). Upon substrate binding, the InsR changes its conformation, which brings kinase domains in proximity to tyrosine phosphorylation sites on the β-chain, allowing the autophosphorylation of tyrosine residues. This leads to two general downstream mechanisms through (i) protein kinase B (PKB, also called AKT), and (ii) the mitogen-activated protein kinase (MAPK). In the first case, the autophosphorylated tyrosine residues on the InsR recruit and phosphorylate downstream signaling proteins, such as the insulin receptor substrate 1 (*e.g.* on residue $IRS1_{Y612}$). Thus, activated IRS1 binds and activates the phosphoinositide 3-kinase (PI3K), which catalyzes the reaction of phosphatidylinositol 4,5-bisphosphate (PIP_2) to Phosphatidylinositol 3,4,5-trisphosphate (PIP_3). PIP_3 acts as a second messenger which activates phosphatidylinositol dependent protein kinase (PDK1), which in turn activates AKT by phosphorylation at Thr_{308} (Alessi *et al.*, 1996). Additionally, AKT activation occurs by Ser_{473} phosphorylation *via* action of mammalian target of rapamycin (mTOR) (Sarbassov *et al.*, 2005). AKT itself acts on a variety of pathways – depending on the affected tissue – including the translocation of GLUT4 vesicles (*via* Tubulin-specific chaperone domain 1 family member 4, TBC1D4) to facilitate glucose uptake, the induction of glycogen synthesis (*via* Glycogen synthase kinase 3, GSK3) and protein synthesis (*via* mTOR), as well as

the suppression of gluconeogenesis (*via* Peroxisome proliferator-activated receptor gamma coactivator 1-alpha, PGC-1α, as well as forkhead box O1/6 proteins, FoxO1/6). The second large insulin signaling pathway includes autophosphorylation sites in the src-homology domains on the insulin receptor, which start a signaling cascade through the proteins Growth factor receptor-bound protein 2 (GRB2), Son of sevenless homolog (SOS), Ras GTPase and c-Raf, down to dual specificity mitogen-activated protein kinase kinase 1/2 (MAP2K1/2) and ultimately Erk1/2. Erk thus finally stimulates cell growth and mitochondrial function in insulin sensitive cells (Taniguchi *et al.*, 2006).

1.3 Insulin sensitivity in white adipose tissue

Insulin sensitivity plays a pivotal role for adipose tissue development and function. Upon insulin binding, the above mentioned signaling cascades are engaged. In the WAT, this leads to four major outcomes of nutrient utilization and WAT expansion: (i) GLUT4 translocation and subsequent glucose uptake, (ii) inhibition of lipolysis, (iii) induction of lipogenesis (*i.e* adipocyte hypertrophy), and (iv) proliferation and differentiation of adipocytes (*i.e* adipocyte hyperplasia).

The first three processes are mainly activated *via* the PI3K-PIP_3-AKT pathway. GLUT4 translocation is induced by phosphorylation of TBC1D4 by AKT, inhibiting its GTPase activity and further triggering activation of downstream Rab proteins, allowing for GLUT4 vesicle translocation to the plasma membrane (Leto *et al.*, 2012).

Lipolysis is a process regulated by hormones that serves to mobilize stored lipids to enter energy generating pathways. Here, glucagon and epinephrine signaling induces conversion of ATP to cyclic AMP (cAMP) which activates protein kinase A (PKA). PKA phosphorylates hormone-sensitive lipase (HSL) and perilipin-1. Phosphorylation of perilipin-1 releases 1-acylglycerol-3-phosphate O-acyltransferase (ABHD5), a co-activator of adipose triglyceride lipase (ATGL) in the lipid droplet. ATGL converts triacylglycerides (TAGs) to diacylglycerides (DAGs). The phosphorylated, and thus activated, HSL then hydrolyzes DAGs into free fatty acids (FFA) and monoacylglycerides (MAG) that are released into the cytosol. MAGs are further hydrolyzed by monoacylglycerol lipase (MGL) into FFAs and glycerol. FFAs can then enter the β-oxidation pathway in the mitochondria to generate ATP. The process of lipolysis is effectively inhibited by insulin by induction of the phosphodiesterase (PDE) through the

PI3K-PIP_3-AKT pathway. PDE degrades the phosphodiester bond in cAMP to reduce the cAMP pool (Lass *et al.*, 2011).

Insulin stimulates *de novo* lipogenesis, a process by which individual adipocytes expand through storage of excess energy as TAGs in lipid droplets, presumably through activation of sterol regulatory element-binding protein 1 (SREBP-1) (Foretz *et al.*, 1999). During lipogenesis, glucose is converted to pyruvate, further to acetyl-CoA and citrate in the mitochondria (Z. Song *et al.*, 2018). Citrate is shuttled to the cytosol, where it serves as substrate to the ATP-citrate lyase (ACLY), which catalyzes its conversion back to Acetyl-CoA. Acetyl-CoA is used by the acetyl-CoA carboxylase 1 (ACC1) to generate malonyl-CoA, which gets converted to palmitic acid by the fatty acid synthase (FASN). Fatty acids are converted to TAGs *via* a reaction catalyzed by diacylglycerol-O-Acyltransferases (Kersten, 2001).

Stimulation of adipocyte proliferation and differentiation by insulin leads to adipose tissue hyperplasia and is mediated *via* the Ras-MAPK pathway activating the nuclear receptor peroxisome proliferator-activated receptor gamma (PPARγ), the master regulator of adipogenesis (Rieusset *et al.*, 1999; Ahmadian *et al.*, 2013). Indeed, loss of the insulin receptor (using an adiponectin-*Cre* driven knockout) leads to a drastic decrease in adipose tissue mass, mitochondrial dysfunction, and whole-body insulin resistance (Boucher *et al.*, 2016).

Complete loss of insulin signaling in the adipose tissue by deletion of InsR, IGF1R, or both, leads to decreased adipose tissue mass, mitochondrial dysfunction, and whole-body insulin resistance (Boucher *et al.*, 2016). These mice also recapitulate features of lipodistrophy, such as excessive ectopic fat deposition. Strikingly, already in the 1970s it has been demonstrated that insulin binding and InsR expression is reduced in the WAT of obese mice and humans, suggesting that the downregulation of the InsR in the WAT is a common mechanism for the occurrence of insulin resistance in mice and humans (Freychet *et al.*, 1972; Olefsky, 1976; Wigand *et al.*, 1979). Interestingly, we could recently show that a decreased expression of the InsR in the white adipose tissue of mice seems to be a common response in a variety of mouse models of obesity and insulin resistance, leading to local and systemic insulin resistance (Hauffe *et al.*, 2020). Further, the upregulation of the InsR through dietary supplementation with sodium selenite alone could – without changing overall body weight – re-instate local as well as whole-body insulin sensitivity, increase adipocyte glucose uptake and differentiation capacity through a mechanism involving the selenoprotein GPx3.

1.4 Insulin resistance

As an adaptive mechanism to limit over-stimulation of cells by insulin, a negative feedback loop will inhibit signaling at the insulin receptor level as well as downstream of it. On a molecular level, phosphatases, such as tyrosine-protein phosphatase non-receptor type 1 (PTPN1, also called PTP1B) or tyrosine-protein phosphatase non-receptor type 11 (PTPN11, also called SHP2) can dephosphorylate the InsR and IRS proteins to inhibit their activity. Additionally, serine/threonine kinases like protein kinase c proteins (PKCs), inhibitor of nuclear factor kB kinase β (IKKβ), or c-Jun N-terminal kinase (JNK) can act on IRS proteins to phosphorylate inhibitory serine residues Ser_{307}, Ser_{636}, or Ser_{1136} (Saltiel *et al.*, 2001). However, in a state of constant over-nutrition, this protective mechanism can derail into a state of chronic insulin resistance. Due to an over-activation of cellular metabolic processes, this normal adaptive mechanism can become chronic. Two key mechanisms work in congress to promote insulin resistance: (i) Low-grade local and systemic inflammation (1.5), and (ii) increased oxidative stress by excess generation of reactive oxygen species (ROS) and subsequent mitochondrial dysfunction (1.6). In a state of constant over-nutrition, insulin resistance in insulin-targeted tissues will lead to a variety of effects. In the central nervous system, the failure to react to insulin leads to increased food intake (Brüning *et al.*, 2000), as well as potential mood disorders, which in and of themselves are a risk factor for obesity (Luppino *et al.*, 2010; Kleinridders *et al.*, 2014). In the liver, gluconeogenesis will not be inhibited after insulin release, arguably increasing to the already elevated blood glucose levels. Adding to this, local insulin resistance in the skeletal muscle and white adipose tissue severely affects their ability to clear the glucose from the bloodstream and adequately store lipids in the adipocytes to avoid lipotoxicity. Interestingly, there seem to be strong sex-dependent differences in the propensity to develop insulin resistance in a state of over-nutrition (Kautzky-Willer *et al.*, 2016).

1.5 Insulin resistance in inflammatory states

In the 1960s initial evidence was found that obese patients suffer from an inflammatory state with an increase of acute-phase inflammation response proteins compared to controls (Fearnley *et al.*, 1959; Ogston *et al.*, 1964). However, only in the early 1990s a series of

publications by Hotamisligil and colleagues was able to report a specific link of obesity and inflammation in the adipose tissue. They could show that obese adipose tissue showed significantly higher levels of the proinflammatory cytokine tumor necrosis factor alpha (TNFα), and that this induced insulin resistance already at the receptor level by inhibiting the receptor's tyrosine kinase activity (Hotamisligil *et al.*, 1993; Hotamisligil *et al.*, 1994; Hotamisligil *et al.*, 1995; Hotamisligil *et al.*, 1996). Furthermore, the absence of TNFα signaling protected rodents from diet-induced insulin resistance (Uysal *et al.*, 1997). Since then, the number of known inflammatory cytokines increased in obese states has expanded, including interleukin (IL)-6, IL-1β and chemokine (C-C motif) ligand 2 (CCL2). The expression of these cytokines is for example induced by the above-mentioned JNK and IKK signaling pathways. JNK itself is activated by a number of stressors, such as oxidative stress, endoplasmic reticulum (ER) stress, UV light, and also cytokines themselves (Vlahopoulos *et al.*, 2004). Prolonged presence of proinflammatory signaling molecules triggers an immune response by recruiting macrophages, memory T cells, and dendritic cells. This changes the tissue environment to an inflammatory state. This state can thus become chronic and lead to a self-sustaining cycle of Ser/Thr kinase (*e.g.* JNK) activation, cytokine release and unresolved immune response.

1.6 Mitochondrial function in metabolism

Another major pathway potentially leading to insulin resistance is based in the energy utilization of nutrients in the mitochondria itself. To generate energy for all cellular processes, cells produce the energy equivalent adenosine tri-phosphate (ATP) through cellular respiration via glycolysis in the cytosol and oxidative phosphorylation in the mitochondria. ATP can subsequently be hydrolyzed into ADP and inorganic phosphate, which releases a substantial amount of energy that is used to drive enzymatic reactions in the cell.

Although many of their proteins are encoded in the nuclear DNA, mitochondria also possess their own independent genome, as well as transcription and translation machinery. This unique organization is commonly explained by the likely bacterial origin of mitochondria. Phylogenetic analysis of conserved ribosomal RNA (rRNA) supports the concept of the incorporation of bacteria into archaeal cells to form early eukaryotes over two billion years ago (Knoll, 2015; Martin *et al.*, 2003). This endosymbiotic relationship allowed utilization

of otherwise toxic O_2 to more efficiently release energy from organic compounds in aerobic respiration. Mitochondrial function is closely linked to their physical organization, specifically their double-membrane. The components of oxidative phosphorylation, the electron transport chain (ETC), are located in the inner membrane, and by pumping protons from the mitochondrial matrix into the intermembrane space generate an electrochemical gradient across the inner membrane that is used by the ATP synthase to produce ATP.

A necessity to maintain a functional ETC complex is the presence of its functional constituents, *i.e.* the enzymes that comprise the ETC. Here, transcriptional and translational control, as well as ensuring proper folding are crucial to the maintenance of ATP generation *via* oxidative phosphorylation. A complex system of mitochondrial protein quality control has evolved, and at its center is the mitochondrial unfolded protein response (UPR^{mt}), which is responsible for both the correct folding of *de novo* synthesized proteins, as well as the degradation of unfolded proteins (Pellegrino *et al.*, 2013; J. Song *et al.*, 2021). A further prerequisite for oxidative phosphorylation is the availability of intracellular glucose and its conversion to pyruvate through the glycolytic pathway, as well as the generation of reducing equivalents nicotinamide adenine dinucleotide hydrogen (NADH). During glycolysis, glucose is converted with use of ADP, inorganic phosphate (Pi) and NAD^+ to pyruvate, ATP, and NADH in a series of ten steps in a reaction that can be summarized as: $C_6H_{12}O_6$ + 2ADP + 2Pi + $2NAD^+ \rightarrow 2C_3H_4O_3 + 2H_2O$ + 2ATP + 2NADH + $2H^+$. Pyruvate is transported into the mitochondria via the mitochondrial pyruvate carrier 1/2 (MPC1/2) and is converted by the pyruvate dehydrogenase complex to acetyl-CoA. Acetyl-CoA in turn is the starting point for the citric acid cycle (or tricarboxylic acid cycle, TCA) in the mitochondria. Here, a series of reactions yield as main products NADH and FADH, that are used as electron donors in the ETC in the mitochondria. The ETC uses a chain of redox reactions through the ETC complexes I-IV to transfer electrons from electron donors (*e.g.* NADH) to electron acceptors. During this process, a proton (H^+) gradient is generated across the inner mitochondrial membrane. This chemical gradient harbors potential energy, that is used in complex V, the ATP synthase to power the final reaction ADP + Pi $\rightarrow$ ATP. Ideally, four electrons and four protons reduce oxygen to water ($4e^-$ + $4H^+$ + $O_2 \rightarrow 2H_2O$).

Whereas glycolysis produces 2 molecules ATP per molecule glucose, shuttling its product pyruvate into the mitochondria to enter the citric acid cycle and coupling it with oxidative phosphorylation in the mitochondria theoretically produces between 30 and 36 molecules

ATP per molecule glucose (Rich, 2003). The mitochondria are further able to utilize fatty acids to generate ATP. Here, fatty acids are converted to acetyl-CoA which can enter the citric acid cycle. Thus, 1 molecule of *e.g.* palmitic acid can theoretically yield $\sim$ 120 - 130 molecules of ATP (Lehner *et al.*, 2016). The values given here are theoretically achievable yields that will in reality be diminished by proton leak across the mitochondrial membranes (Porter *et al.*, 1995).

Apart from the generation of the energy equivalent ATP, mitochondria are found at the intersection of multiple cellular functions and signaling pathways. During ATP synthesis reactive oxygen species are generated that take part in various signaling pathways ((Finkel, 2011), see also section 1.7). Next, lipid metabolism is in large part dependent on mitochondrial function. First, as β-oxidation of fatty acids takes place in the mitochondrial matrix, but second, also as the main source for Acetyl-CoA and other phospholipid precursors, which in turn are needed for synthesis of membrane phospholipids, *e.g.* cholesterol, in the endoplasmic reticulum (Fagone *et al.*, 2009). Further, through controlled uptake and release, mitochondria are regulating the cellular Ca^{2+} levels, which in turn impact a variety of physiological processes, such as cell migration, cell growth, neuronal excitability, and muscle contraction (Finkel Toren *et al.*, 2015; Giorgi *et al.*, 2018). Despite the indispensability of mitochondria for eukaryotic life, they are also often essential for the initiation cell death (apoptosis). Through a process called mitochondrial outer membrane permeabilization, mitochondrial intermembrane proteins (most prominently cytochrome c) are released into the cytosol and activate caspases, which results in apoptosis (Tait *et al.*, 2013).

Thus, functional mitochondria are central to regulating cell function health as well as controlled cell death (Fig. 1.2).

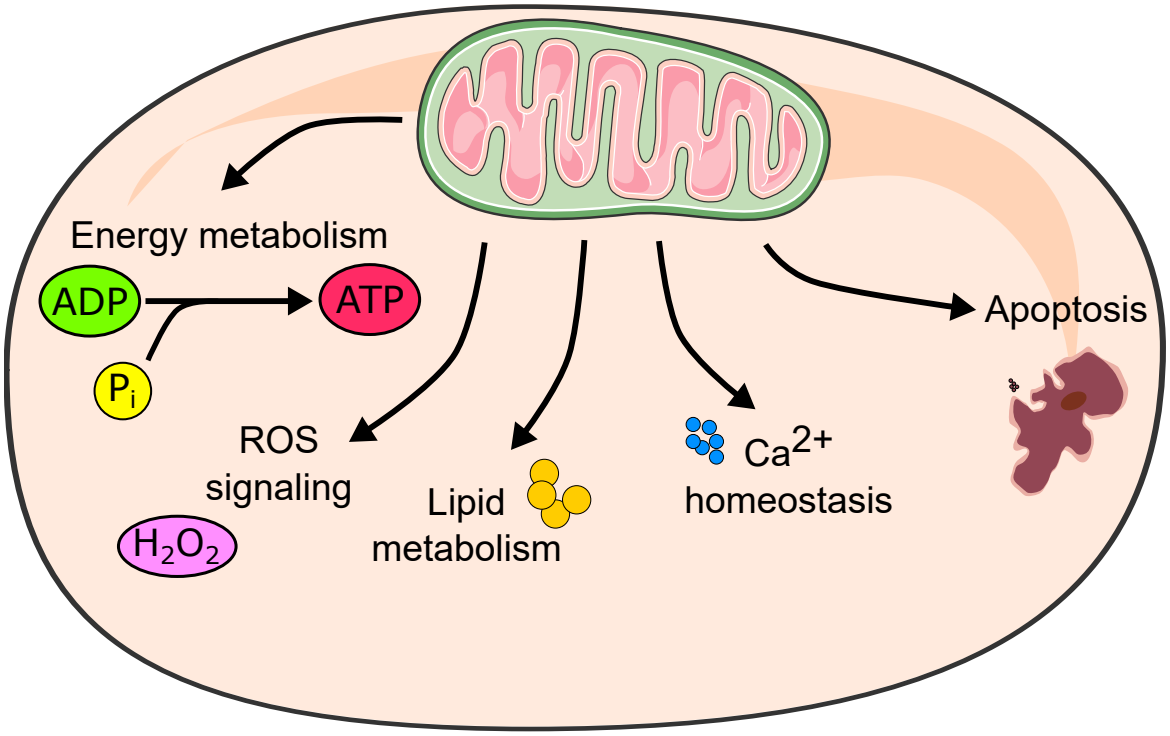

Figure 1.2: Mitochondria impact a wide range of cellular functions.
Mitochondria provide the majority of the cells ATP pool. ROS generated during this process perform important signaling function to *e.g.* inform about the energy metabolism status. Lipid metabolism does not only include the generation of ATP from lipids *via* β-oxidation, but also synthesis of Acetyl-CoA and phospholipid precursors. Control of intracellular Ca^{2+} levels regulates Ca-dependent processes (muscle contraction, neuron excitability *etc.*). Through release of mitochondrial intermembrane proteins (*e.g.* cytochrome c) apoptopic processes can be induced.

1.7 Mitochondrial dysfunction and insulin resistance

During the reduction of O_2 potentially harmful intermediates such as superoxide radicals or peroxides can occur, collectively called reactive oxygen species (ROS). These highly reactive oxidizing agents diffuse freely across membranes and readily react with cellular components. Uncontrolled protein, lipid, or nucleic acid oxidation damages cell components, disturbing cellular processes and signaling pathways (Sies *et al.*, 2017). Thus, excessive ROS generation is harmful to cells. Cells possess a variety of mechanisms to detoxify these by-products, for example the mitochondrial enzyme superoxide dismutase (SOD2) that catalyzes the reaction from superoxide anion radicals to oxygen and the less harmful hydrogen peroxide ($2H^+ + 2O_2^- \rightarrow H_2O_2 + O_2$). Thus, deletion of SOD2 in mice leads to severe

neurodegeneration and early lethality (Oh *et al.*, 2012). Even just a heterozygous deletion leads to mitochondrial dysfunction and increased apoptosis highlighting the need to eliminate excessive ROS to ensure cellular survival (Van Remmen *et al.*, 2001). However, an adipose tissue-specific deletion of SOD2 (targeted via an adiponectin promoter-*Cre* transgene) protected mice from diet-induced obesity, primarily through induction of mitochondrial biogenesis and mitochondrial fatty acid oxidation (Han *et al.*, 2016). Simultaneously however, ROS themselves take part in essential signaling pathways relating to mitochondrial function and insulin sensitivity. Accordingly, overexpression of GPx1, which uses glutathione to detoxify H_2O_2, causes insulin resistance (McClung *et al.*, 2004). Further, intake of antioxidants vitamin C or E after exercise has been shown to decreases exercise-induced insulin sensitivity in skeletal muscle in humans. Interestingly, the exercise-induced upregulation of the aforementioned antioxidative enzymes SOD2 and GPx1 was impeded by use of antioxidants, suggesting the need for signaling pathways involving elevated ROS levels for a healthy metabolism (Ristow *et al.*, 2009). Adipose tissue seems to be especially susceptible to aberrant changes of redox status, since either artificial reduction, or induction lead to impairment of adipocyte differentiation and insulin sensitivity. For example, both hyperoxic culture conditions and treatment with antioxidants, such as N-acetylcysteine (NAC), impair differentiation of 3T3-L1 preadipocytes to mature adipocytes (Fernando *et al.*, 2020; Calzadilla *et al.*, 2011). Further, H_2O_2 treatment markedly increases adipocyte differentiation *in vitro* (H. Lee *et al.*, 2009), presumably by increasing expression of peroxisome proliferator-activated receptor γ (PPARγ). Furthermore, mitochondrial dysfunction can lead to insulin resistance at the post-receptor level. An unrestrained increase in ROS production can activate serine/threonine kinases, which lead to inhibitory serine phosphorylation of IRS1. For example, downregulation of the key enzyme for the proper folding of mitochondrial proteins, the heat-shock protein 60 (HSP60), directly leads to mitochondrial dysfunction and insulin resistance *in vitro* and *in vivo* via induction of JNK and subsequent increase in inhibitory $IRS1_{S307}$ phosphorylation (Kleinridders *et al.*, 2013).

A variety of naturally occurring mitochondrial pathologies are described in humans. Symptoms are diverse, but most often associated with neurological or muscular deficits, such as visual or learning disabilities, poor growth, loss of muscle coordination, or heart disease. However, they are also implicated in a variety of acquired neurological disorders, such as Alzheimer's disease, Parkinson's, disease, and Huntington's disease, as well as

cancer (Alzheimer's-Association, 2018; Rohan de Silva *et al.*, 2000; Albers *et al.*, 2000; Hsu *et al.*, 2016). In diabetes, genetic mutations leading to mitochondrial dysfunction lead to β-cell failure, due to their inability to adequately react with an increase in ATP production after glucose uptake (Ma *et al.*, 2011). Additionally, mutations leading to major defects in mitochondrial function could conceivably impair their ability to adapt to increased nutrient loads, increasing the susceptibility to the development of insulin resistance and obesity. Therefore, mitochondrial function is arguably intricately linked to insulin sensitivity and the development of insulin resistance.

1.8 Models of mitochondrial dysfunction show diverse phenotypes

In the past years, various studies have used mouse models to target different components and aspects of mitochondrial function, which yielded interesting results on both organ-specific and whole-body metabolism. Thus, an adipocyte protein 2 (aP2) targeted over expression of the crucial mitochondrial regulator of iron influx mitoNEET drastically enhanced lipid uptake and storage in the WAT, leading to massive fat accumulation in white adipocytes and resulting in gross obesity. However, overall insulin sensitivity was preserved. The authors argue that overexpression of mitoNEET limits the mitochondrial iron content – the rate limiting factor for electron transport in the ETC – and thereby limiting β-oxidation and consequently lowering mitochondrial membrane potential and ROS-induced oxidative damage. Further, the authors generated a systemic doxycyclin-inducible mitoNEET knockdown mouse. Interestingly, in clear reverse of the overexpression model, the reduction of mitoNEET protected mice from diet induced obesity, but increased β-oxidation, oxidative damage and thus impaired overall glucose tolerance (Kusminski *et al.*, 2012).

A deletion of the master regulator of mitochondrial DNA transcription, the mitochondrial transcription factor A (TFAM) in adipose tissue (aP2-*Cre* transgene), protected mice from diet-induced obesity and insulin resistance, exemplified by lower glycemia and insulinemia, as well as increased sensitivities in both glucose and insulin tolerance tests. Strikingly, although loss of TFAM should limit mitochondrial biogenesis, a crucial prerequisite for adipogenesis, these mice display adipocyte hyperplasia. These adipocytes showed increased oxygen consumption without increased ATP generation. The authors argue that this leads

to a futile energy cycle, where energy is taken up and consumed without generating energy equivalents, ultimately explaining the protection from excessive weight gain and associated metabolic complications (Vernochet *et al.*, 2012). However, this TFAM knockout using the aP2-*Cre* did not lead to TFAM ablation in all adipose tissue depots. Therefore, the authors performed further studies using a adiponectin-*Cre* directed TFAM knockout. Here, mice showed pronounced mitochondrial dysfunction, lower fat mass but impaired glucose tolerance (Vernochet *et al.*, 2014).

In another approach, an adipose tissue specific knockout of PGC-1α was achieved by using the *Cre* recombinase under control of the adiponectin promoter (Kleiner *et al.*, 2012). PGC-1α is essential for mitochondrial biogenesis, which in turn is crucial for adipocyte proliferation. As such, reduced levels should lead to impaired adipose tissue function when challenged with a HFD. Indeed, the authors observed a reduction of genes involved in oxidative phosphorylation and the citric acid cycle. Further, mice lacking PGC-1α in the adipose tissue showed glucose intolerance and insulin resistance, interestingly without differences in body weight development (Kleiner *et al.*, 2012).

In summary, models of mitochondrial dysfunction lead to a wide range of phenotypes, depending on the specific underlying cause, such as *e.g.* altered biogenesis, fatty acid oxidation, or oxidative respiration. One common factor in most models however are alterations in mitochondrial protein homeostasis, *i.e.* abnormal alterations in the content of functional proteins and protein complexes, that arguably have large implications for local and systemic metabolic health. Thus, a key component for maintaining adequate mitochondrial function is the maintenance of mitochondrial proteostasis.

1.9 The molecular chaperone HSP60

Central for maintenance of mitochondrial proteostasis is correct folding of *de novo* synthesized proteins. An increased demand for mitochondrial activity leads to an increase in expression of genes coding for enzymes necessary for theses functions, *e.g.* members of the ETC or ROS detoxifying enzymes. Following the necessity for the correct folding of these proteins rises equally. Most of the mitochondrial proteins are encoded in the nuclear DNA. Therefore, they are transcribed in the nucleus and translated in the cytosol. The resulting peptide chain is targeted to the mitochondria with a mitochondrial localization sequence

(Omura, 1998). Once transported across the mitochondrial membranes into the mitochondrial matrix, they are processed and converted from their unfolded, non-functional forms to their properly folded and functional conformations. In mitochondria, the protein folding is mainly achieved through the activity of the HSP60/10 chaperonin complex. This molecular chaperone is highly conserved throughout all domains of life. Indeed, its function is conserved to a degree where the bacterial homologues GroEL and GroES, can be substituted for with their mammalian counterparts without loss of functionality (Nielsen *et al.*, 1999). The two chaperonin subunits HSP60 and HSP10 are controlled by a bi-directional promoter leading to a theoretical 1:1 expression stoichiometry (J. Hansen *et al.*, 2003). HSP60 is a 60 kilodalton protein that is arranged in two stacked heptameric rings in a barrel-like structure. The 10 kilodalton protein HSP10 forms two heptameric rings that seal the HSP60 barrel on both ends to form a hydrophilic cavity favoring ATP-dependent protein folding of unfolded proteins (Saibil *et al.*, 2013; Ryabova *et al.*, 2013; Nisemblat *et al.*, 2015; Taguchi, 2015, Fig. 1.3).

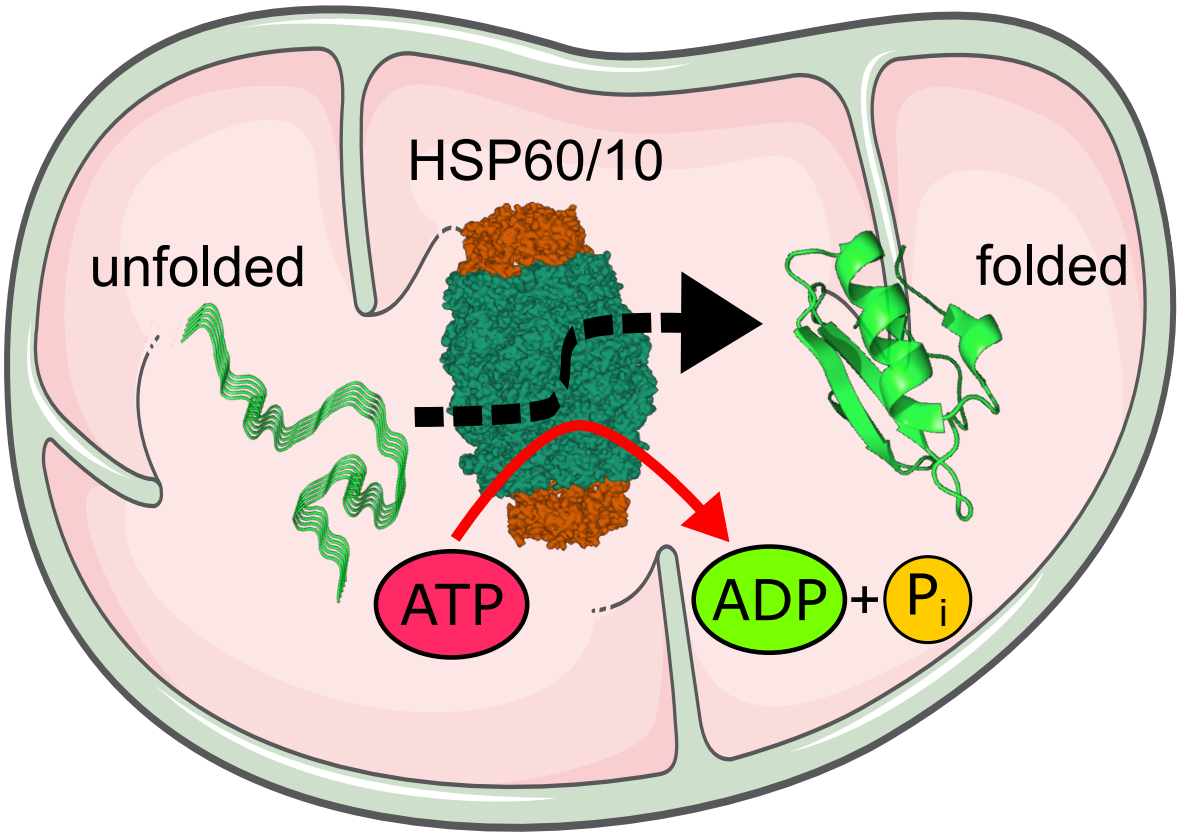

Figure 1.3: The HSP60/10 chaperonine folds proteins in the mitochondrial matrix.
Two stacked heptameric rings of HSP60 are capped on either side by a heptameric ring of HSP10. The hydrophobic inner cavity facilitates protein folding. ATP is used for a confirtmational change, releasing the now folded protein and allowing for another cycle of protein binding and folding.

HSP60 is known to be responsible for the correct folding of over 300 mitochondrial proteins (Kerner *et al.*, 2005; Hartl *et al.*, 2009; Bie *et al.*, 2020). Thus, it plays a pivotal role in maintaining mitochondrial integrity and thereby cellular metabolism (Fig. 1.4). Besides its protein folding function, HSP60 can also act as a pro-inflammatory agent in the adipose tissue. Released by cells through an as of yet unknown mechanism, it has been shown to directly activate toll-like receptors (TLRs) to induce the release of inflammatory cytokines *via* nuclear factor kappa-light-chain-enhancer of activated B cells (NF-κB) (Märker *et al.*, 2012).

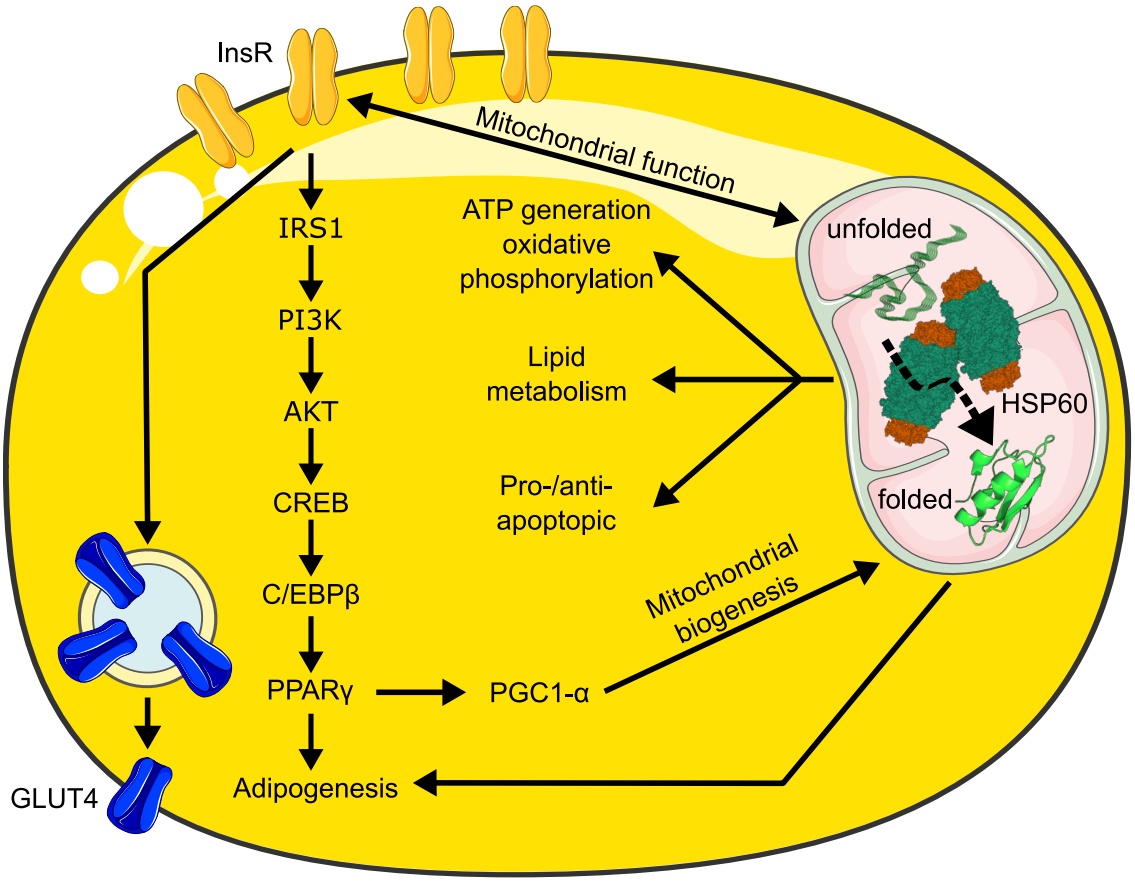

Figure 1.4: Processes mediated by functional mitochondria in the white adipose tissue.

Insulin signaling induces GLUT4 translocation to increase glucose uptake, and acts through the PI3K-AKT signaling cascade to activate C/EBPβ and PPARγ, leading to an induction of PGC1-α mediated mitochondrial biogenesis, a prerequisite of adipogenesis. Here, a functional protein folding machinery in the mitochondria forms the basis for as the need to increase growth-related functions also increases the need for *de novo* synthesized proteins and their correct folding.

A pathological accumulation of unfolded proteins triggers the UPR^{mt}, a retrograde signaling mechanism that results in the upregulation and activation of two main enzymatic systems: (i) the folding of proteins by the above described HSP60/10 chaperonin system, and (ii) the degradation of unfolded or misfolded proteins by proteases Lon protease homolog (LonP) and caseinolytic peptidase X and P (ClpXP) protease system. LonP is an ATP-dependent serine protease with a well described role in the degradation of unfolded,

misfolded, or oxidatively damaged proteins. ClpX and ClpP join together to form the ATP-dependent ClpXP protease system. These systems prevent an accumulation of unfolded proteins when the chaperonin system is at maximum capacity or in cases where proteins are not correctly folded or damaged by oxidation due to excessive ROS generation (J. Song *et al.*, 2021). Thus, these two processes, protein folding and degradation, act in concert to promote proper mitochondrial function by maintaining protein homeostasis. Interestingly, the components of the UPR^{mt} are among the first to be upregulated after insulin stimulation of cells, presumably to anticipate the demand for increased protein folding and degradation (Wardelmann *et al.*, 2019).

Following its central role in folding many mitochondrial proteins, a homozygous deletion of HSP60 results in embryonic lethality (IMBC MGI:96242 and Christensen *et al.*, 2010). Disease-related mutations in humans in the gene coding for HSP60, *HSPD1*, are the likely cause of Hereditary Spastic Paraplegia SPG13, and a form of neurodegenerative hypomyelinating leukodystrophy, respectively (J. J. Hansen *et al.*, 2002; J. Hansen *et al.*, 2007; Bross *et al.*, 2007; Magen *et al.*, 2008). Further, two case studies in humans reported HSP60 deficiency leading to systemic organ failures due to severe mitochondrial dysfunction and early patient death (Agsteribbe *et al.*, 1993; Briones *et al.*, 1997). Heterozygous deletion of HSP60 ($Hsp60^{+/-}$) in mice – which leads to a 50 % reduction in HSP60 protein levels – mirrors human HSP60 deficiencies with late onset motoneuron disorder as a feature of SPG13 (Magnoni *et al.*, 2013). Interestingly, the same level of HSP60 reduction can be seen in diabetic mice, as well as *post-mortem* brain samples in humans Further, as mentioned earlier, $Hsp60^{+/-}$ mice are already on a baseline less insulin sensitive than control litter mates, although they do not show any other phenotype (Kleinridders *et al.*, 2013). For HSP10, there are currently no knockout models described (MGI:104680). A human case study of infantile spasms describes a likely causative genetic mutation in the HSP10 gene, leading to a 2-fold decrease in HSP10 to HSP60 ratio and a 2-fold increase in cellular superoxide levels (Bie *et al.*, 2016).

In conclusion, a sustained situation of nutrient influx can lead to increased ROS generation and oxidative damage, causing successive breakdown of UPR^{mt} signaling and its individual components, leading to mitochondrial dysfunction.

1.10 Mitochondrial dysfunction and autophagy

A sustained situation of mitochondrial dysfunction can lead to damaged mitochondria. A complex process of mitochondrial fission and fusion events, together termed mitochondrial dynamics, regulates both mitochondrial biogenesis and degradation (Dorn, 2019). Disposal of damaged mitochondria is processed through the autophagic system responsible for the degradation of intracellular components and is consequently termed mitophagy (Kissová *et al.*, 2004; Youle *et al.*, 2012). Besides the neutralization of damaged cell parts, this also recycles the molecular components and adds them back to the cellular resource pool. The most common activator of autophagy is nutrient starvation, leading to an increase in ADP-to-ATP ratio. This activates a signaling cascade through the cellular energy sensor AMP-activated protein kinase (AMPK), which inhibits mammalian target of rapamycin (mTOR) activity, thereby reducing Unc-51 like autophagy activating kinase 1 (ULK1) phosphorylation and facilitating its release from the mTOR complex 1 (mTORC1) (J. W. Lee *et al.*, 2010; D. F. Egan *et al.*, 2011; J. Kim *et al.*, 2011; Shang *et al.*, 2011; Singh *et al.*, 2011). Additionally, ULK1 is activated by AMPK directly to favor its translocation to the site of autophagosome formation. (J. Kim *et al.*, 2011). The assembly of the autophagosome is a process involving at an initial central point Beclin 1. Beclin 1 activity leads to the activation of class III Phosphoinositide 3-kinase and the recruitment of an isolation membrane. Through action of various autophagy related proteins (ATGs) and microtubule-associated protein 1A/1B light chain 3B (LC3) – and its conversion from LC3-I to LC3-II – the autophagosome is formed. Finally, fusion with a lysosome gives rise to the autophagolysosome, where the degradation of cell components takes place (Mizushima *et al.*, 2008; Singh *et al.*, 2011). Interestingly, there is a strong correlation of increased autophagy and the prevalence of obesity and T2D (Kovsan *et al.*, 2011; Clemente-Postigo *et al.*, 2020). Further, targeted disruption of autophagy by deletion of ATG5 or ATG7 impairs adipogenesis in the WAT (Baerga *et al.*, 2009; Singh *et al.*, 2009; Zhang *et al.*, 2009; Goldman *et al.*, 2010). Therefore, severe and sustained damage can lead to breakdown of mitochondria, leading to the release of cytochrome c (CytC), a well-known inducer and marker of apoptosis. As mentioned above, this would also increase cytosolic, and presumably circulating, HSP60 levels, increasing inflammatory signaling. Ultimately, this can lead to a vicious self sustaining cycle of increasing mitochondrial dysfunction, inflammation, and insulin resistance.

1.11 Aim of this study

To date, it remains largely unknown how the various components of mitochondrial function and protein homeostasis act to promote or prevent mitochondrial dysfunction in obesity, or indeed if one necessarily causes the other. Central to mitochondrial function is the regulation of mitochondrial protein homeostasis which in turn impacts local as well as whole-body metabolism.

This thesis is aiming to understand the impact of a dysfunctional mitochondrial proteostasis on mammalian metabolism during diet-induced obesity.

To achieve this I used C57BL/6N Hsp60$^{+/-}$ mice as an *in vivo* model of altered mitochondrial proteostasis. The Hsp60$^{+/-}$ mouse bears a heterozygous deletion of the Hsp60 gene and consequently a comparable 50 % reduction in protein levels, and thus serves as a model of a preexisting disturbance of mitochondrial protein homeostasis as it is found in diet-induced obesity and diabetes. Both NCD and HFD feeding regimes in conjunction with an extensive metabolic phenotyping were used to decipher a possible gene-nutrient interaction and its effects on DIO.

Following, probable target tissues that are found at the intersection of mitochondrial function and whole-body metabolism, such as adipose tissue, skeletal muscle and the hypothalamus, were further analyzed on a molecular level. Further, depending on the tissues most affected, a suitable *in vitro* cell culture system was chosen, and a knockdown of HSP60 achieved *via* infection with lentiviral particles targeting HSP60.

Material and Methods

2.1 Figures and statistics

Graphical representations of concepts in the introduction as well as the proposed model were created by me in Inkscape V1.01 by using modified templates from Servier Medical Art (licensed under a Creative Commons Attribution 3.0 Unported License). The structure of the HSP10/60 chaperonine complex was visualized with the online tool Mol* from the Research Collaboratory for Structural Bioinformatics Protein Data Bank (RCSB PDB, Sehnal *et al.*, 2018) using the PDB ID 4PJ1 based on the findings of Nisemblat and colleagues (Nisemblat *et al.*, 2015).

If not stated otherwise, visual representation of data as well as statistical analysis in the results was done using GraphPad Prism 9.

2.2 Cell culture

In vitro experiments presented in this work were performed with the well described murine fibroblast cell line 3T3-L1 (Green *et al.*, 1975). These cells are capable of adipogenic differentiation, yielding mature adipocytes. Cells were cultivated at 37 °C and 5 % CO_2 in Dulbecco's Modified Eagle Medium (DMEM) GlutaMAX^{TM} (Gibco) supplemented with 10 % fetal bovine serum (FBS), 1 mM sodium pyruvate and 1 % Penicillin/Streptomycin (P/S). 3T3-L1 culture maintenance and/or seeding on smaller well plates for experiments was carried out as follows:

1. Grow cells on a 10 cm plastic dish to 90 % confluency.
2. Aspirate media and add 10 mL 1x PBS to wash cells, aspirate PBS
3. Incubate with trypsin to detach cells from culture dish for 5 minutes at 37 °C
4. Add 10 mL DMEM, completely detach cells and transfer to 15 mL plastic tube

5. Centrifuge for 3 minutes at 1200 RPM and room temperature (RT)
6. Aspirate supernatant
7. Re-suspend cell pellet carefully in 10 mL fresh DMEM
8. For seeding on multiwell plates, otherwise continue with 9.:
   (a) transfer 10 μL of cell suspension onto a Neubauer Improved counting chamber
   (b) Count cells in 4 individual 4 by 4 squares under a microscope
   (c) Calculate cell number as $\frac{Total\ cell\ count}{4}\ x\ 10.000$, which gives cell number per mL
   (d) Calculate appropriate volume for the given experiment and dish size and add to multi well dish
   (e) Incubating as experimental procedure dictates
9. In a new dish, add 1 mL re-suspended cells to 9 mL fresh DMEM
10. Incubate at 37 °C and 5 % CO_2

2.2.1 Lentiviral infection for siRNA mediated knockdown of HSP60

The lentiviral infection is a well established method for stable integration of small interfering RNA sequences into the genome of target cells. Lentivirae are a genus of retroviruses and as such are able to integrate their genetic material into the host genome. For this work, 3T3-L1 cells were infected using lentiviral transduction particles with pLKO.1 plasmid containing shRNA targeting either the murine *Hspd1* gene (HSPD1 MISSION shRNA Lentiviral Transduction Particles, SHCLNV NM010477, Merck KG; Hsp60KD) or control transduction particles targeting no known mammalian genes (MISSION pLKO.1-puro Non-Mammalian shRNA Control Transduction Particles, SHC902V, Merck KG; NT ctrl) according to manufacturer's instructions. Further, 12 μg/mL hexadimethrine bromide (polybrene) was added for incubation overnight. The following day, the media was changed to fresh DMEM. After an additional 6 hours, 5 μg/mL of puromycin was added to the media for antibiotic selection of infected cells. Selection continued for at least one week. Knock down was confirmed *via* qPCR.

2.2.2 *In vitro* adipogenic differentiation

In vitro adipogenic differentiation was performed as described in Zebisch *et al.*, 2012. After reaching a state of growth arrest, 3T3-L1 cells can be readily differentiated into mature

adipocytes by the addition of pro-differentiative agents insulin, dexamethasone, 3-isobutyl-1-methylxanthine (IBMX) and Rosiglitazone. The differentiation was carried out as follows:

1. Grow cells in DMEM 10 % FBS, 1mM sodium pyruvate, 1 % P/S let reach confluency and incubate for an additional 24 h
2. Change media to induction media (table 2.1)
3. Let cells incubate for 72 h
4. Change media to differentiation media (table 2.2)
5. Change media every 48 h to fresh differentiation media
6. Commence differentiation for 8 days

Using this protocol, first lipid droplets are visible after around 4 days of differentiation. After 8 days, successful differentiation was confirmed visually, as well as with an Oil Red O stain, performed as follows:

1. Carefully wash differentiated adipocytes with PBS
2. Fix cells for 20 minutes with 4 % formaldehyde
3. Wash once with PBS
4. Stain 30 minutes with Oil red O (0.3 % 60 % Isopropanol)
5. Wash 4 times with H_2O
6. Air-dry for $\sim$ 30 minutes
7. Lyse stained cells in DMSO and 5 minutes shaking
8. Transfer 100 μL per sample on a 96-well plate
9. Measure absorbance at 520 nM on a microplate reader

Table 2.1: Adipogenic induction media

Compound	Concentration
FBS	10 %
Sodium pyruvate	1 mM
Penicillin/Streptomycin	1 %
Insulin	100 nM
Dexamethasone	0.25 μM
IBMX	0.5 mM
Rosiglitazone	2 μM

Table 2.2: Adipogenic differentiation media

Compound	Concentration
FBS	10 %
Sodium pyruvate	1 mM
Penicillin/Streptomycin	1 %
Insulin	100 nM

2.2.3 Neutral Red assay

The compound Neutral Red (3-Amino-7-dimethylamino-2-methylphenazine hydrochloride) is used in cell viability assays first described in 1985 (Borenfreund *et al.*, 1985). Neutral Red incorporates into active lysosomes (Winckler, 1974). Thus, it was used here as a proxy for lysosomal activity as increased cellular lysosomal activity would likely correspond with an increased lysosome number and therefore increased Neutral Red incorporation. The Neutral Red assay for this purpose was carried out as follows:

1. Seed 50.000 cells/well in a 96-well plate and incubate over night at 37 °C and 5 % CO_2 in 200 μL DMEM 10 % FBS
2. Wash cells with PBS and add 100 μL Neutral Red medium per well (final concentration of Neutral Red 40 μg/mL in DMEM 10 % FBS) and incubate for 2 h at 37 °C and 5 % CO_2
3. Decant the media and wash with 150 μL of PBS
4. Add 150 μL lysis solution per well (1 % acetic acid in 50 % ethanol) and lyse cells for 10 minutes and vigorous shaking
5. Transfer 100 μL of lysate to a fresh 96-well microplate and measure Neutral Red absorption at 540 nm or fluorescence at 630 nm after excitation at 530 nm

2.2.4 MTT assay

The tetrazolium dye MTT (3-(4,5-dimethylthiazol-2-yl)-2,5-diphenyltetrazolium bromide) is used in a colorimetric cell viability assay (Mosmann, 1983). MTT is reduced by NAD(P)H-dependent cellular oxidoreductases to the purple colored formazan (Berridge *et al.*, 1993). The assay was carried out as follows:

1. Seed 50.000 cells/well in a 96-well plate and incubate over night at 37 °C and 5 % CO_2 in 200 μL DMEM 10 % FBS
2. Add 20 μL MTT solution (5 mg/mL in PBS, freshly prepared), incubate on a rotary shaker at 150 rpm for 5 minutes
3. Incubate for 3 h at 37 °C and 5 % CO_2
4. Decant the media
5. Lyse cells in 200 μL DMSO for 5 minutes and vigorous shaking
6. Read absorption at 560 nM

2.3 Animal studies

2.3.1 Animal husbandry

C57BL/6N Ctrl and Hsp60$^{+/-}$ mice were bred in-house and housed in mixed genotype groups in a temperature-controlled room (22 ± 1 °C) on a 12-hour light/12-hour dark cycle with free access to food and water. Mice were kept on the experimental diets for 16 weeks starting at 4 weeks of age. For the HFD (60 % of calories from fat, ssniff Spezialdiäten GmbH, Germany), the HFD was slowly added to the NCD over the course of 2 weeks to allow adaptation to the new diet. Euthanasia and organ sampling was carried out at 20 weeks of age.

2.3.2 Genotyping Polymerase Chain Reaction (PCR)

The Hsp60$^{+/-}$ mice have only one functioning *Hspd1* gene. This has been achieved by an inactivating insertion using a gene-trap approach (Christensen *et al.*, 2010). For confirmation of the genotypes and subsequent assigning to the experimental groups, a genotyping PCR targeted at the sequence of the *Hspd1* gene was performed using reagents from Promega (table 2.3, 2.4 and 2.5). The expected PCR products have sizes for the wildtype alelle of 497 base pairs, and for the trapped allele of 416 base pairs. Thus, control mice show one band on a resulting agarose gel, whereas heterozygous mice show two (Fig. 2.1). Mouse tail genomic DNA was purified with an isopropanol-ethanol precipitation as follows:

1. Digestion of a $\sim$ 5 mm tail biopsy in 100 μL lysis buffer (10 mM Tris-HCl (pH 8.0), 10 mM EDTA, 150 mM NaCl, 0.2 % SDS) at 56 °C over night
2. Add 100 μL isopropanol and centrifuge for 10 minutes at maximum speed

3. Decant the supernatant and resolubilize the pellet in 70 % ethanol, centrifuge for 10 minutes at maximum speed
4. Decant the supernatant and dry the pellet
5. Resolubilize the pellet in TE buffer (10 mM Tris pH 8.0, 1 mM EDTA)

Table 2.3: Genotyping PCR primers

Primer name	5' to 3' sequence
Hsp60 P1	TAAGACAGCATTTCTCCGGTAG
Hsp60 P2	CTGAGTGTTGGGATTATGCAG
Hsp60 P3	GCCAGTCCTCCGATTGAC

Table 2.4: Components for the genotyping PCR, 25 μL total reaction volume

Component	final concentration
5X GoTaq® Green buffer	1X
dNTPs	200 μM
$MgCl_2$	3 mM
Primer P1	1 μM
Primer P2	1 μM
Primer P3	1 μM
GoTaq® G2 DNA polymerase	1.25 U
Purified DNA	2 μL
H_2O	to 25 μL

Table 2.5: Genotyping PCR protocol

Step	Temperature [°C]	Time [seconds]	Cycles
Initial denaturation	95	120	1
Denaturation	95	30	40
Annealing	54	30	
Elongation	72	30	
Final Elongation	72	60	1

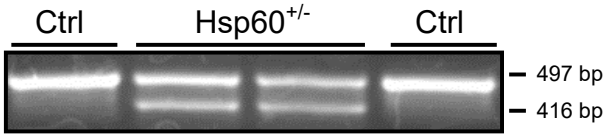

Figure 2.1: PCR genotyping C57BL/6N Ctrl and Hsp60$^{+/-}$ mice.
Representative picture of genotyping PCR products separated on a 2 % agarose gel and visualized with ethidium bromide.

2.3.3 Measurement of basic metabolic parameters

Body weight of mice was measured daily for the first week to assess tolerance of the experimental diet, and then weekly to monitor weight gain. Blood was taken out of the tail vein at 4 weeks of age as a baseline, and for fasted values at the 0 minute timepoint during the oGTT.

2.3.4 Intraperitoneal insulin tolerance test (ITT)

For measurements of insulin tolerance an ipITT was performed. Mice were single-caged just prior to the experiment, with free access to water. Animals were then injected intraperitoneally with 0,75 U insulin per kilogram body weight, and blood sugar was measured at 15, 30, and 60 minutes.

2.3.5 Oral glucose tolerance test (oGTT)

For measurements of glucose tolerance an oGTT was performed. Mice were single caged and deprived of food 16 hours prior to the experiment, with free access to water. Animals were then given 2 g glucose per gram body weight *via* oral gavage, and blood samples were taken from the tail vein at 2, 15, 30, 60. 90, and 120 minutes.

2.3.6 Intraperitoneal pyruvate tolerance test (PTT)

For measurements of pyruvate tolerance as an approximation of hepatic gluconeogenesis an ipPTT was performed. Mice were single caged and deprived of food 16 hours prior to the experiment, with free access to water. Animals were then injected intraperitoneally with 2 g pyruvate per kilogram body weight, and blood sugar was measured at 15, 30, and 60 minutes.

2.3.7 Body composition measurement *via* Nuclear Magnetic Resonance

With the help of nuclear magnetic resonance (NMR), body composition can be determined by observing and measuring the interaction of hydrogen proton spins when placed in a powerful magnetic field. Due to composition differences of fat and lean tissues, their respective proportion can be inferred. In this work, the EchoMRI (EchoMRI LLC, USA) was used.

2.3.8 Indirect calorimetry

For measurement of energy expenditure and respiratory quotient the PhenoMaster indirect calorimetry system (TSE Systems GmbH, Germany) was used. Mice were caged individually and the gas composition of outflowing from each cage was analyzed.

2.3.9 Determination of fecal energy content and body temperature

Mice were individually caged for 48 hours with free access to food and water. The cages were lined with a double layer of 3 mm Whatman filter paper to allow efficient sample collection. Twice daily body temperature was measured and feces collected. Fecal energy content was measured using bomb calorimetry (IKA C5003; IKA Werke, Staufen, Germany). First, fecal samples were freeze-dried and around 1 g total dried sample was pressed into a pellet. The pellet was completely combusted in the bomb calorimeter. The processing of frozen and dried feces as well as the caloric bomb measurement was performed by Ms. Carola Gehrmann (Max Rubner Laboratorium (MRL)) of the German Institute of Human Nutrition (DIfE).

2.3.10 *Vena cava* insulin injection

To assess local insulin sensitivity in DIO, mice were kept on HFD for 16 weeks. Under deep anesthesia, the abdominal cavity was opened and the *vena cava* located. Then, saline as control substance or 5 U of insulin were injected directly into the *vena cava*. Organs were harvested after the time points in parentheses: Liver (2 minutes), quadriceps (5 minutes), gonadal and subcutaneous WAT (5 minutes), brown adipose tissue (10 minutes), and brain (10 minutes). As a read out for insulin sensitivity, protein samples from these organs were

probed for Akt_{S473} phosphorylation in a Western Blot (2.5.3). The insulin injection was performed by Ms. Michaela Rath (now Molecular and Experimental Nutritional Medicine (MEM) at the University of Potsdam).

2.3.11 Ovariectomy of female mice

To analyze the potential effect of the female sex hormone estrogen, mice were ovariectomized at 4 weeks of age under anesthesia by dorsal incision and subsequent cauterization of the ovaries (OVX group). For non-ovariectomized controls, the ovaries were exposed, but not damaged (Sham group). The dorsal cuts were stitched and the mice kept on analgesic food for 3 consecutive days.

2.3.12 Isolation of stromal vascular fraction (SVF)

Mice were kept on the HFD for 16 weeks, anesthetized, and killed *via* cervical dislocation. Then, the gonadal WAT was surgically removed, finely minced with sterile scissors in Hank's buffered salt solution (HBSS, table 2.6), and treated as follows:

1. Tissue digestion in 2 mg/mL collagenase II solution for 60 minutes at 37 °C and gentle agitation
2. Add 1 mL of FBS
3. Centrifuge at 1200 rpm for 10 minutes
4. Aspirate the supernatant (the supernatant contains mature adipocytes, keep them for further analysis)
5. Resuspend pellets in 10 mL of 2 % FBS-HBSS and filter through a 100 μm cell strainer into a fresh 50 mL tube
6. Wash old tube with another 10 mL of 2 % FBS-HBSS and filter through the same cell strainer
7. Centrifuge at 1200 rpm for 7 minutes
8. Completely remove supernatant and re-suspend pellets in 2 mL ACK lysis buffer (2.7), incubate on ice for 3 minutes
9. Dilute ACK by adding 20 mL 2 % FBS-HBSS, filter through 40 μm cell strainer into a new tube, and wash tube and strainer with an additional 10 mL 2 % FBS-HBSS
10. Centrifuge at 1200 rpm for 7 minutes

11. Resuspend pellet in appropriate volume of DMEM/F12 growth media (10 % FBS and 1 % P/S)
12. Count and seed onto plates at a density of $2.5\ x\ 10^4\ \frac{cells}{cm^2}$

Induction of adipogenic differentiation was carried out as described above (2.2.2).

Table 2.6: Hank's buffered salt solution (HBSS)

Compound	Concentration [mM]
Sodium chloride (NaCl)	140
Potassium chloride (KCl)	5
Calcium chloride ($CaCl_2$)	1
Magnesium sulphate ($MgSO_4$)	0.4
Magnesium chloride ($MgCl_2$)	0.5
Disodium phosphate (Na_2HPO_4)	0.3
Monopotassium phosphate (KH_2PO_4)	0.4
Sodium bicarbonate ($NaHCO_3$)	4
Glucose	6

Table 2.7: ACK lysis buffer

Compound	Concentration [mM]
Ammonium chloride (NH_4Cl)	150
Potassium bicarbonate ($KHCO_3$)	10
Ethylenediaminetetraacetic acid(EDTA)	0.01

2.3.13 *Ex vivo* radioactive glucose uptake assay

2-Deoxy-d-glucose (DOG) can be taken up *via* glucose transporters present in adipocytes. However, due to the replacement of the 2-hydroxyl group with hydrogen it cannot undergo conversion to glucose-6-phosphate by glucose-6-phosphate isomerase during glycolysis (Wick *et al.*, 1957). Thus, it accumulates inside the cells. By labeling DOG with the radioactive carbon isotope ^{14}C, the amount of accumulated ^{14}C-DOG can be measured using liquid scintillation counting. Here, radioactive decay of the ^{14}C releases beta particles, that transfer energy to solvent molecules in the scintillation liquid. This energy in turn is transferred to the primary phosphor that emits light after absorption of energy. Therefore, the

amount of ^{14}C-DOG present in a sample is directly proportional to the emitted light. For the assay used during this work, mice were kept on the HFD for 16 weeks, anesthetized, and killed *via* cervical dislocation. Then, the gonadal WAT was surgically removed and the following steps were carried out:

1. Cut and weigh replicates of WAT tissue and place in 37 °C Krebs-Ringer-HEPES(KRH)-0.2 % BSA (table 2.8) in a 24-well plate
2. Wash tissue 2x with KRH-0.2 % BSA
3. Incubate 45 min at 37 °C in KRH-1 % BSA and additives
    - Basal: KRH-1 % BSA
    - Insulin: KRH-1 % BSA + 250 nM Insulin
    - Cytochalasin B: KRH-1 % BSA + 10 μM Cytochalasin B
4. Incubate 10 min with KRH-1 % BSA + 2 mM ^{14}C-DOG
5. Place plates on ice and wash 3x with ice-cold KRH-0.2 % BSA
6. Transfer the tissue piece into a scintillation vial containing 9 mL Scintillation Cocktail; additionally, prepare 2 standard vials with 9 mL Scintillation Cocktail and 5 μL 2 mM 14C 2-Deoxy-D-glucose as well as 2 vials with 9 mL Scintillation Cocktail as blanks
7. Shake vials for 2 h
8. Put vials in β-counter to measure signal from accumulated ^{14}C-DOG

Table 2.8: Krebs-Ringer-Hepes buffer (add either 0.2 or 1 % BSA)

Component	Concentration [mM]
Sodium chloride (NaCl)	136
Potassium chloride (KCl)	4.7
Magnesium sulphate ($MgSO_4$)	1.25
Calcium chloride ($CaCl_2$)	1.25
Hepes	10

2.3.14 *Ex vivo* mitochondrial activity measurement with the Agilent Seahorse Flux Analyzer

The Agilent Seahorse Flux Analyzer measures the oxygen consumption rate in presence of glucose and pyruvate as substrates. Additionally, various agents are serially injected to inhibit or engage different components of the electron transport chain (ETC). Here, Oligomycin (solution A) inhibits complex V (ATP synthase) to inhibit ATP generation. Carbonyl cyanide-4-(trifluoromethoxy)phenylhydrazone (FCCP, solution B) uncouples oxygen consumption from ATP production. Finally, a mix of Rotenone and Antimycin A inhibit complex I and III, respectively. By measuring the oxygen consumption over time during these treatments it is possible to calculate basal and maximal respiration, ATP production, proton leak, and spare capacity. One day prior to the assay, the Seahorse cartridge was hydrated by filling the utility plate with sterile H_2O and incubation at 37 °C in a CO_2-free incubator. To asses mitochondrial function in the gWAT during this work mice were kept on the HFD for 16 weeks, anesthetized, and killed *via* cervical dislocation. Then, the gonadal WAT was surgically removed. On the assay day, all compounds and injection media were freshly prepared and kept at 37 °C. The proprietary Agilent Seahorse media was supplemented with 10 mM D-Glucose, 2 mM L-Glutamine, and 1 mM pyruvate to yield the assay medium. For the assay itself, the following steps were carried out:

1. Cut and weigh replicates of gWAT tissue and place in 37 °C PBS in a 24-well Seahorse islet measure plate
2. Cover tissue pieces with capture screens
3. Incubate microplate at 37 °C in a CO_2-free incubator
4. Replace the water in the utility plate with Seahorse Calibrant solution
5. Load the hydrated cartridge with the compounds
    - Solution A: 2 μM Oligomycin in assay medium
    - Solution B: 1 μM FCCP in assay medium
    - Solution A: 1 μM Rotenone and 2 μM Antimycin A in assay medium
6. Place loaded cartridge into the Agilent Seahorse Flux Analyzer to perform plate calibration
7. Replace utility plate with the islet measure plate
8. Start assay

2.3.15 Analytics of blood and plasma metabolites

Blood glucose was measured with a Glucometer – Contour XT (Bayer, Leverkusen, Germany). Plasma Insulin and Adiponectin were measured with ELISAs from Alpco (Alpco Salem, BioCatGmbH, Switzerland). Plasma HSP60 was measured with an ELISA from Elabscience (Elabscience Inc., USA. Leptin was measured using an ELISA from R & D Systems (R & D Systems/ Bio-Techne GmbH, Germany), Plasma Glucagon levels with an ELISA from Yanaihara (Yanaihara Institute Inc., Awakura, Japan). All ELISAs were performed according to manufacturer's guidelines. Triacylglycerols were measured with Triglyceride Reagent from ABX and NEFA were measured with the NEFA-HR assay according to manufacturer's guidelines (FUJIFILM Wako Chemicals Europe GmbH, Germany). All ELISAs were performed by Ms. Katrin Ritter (now in the junior research group Neurocircuit Development and Function (NDF), DIfE).

2.3.16 Immunohistochemistry

To determine tissue morphology, an immunohistochemistry approach was used. Here, tissues were taken as in 2.3.1 and tissues submerged in a 4 % formaldehyde solution for 24 hours. After washing with PBS, the tissues were embedded in paraffin. After fixation, tissue sections can be cut and stained with compounds dying specific organelles. Tissue embedding and cutting was performed by Ms. Elisabeth Meyer (Max Rubner Laboratorium (MRL)) of the German Institute of Human Nutrition (DIfE). Then, tissue sections were stained with hematoxylin and eosin to visualize nuclei and the cytoplasm, respectively. Pictures were taken with a Zeiss light microscope. Counting and calculation of adipocyte area was done semi-automatically using a macro written for ImageJ Fiji, version 1.53c (see Appendix B).

2.4 Gene expression analysis using quantitative real-time PCR

The quantitative real-time polymerase chain reaction (qPCR) is a commonly used technique to determine the amount of a given RNA transcript within a sample and consists of the three steps RNA isolation, cDNA synthesis, and the qPCR itself. In theory, all mRNA present at the point of cell or tissue extraction is reverse transcribed into cDNA in a one-to-one manner. Therefore, the higher a gene was expressed, the higher the corresponding mRNA levels and cDNA of that transcript, and therefore ultimately the signal in the qPCR will be higher as well.

With this it is possible to assess the differences in expression of genes in regard to external stimuli, such as different diets in mice.

2.4.1 RNA isolation

During this work, two methods were used to extract RNA, depending on the type of sample. For cells out of cell culture experiments, a guanidinium thiocyanate-phenol-chloroform extraction was performed (with QIAzol reagent, Qiagen, Germany), whereas for animal tissue samples, RNA was extracted using a commercial column affinity based kit was used (RNeasy Mini Kit, Qiagen).

The QIAzol/chloroform extraction method employs different solubilities of cellular components in organic and aqueous solutions as well as their separations due to different densities of these solutions (Chomczynski *et al.*, 1987). After mixing a given aqueous solution (*i.e.* the cytosol) with an acidic phenol/chloroform solution and subsequent centrifugation three distinct layers will have formed. The lower organic phase containing precipitated DNA as well as lipids, the interphase containing the proteins, and an upper aqueous phase containing the RNA. The upper phase can then be subjected to a isopropanol/ethanol precipitation of RNA. Here, the combination of high concentrations of positive ions as well as the lower dielectric constant of ethanol as opposed to water (24.3 vs. 80.1) results in precipitation of nucleic acids, in this case the RNA. These can be pelleted by centrifugation and resolubilized in water. The following steps were performed to extract RNA using the phenol/chlorofrom extraction after any given cell culture experiment:

1. Add QIAzol reagent to the well (250 μL for 12 well)
2. Transfer QIAzol lysate to a microcentrifuge tube
3. Incubate for 5 minutes at RT
4. Add 100 μL of chloroform, and mix well by vortexing
5. Incubate for 2 minutes at RT
6. Centrifuge for 15 minutes at 10000 RCF and 4 °C
7. Carefully pipet the upper aqueous phase into a new tube containing 300 μL isopropanol
8. Incubate for 10 minutes at RT
9. Centrifuge for 10 minutes at 10000 RCF and 4 °C
10. Decant the supernatant

11. Resolubilize the pellet in 500 μL of 75 % ethanol (4 °C)
12. Centrifuge for 5 minutes at 10000 RCF and 4 °C
13. Decant the supernatant and air-dry the pellet for 30 - 60 minutes at RT
14. Resolubilize the dried pellet in 25 μL RNAse-free water
15. Incubate for 10 minutes at 55 °C
16. Measure RNA content using a photometric assay (NanoDrop)

RNA extraction from animal tissue was performed with the RNAeasy Mini Kit (Qiagen) or ReliaPrep RNA Tissue Miniprep System (Promega) according to manufacturer's instructions, including DNAse I treatment.

2.4.2 cDNA synthesis

Preparation of a library of complementary DNA (cDNA) is the prerequisite to perform a qPCR. Here, RNA is reverse transcribed by a reverse transcriptase in a regular PCR reaction (table 2.9). With the use of random hexameric primers, which bind random parts of the RNA in solution, and oligo(dT)15 primers, which bind the poly(A) tail of mRNA, an efficient reverse transcription of the mRNA present is achieved.

The cDNA synthesis was performed with reagents from the Moloney Murine Leukemia Virus Reverse Transcriptase (M-MLV RT) Kit from Promega as follows:

1. Between 250-1000 ng RNA is added to a RNAse-free plastic tube
2. Add RNAse-free water up to 13 μL total volume
3. Add 1 μL of a pre-made 1:1 mix of random hexameric primers and Oligo(dT)15 primers
4. Incubate at 70 °C for 5 minutes
5. Incubate on ice for 5 minutes
6. Add 4 μL 5X M-MLV reaction buffer, 1 μL of 40 nM dNTP mix, and 1 μL M-MLV reverse transcriptase per reaction
7. Run the cDNA synthesis PCR protocol (table 2.9)
8. Dilute the cDNA to 5 ng/μL

Table 2.9: cDNA synthesis PCR protocol

Step	Temperature [°C]	Time [minutes]
Annealing	25	5
DNA polymerization	42	60
Inactivation	70	15

2.4.3 qPCR

To assess the amount of a given transcript within a cDNA library gene-specific primers are used to amplify this transcript as is the case in a regular PCR. However, during each amplification cycle, a DNA intercalating dye (SYBRgreen, Promega) gives a fluorescent signal if it was incorporated into double-stranded DNA. The cycle at which the earliest signal for a target gene is detected is the so-called Threshold Cycle (C_t) value. Thus, the earlier a fluorescent signal is detected in a sample, the more cDNA of that specific gene was present in the original sample. Due to the exponential nature of the PCR, a C_t difference of one indicates a two-fold expression difference. Further, by comparing this value to value of an internal control gene, called the housekeeping gene, one can quantify the expression rate of the target gene. The housekeeping gene used throughout this work was the TATA-Box binding protein (*Tbp*). Table 2.11 lists the gene-specific primers used during this work.

The qPCR was performed with GoTaq® qPCR Master Mix from Promega as follows:

1. Add 2 μL (10 ng) cDNA in duplicate per target on a 384-well qPCR plate
2. Add of 8 μL SYBRgreen Master Mix containing 0.25 μmol gene-specific primers
3. Seal the microwell plate with adhesive plastic
4. Centrifuge for 1 minute at 1200 RCF
5. Run the qPCR protocol (table 2.10)

Table 2.10: Real-Time qPCR protocol

Step	Temperature [°C]	Time [seconds]	Cycles
Polymerase activation	95	60	1
Denaturation	95	15	40
Annealing and extension	60	60	

To calculate expression rates, the $2^{-\Delta\Delta C_t}$ method was used. Here, first the C_t value of the housekeeping gene is subtracted from the C_t of the target gene, yielding the ΔC_t. Next,

the mean ΔC_t value of the control group is subtracted from each individual ΔC_t to arrive at the $\Delta\Delta C_t$ for each sample. Since all values are in logarithm base 2, to arrive at the fold increase, the $2^{-\Delta\Delta C_t}$ is calculated. Finally, expression values are expressed as a percent value of the control group (% of ctrl).

Table 2.11: Primer pairs used for qPCR

Target gene	forward sequence	reverse sequence
Tbp (TATA-binding-protein)	CTGGAATTGT ACCGCAGCTT	ATGATGACTG CAGCAAATCG
Acadl (Acyl-CoA dehydrogenase, long chain)	GGTGGAAAAC GGAATGAAAGG	GGCAATCGGA CATCTTCAAAG
Acadm (Acyl-CoA dehydrogenase, medium chain)	TGTTAATCGG TGAAGGAGCAG	CTATCCAGGG CATACTTCGTG
Acads (Acyl-CoA dehydrogenase, small chain)	CCTGGGATGG GCTTCAAAATAG	GGTTCTCGGC ATACTTCACAG
Adrb3 (Beta-3 adrenergic receptor)	TGAAACAGCA GACAGGGACA	GGTTCTCGGC ATACTTCACAG
Ap2 (Adipocyte protein 2)	AAGGTGAAGA GCATCATAACCCT	GGCGTCCTGT CTTGACACTC
Atf4 (Activating transcription factor 4)	CCTGAACAGC GAAGTGTTGG	TGGAGAACCC ATGAGGTTTCAA
Cidea (Cell death activator CIDE-A)	TGCTCTTCTG TATCGCCCAGT	GCCGTGTTAA GGAATCTGCTG
Chop (C/EBP homologous protein)	CTGCCTTTCA CCTTGGAGAC	CGTTTCCTGG GGATGAGATA
Dio2 (Deiodinase 2)	TTTGATGTGT CAGGAGTCGGG	CCAACATTCC CTACCCCAAGA
Fasn (Fatty acid synthase)	GAGGACACTC AAGTGGCTGA	GTGAGGTTGC TGTCGTCTGT
Glut1 (Solute carrier family 2, facilitated glucose transporter member 1)	GATTGGTTCC TTCTCTGTCGG	CCCAGGATCA GCATCTCAAAG
Glut2 (Solute carrier family 2, facilitated glucose transporter member 2)	GTCACTATGC TCTGGTCTCTG	CAAGAGGGCT GACCCATAGC
Glut3 (Solute carrier family 2, facilitated glucose transporter member 3)	CGCTTCTCAT CTCCATTGTCC	TGAAGATAGT ATTGACCACGCC
Glut4 (Solute carrier family 2, facilitated glucose transporter member 4)	CATTCCCTGG TTCATTGTGG	GAAGACGTAA GGACCCATAGC

Table 2.11: Primer pairs used for qPCR (continued)

Target gene	Forward sequence	Reverse sequence
Glut8 (Solute carrier family 2, facilitated glucose transporter member 8)	CCCTTCGTGA CTGGCTTTG	TGGGTAGGCG ATTTCCGAGAT
Hsp60 (heatshock protein 60)		
Pat2 (Proton-coupled amino acid transporter 2)	GTGCCAAGA AGCTGCAGAG	TGTTGCCTTT GACCAGATGA
P2RX5 (P2X purinoceptor)	CCTTCCCAGA AAGGAAAAGG	CAGGAGTCAA CAGGATGCAA
PPARγ (Peroxisome proliferator activated receptor gamma)	CCCAGAGCAT GGTGCCTTCGC	AGTTGGTGGG CCAGAATGGCA
Scd1 (Stearoyl-CoA desaturase-1)	CTGACCTGAA AGCCGAGAAG	AGAAGGTGCT AACGAACAGG
Socs3 (Suppressor of cytokine signaling 3)	CCTATGAGAA AGTGACCCAGC	TTTGTGCTTG TGCCATGTG
Ucp1 (Uncoupling protein 1)	GGCCTCTACG ACTCAGTCCA	TAAGCCGGCT GAGATCTTGT

2.5 Protein expression analysis using SDS-PAGE and Western Blot

There are a multitude of regulatory mechanisms between mRNA transcription (as assessed via qPCR) and physiological function of a resulting protein. The mRNA could get degraded before translation, and the translation rate itself can be subject to regulation. Further, newly synthesized protein chains need to be folded correctly to reach their functional conformation. Finally, differential post-translational modifications, such as phosphorylations, glycosylations, acetylations, or palmitoylation, can modify a proteins activity. Thus, it is important to investigate potential physiological changes on a protein level, as well as the phosphorylation status of key proteins in signaling pathways, as an indication of their activity. To assess the expression patterns or phosphorylation status of proteins in a sample, it is necessary to separate the complex protein mixture and then visualize the expression pattern or phosphorylation status of a specific protein of interest. To achieve this, a combination of two electrophoretic methods, SDS-PAGE (sodium dodecyl sulphate-polyacrylamide gel

electrophoresis 2.5.2) and Western Blotting (2.5.3), is used. Afterwards, primary antibodies specific to the protein of interest are applied. These in turn can be bound to a secondary antibody conjugated to the horse radish peroxidase (HRP), which catalalyzes an enzymatic chemiluminescence reaction, ultimately visualizing protein expression or phosphorylation status, respectively. In the chemiliuminescent reaction the HRP uses H_2O_2 to oxidize luminol to an excited intermediate form, 3-aminophtalate. This intermediate spontaneously falls back to a lower energy state and thereby releases energy in the form of visible light. Thus, the amount of detected light is directly proportional to the oxidation reactions caused by HRP bound to the target proteins. This allows for qualitative an quantitative comparisons of protein expressions between samples on a Western Blot.

2.5.1 Protein isolation

Proteins from cultured cells or animal tissue were isolated using RIPA buffer with protease and phosphatase inhibitors (Merck #4693116001 and #4906837001, table 2.12), combined with a mechanical shearing of cells with a manual potter as follows. All steps are carried out on ice. Cell culture plates are washed twice with ice-cold PBS before addition of RIPA lysis buffer. Animal tissues are first homogenized using liquid nitrogen-cooled stainless steel mortar and pestle.

1. Addition of RIPA lysis buffer to cultured cells or frozen tissue
   (a) for cultured cells: 50 μL for 12-well, 100 μL for 6-well plates
   (b) for tissue: weigh 20-50 mg homogenized tissue, depending on the tissue type
2. Mechanical shearing of samples with the handpotter
3. Incubation on ice for 30 minutes
4. Centrifugation at 21.000 RCF and 4 °C for 45 minutes
5. In case of adipose tissue, a relatively firm layer of lipids will form above the supernatant, which can be pushed to the side with a pipette tip
6. Transfer of the supernatant containing the proteins to a fresh microcentrifuge tube, taking care not to transfer any lipids

Isolated proteins were then quantified with a colorimetric assay using the Pierce^{TM} 660 nm Protein-Assay (ThermoFisher Scientific, Germany). This reagent employs a proprietary

Table 2.12: RIPA protein isolation buffer (10 mL)

Component	Concentration
Tris-HCl	50 mM
NaCl	150 mM
EDTA	1 mM
Na-deoxycholate	0.25 %
Triton X-100	1 %
Complete protease inhibitor	1 tablet
PhosSTOP	1 tablet

solution that changes its color upon protein binding. The intensity of the color change is directly proportional to the amount of protein present in a sample and can be measured with a photometer at an absorbance wavelength of 660 nm. By using a standard curve method, protein concentrations can be calculated. Therefore, 1 μL of each sample was added on a 96-well clear microplate. Additionally, 1 μL of defined solutions containing bovine albumin serum protein (BSA) was added in triplicate to generate a standard curve. After adding 150 μL of Pierce reagent and incubation for 5 minutes, the absorbance was measured at 660 nm. From the values of the standard solution a standard curve was generated and the protein concentrations of the samples calculated. For further applications, a sample volume containing 15 μg protein is mixed with a Laemmli loading buffer (table 2.13) and denatured for 5 minutes at 95 °C.

Table 2.13: Laemmli loading buffer

Component	Concentration
Glycerol	20 %
SDS	8 %
EDTA	10 mM
Tris	250 mM
Bromophenol blue	0.1 %
β-mercaptoethanol	10 %

2.5.2 SDS-PAGE

The SDS-PAGE is a widely used method to separate complex protein mixtures and was first published in its current form in 1970 by Ulrich Laemmli (Laemmli, 1970). Biochemically, SDS binds to hydrophobic amino acid side chains of denatured (*i.e.* linearized) proteins. By binding all along the protein, SDS masks the intrinsic charge of a protein, making the overall charge of the SDS-protein complex negativ. Thus, the remaining differentiating characteristic of these complexes is their amino acid chain length, and therefore their mass. This allows subsequent protein separation by mass by applying an electrical current through a gel matrix. From the primary protein structure (amino acid sequence) a theoretical migration size in the gel can be predicted, *i.e* a size corresponding to a certain running distance in the gel. It is of note however, that for special cases this can be misleading. For example, proteins rich in hydrophobic amino acids (as is the case for *e.g.* large multi-membrane spanning proteins) bind proportionally more SDS relative to their predicted size, letting them run differently than expected in a gel. Additionally, post-translational modifications, such as glycosylations, can add weight to a protein, affecting its migration behavior. The polyacrylamide gel is freshly cast at a final acrylamide concentration of 8-15 % , depending on the size range desired for a certain experiment. The gel is divided in a lower running (or separation) gel (table 2.14), and an upper stacking gel (table 2.15). The stacking gel contains pockets for loading the protein samples, prepared as in 2.5.1. Additionally, a protein ladder (Precision Plus Protein^{TM} Dual Color, BioRad). is used for visual confirmation of protein separation. Upon application of an electrical current, the negatively charged proteins move towards the positively charged anode, until the desired degree of separation is reached.

Table 2.14: SDS-polyacrylamide running gel (10 %)

Component	Amount [mL]
Deionized water	4
Acrylamide (30 %)	3.3
Tris buffer 1.5 M pH 8.8	2.5
SDS (10 %)	0.1
Ammonium persulfate (10 %)	0.1
TEMED	0.004

Table 2.15: SDS-polyacrylamide stacking gel (5 %)

Component	Amount [mL]
Deionized water	1.7
Acrylamide (30 %)	0.4
Tris buffer 1 M pH 6.8	0.3
SDS (10 %)	0.025
Ammonium persulfate (10 %)	0.025
TEMED	0.0025

2.5.3 Western Blot

Proteins separated in a gel matrix can be visualized using dyes that penetrate the gel and bind proteins, such as Coomassie blue or silver stains. However, to detect specific proteins, it is necessary make them accessible to antibody binding. Therefore, the separated proteins are transferred to a polyvinylidene difluoride (PVDF) membrane. To achieve this, the gel is brought into immediate contact with the PVDF membrane in a buffer filled tank (1x Tris/Glycine Buffer (Bio-Rad), and 20 % methanol) and subjected to electroblotting. Through application of an electrical current, the negatively charged proteins are pulled towards the positively charged anode onto the PVDF membrane. The electroblotting is allowed to run at a constant voltage of 90 V for 3 hours. After completion of the transfer, the membrane is stained with Ponceau staining solution (0.2 % Ponceau S, 3 % trichloroacetic acid, 3 % sulfosalicylic acid), which reversibly binds all proteins on the membrane. This is used to confirm equal loading as well as later normalization of protein expression to total protein content. Then the membrane is destained using Tris-buffered saline with 0.05 % Tween-20 (TBS-T). Afterwards, the following steps are carried out:

1. Blocking of unoccupied binding sites on the PVDF membrane with StartingBlock ™ blocking solution (Pierce) for 15 minutes at RT and gentle agitation
2. Washing 3 x 5 minutes in TBS-T and gentle agitation
3. Incubation with primary antibody (table 2.16) over night at 4 °C and gentle agitation
4. Washing 4 x 4 minutes in TBS-T and strong agitation
5. Incubation with appropriate secondary antibody (table 2.16) for 60 minutes at RT and gentle agitation
6. Washing 4 x 4 minutes with TBS-T and strong agitation

7. Application of a 1:1 mix of H_2O_2 and luminol reagent (Advansta Inc.) to the membrane and incubation for 2 minutes at RT
8. Visualization of the chemiluminescence signal on the BioRad ChemiDoc Imaging System

Calculating the expression values of target proteins relative to the Ponceau staining signal was then used to compare expression or phosphorylation intensities between samples.

Table 2.16: Antibodies used for Western Blot

Target protein	Host species	Catalogue number	Company
Anti mouse-HRP	NA	#7076	Cell Signaling
Anti rabbit-HRP	NA	#7074	Cell Signaling
AKT1 (Protein kinase B)	rabbit	#9272	Cell Signaling
$AKT1_{S473}$	rabbit	#4060	Cell Signaling
β-Actin-HRP	NA	A3854	Sigma Aldrich
DNP (Dinitrophenol)	rabbit	#14681	Cell Signaling
GLUT8 (Solute carrier family 2, facilitated glucose transporter member 8)	rabbit	Self made (Lisinski *et al.*, 2001)	DIAB, DIfE
GPx1 (Glutathione peroxidase 1)	rabbit	ab22604	Abcam
HSP60 (Heat-shock protein 60)	rabbit	#4870	Cell Signaling
LC3 I/II (Microtubule associated protein 1A/1B light chain 3)	rabbit	#12741	Cell Signaling

2.6 Lysosomal activity

To measure lysosomal activity in the gWAT, a non-denaturing protein isolation was carried out as follows:

1. Weigh in $\sim$ 30 mg of gWAT previously homogenized in liquid nitrogen
2. Add 150 μL lysis buffer (sterile H_2O with 1 mM dithiothreitol (DTT))
3. Add steel ball and shake for 2 minutes at 30 Hz in a ball mill
4. Remove steel ball
5. Incubate 60 minutes at 4 °C on a shaker
6. Treat samples with ultrasound, 10 times with 80 ° amplitude and a 0.5 cycle
7. Centrifuge for 10 minutes at 20000 RCF and 4 °C
8. Transfer supernatant to a fresh microcentrifuge tube

The following lysosomal activity assay was performed by Ms. Stefanie Deubel (Molecular

Toxicology (MTOX), DIfE). Tissue lysates (0.25 μg/ well) were incubated with lysosome activity incubation buffer (containing 24 mM Cystein*HCL, 150 mM Na-Acetate, 3 mM EDTA Dihydrate, pH 4.0) for 10 min at room temperature. To measure cysteine cathepsins, OmniCathepsin fluorogenic substrate Z-FR-AMC, Z-Phe-Arg-AMC (Enzo, catalogue number BML-p-139) was used, final substrate concentration 166 µM/well. AMC liberation was measured in a black 96-well plate and monitored every 180 seconds for 90 min at 37 °C, using a fluorescence microplate plate reader (excitation: 360 nm, emission: 460 nm). Proteolytic cathepsins activity was calculated using free 7-amino-4-methylcoumarin (AMC) as fluorogenic calibration standard. Protein concentration of gWAT lysates was determined using Bradford protein assay and proteolytic activity was verified using a protease inhibitor cocktail (Sigma-Aldrich, P8340, diluted according manufacturer's instructions).Thus, lysosomal activity was determined as $\frac{substrate\ turnover\ /\ hour}{mg\ protein}$.

2.7 Transcriptome analysis of gonadal adipose tissue

For determination of changes in the gene expression patterns between Ctrl and Hsp60$^{+/-}$ mice fed a HFD for 16 weeks, a transcriptomic analysis using a microarray approach was used. RNA was isolated as described in 2.4.1. Then, RNA quality control was performed with the Agilent 2100 Bioanalyzer. A RNA Integrity Number (RIN) above 8.0 was considered as sufficient for use in the microarray. The microarray itself was performed by OakLabs GmbH on an Agilent 8X60K chip. Raw data was transformed to a analysable Excel format by Markus Jähnert (DIAB, DIfE). Mr. Jähnert also performed the analysis with the proprietary Ingenuity Pathway Analysis (IPA) software from Qiagen. Further, I used the online tools ClustVis and the Gene Ontology enRIchment anaLysis and visuaLizAtion tool GOrilla. Additionally, gene set enrichment analysis was done using the free software Gene Ontology enRIchment anaLysis and visuaLizAtion tool GSEA from the Broad Institute.

Results

3.1 Phenotypic consequences of an HSP60 reduction in mice fed a normal chow diet

HSP60 is the key component for maintaining normal mitochondrial function through control of mitochondrial protein homeostasis, which in turn is intricately linked to insulin sensitivity. A reduction in HSP60 protein levels has been shown to negatively impact mitochondrial function and insulin sensitivity (Kleinridders *et al.*, 2013; Wardelmann *et al.*, 2019 and as described in 1.6). A gene-trap approach introduces an inactivating insertion in the gene coding for HSP60 on only one allele. Thus, the heterozygous $Hsp60^{+/-}$ mouse shows an average reduction in HSP60 protein expression of 50 % in all tissues, which is also present in type 2 diabetes (Christensen *et al.*, 2010; Kleinridders *et al.*, 2013, see also data from the Attie Lab database in Appendix Fig. A.1). Therefore, the $Hsp60^{+/-}$ mouse can serve as a model of a preexisting disturbance of mitochondrial protein homeostasis (proteostasis) and can thus help in understanding the impact of mitochondrial proteostasis on the development of obesity, insulin resistance and diabetes. To this end C57BL/6N control (Ctrl) and $Hsp60^{+/-}$ mice were fed normal chow diet (NCD) or high fat diet (HFD, containing 60 % of calories from fat) for 16 weeks and subjected to metabolic phenotyping to investigate the effect of a reduced mitochondrial protein folding capacity on metabolism.

Hsp60 mRNA expression is reduced across all tissues in $Hsp60^{+/-}$ mice (Christensen *et al.*, 2010). Of note however, not all heterozygous animals show a haploinsufficiency of HSP60, as the reduction in expression varies between 25 % and 66 % for an average reduction of 50 % (Fig. 3.1 A). Interestingly, when fed normal chow diet, there are no major metabolic differences between groups. Neither final body weight, body composition (measured *via* nuclear magnetic resonance NMR), or random fed blood glucose levels are

markedly changed (Fig. 3.1 B-D). Measuring insulin tolerance by an intraperitoneal insulin tolerance test shows no changes either (Fig. 3.1 E). Further, glucose or pyruvate tolerance tests show no differences between groups (Fig. 3.1 F and G). However, Hsp60$^{+/-}$ mice do have a slight (7 %), but significant, increase in energy expenditure relative to lean mass specifically during the active phase (Fig. 3.1 H).

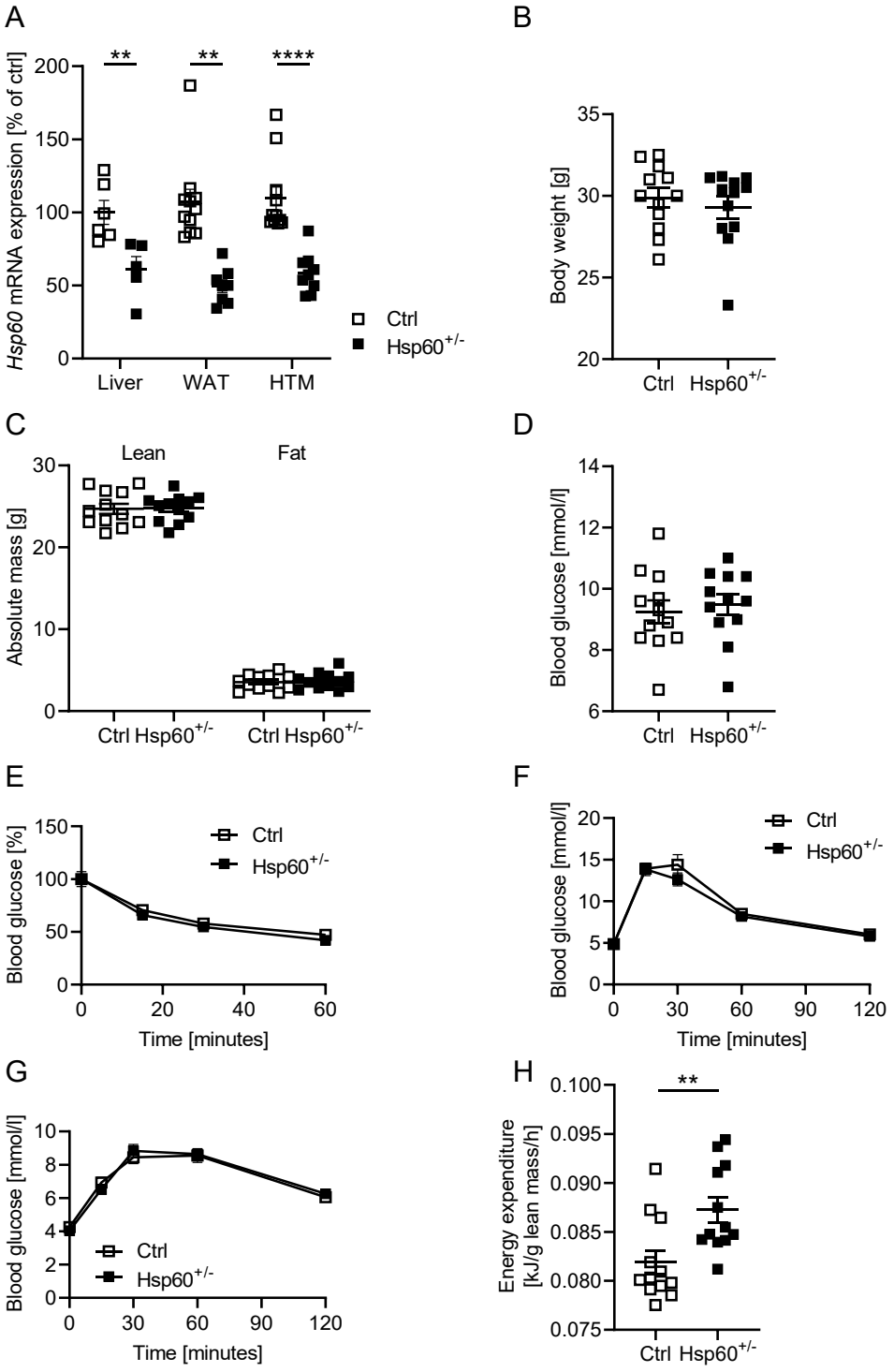

Figure 3.1: HSP60 deficiency selectively impacts energy expenditure in mice on a NCD.

A: Hsp60 mRNA expression in a variety of tissues of Ctrl and Hsp60$^{+/-}$ mice.**B:** Final body weight measurements. **C:** Body composition as measured *via* NMR. **D:** Final blood glucose values. **E:** Blood glucose values during an i.p.ITT. **F:** Blood glucose values during an oGTT. **G:** Blood glucose values during an i.p.PTT. **H:** Energy expenditure relative to lean mass. ** $P < 0.01$ and **** $P < 0.0001$ after 2-tailed Student's *t* test. All data are presented as mean $\pm$ SEM.

3.2 Phenotypic consequences of an HSP60 reduction in male mice fed a high fat diet

A higher energy expenditure could lead to improved outcomes under increased metabolic load through elimination of excess energy equivalents. Indeed, when feeding mice a HFD containing 60 % calories from fat, Hsp60$^{+/-}$ mice show decreased body weight gain with an average reduction of 16 % in final bodyweight (Ctrl = 44.02 g *vs.* Hsp60$^{+/-}$ = 36.79 g, Fig. 3.2 A). This is due to a decrease in total fat mass as measured *via* NMR by almost 50 % when comparing groups (Ctrl = 16.28 g *vs.* Hsp60$^{+/-}$ = 10.94 g, Fig. 3.2 B).

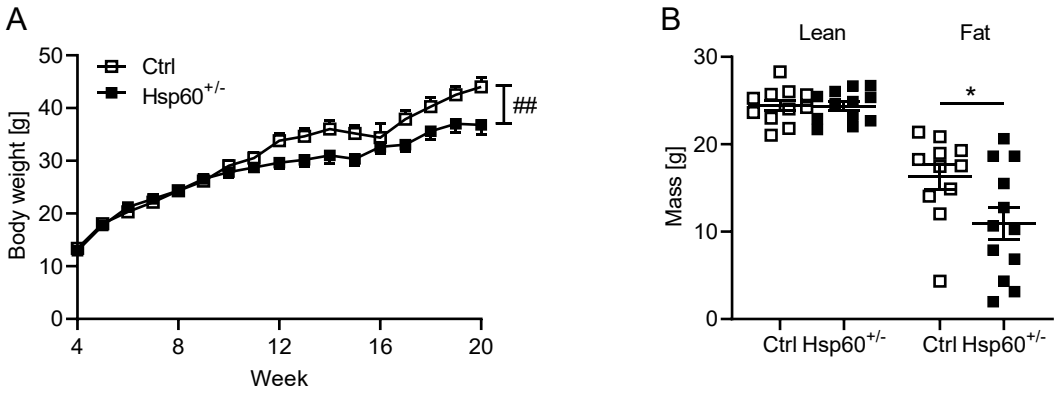

Figure 3.2: HSP60 deficiency in male mice decreases weight gain in DIO.
A: Final body weight measurements after 16 weeks of HFD. **B:** Body composition as measured *via* NMR after 14 weeks of HFD. * $P < 0.05$, and $^{\#\#}$ $P < 0.01$ after 2-way ANOVA with Šidák's *Post-hoc* test. All data are presented as mean $\pm$ SEM.

Interestingly, this does not lead to improved insulin tolerance during an intraperitoneal insulin tolerance test (Fig. 3.3 A). When measuring insulin levels during the oral glucose tolerance test however, it became apparent that Hsp60$^{+/-}$ mice need less insulin to maintain comparable blood glucose levels to Ctrl mice. Already at a basal fasted level, male Hsp60$^{+/-}$ mice show a reduction in insulin levels by 54 % (Ctrl = 1.46 ng/mL *vs.* Hsp60$^{+/-}$ = 0.67 ng/mL). This persists throughout the test with insulin levels that are reduced by an average of 40 % at each time point measured. (Fig. 3.3 B). Two commonly used markers for insulin resistance or sensitivity are the HOMA-IR (Homeostatic Model of Insulin Resistance) and the Matsuda insulin sensitivity index. The HOMA-IR is calculated from fasted insulin and glucose levels with a calculation factor of 22.5, which was empirically determined in human studies

(Turner *et al.*, 1979; Matthews *et al.*, 1985; Rudenski *et al.*, 1991). Its applicability to murine studies is therefore questionable. Nevertheless, it remains used in the literature and has also been calculated here as an additional value to gauge insulin sensitivity. The Matsuda Index on the other hand uses only the values of insulin and glucose and their respective changes over the course of a glucose tolerance test and can thus be an useful determinant of insulin sensitivity (Matsuda *et al.*, 1999). In humans, HOMA-IR values $>$ 2.50 indicate insulin resistance, whereas value $>$ 5.00 are found in type-2 diabetic patients. Calculating the HOMA-IR here results in average values for Ctrl mice of 7.51, and for Hsp60$^{+/-}$ mice of 2.52 (Fig. 3.3 C). Confirmatory, the calculated Matsuda Index yields average values of 2.02 in Ctrl mice *vs.* 4.18 in heterozygous mice (Fig. 3.3 D). For the Matsuda Index, values $<$ 3.0 are associated with insulin resistance in humans. The given reference values are not applicable to mice, but qualitative increases or decreases in those indices can still be useful when comparing experimental groups strictly with each other. Thus, driven by lower insulin values in Hsp60$^{+/-}$ mice, calculating both indices shows significantly lower insulin resistance and higher insulin sensitivity scores, respectively.

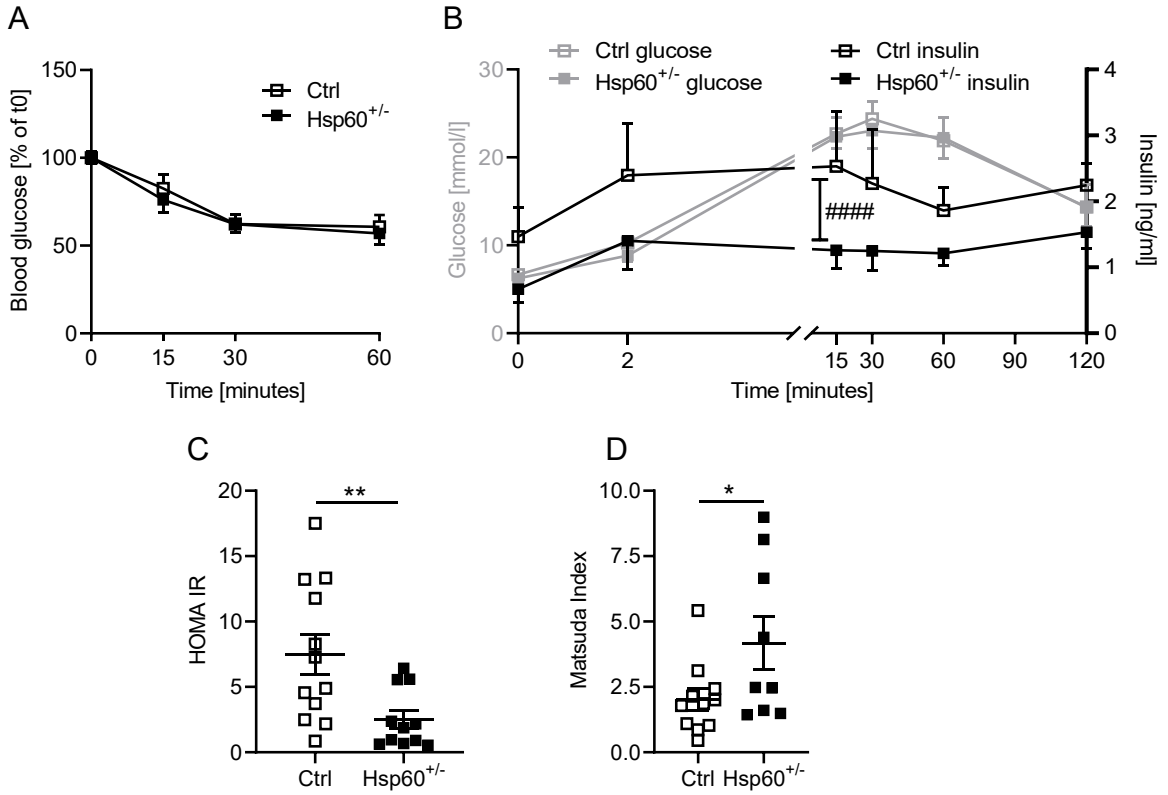

Figure 3.3: HSP60 deficiency in male mice improves insulin sensitivity in DIO.
A: Blood glucose values during an i.p.ITT after 10 weeks of HFD. **B:** Blood glucose (left Y-axis in grey) and insulin (right Y-axis in black) values during an oGTT after 11 weeks of HFD. **C:** Homeostatic Model Assessment of Insulin Resistance (HOMA-IR) values. **D:** Matsuda Index of insulin sensitivity values. * $P < 0.05$ and ** $P < 0.01$ after 2-tailed Student's *t* test. All data are presented as mean $\pm$ SEM.

Lower body weight and increased insulin sensitivity could lead to beneficial alterations in metabolic blood parameters in DIO. Here, leptin levels are significantly lower in Hsp60$^{+/-}$ mice with an average reduction of 45 % (Fig. 3.4 A). Measuring adiponectin as another important adipokine associated with insulin sensitivity showed no differences between groups (Fig. 3.4 B). Systemic insulin resistance is also associated with increased fasting glucagon levels (Færch *et al.*, 2016), but in this study, glucagon levels are similarly unaltered between groups (Fig. 3.4 C).

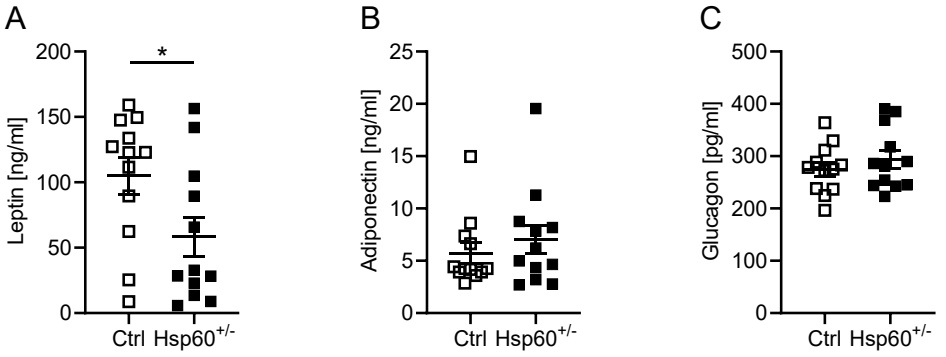

Figure 3.4: No marked changes in circulating adipokines in male Hsp60$^{+/-}$ mice in DIO.
A-C: Plasma content of leptin (A), adiponectin (B), and glucagon (C) from mice fed a HFD for 16 weeks. * $P < 0.05$ after 2-tailed Student's *t* test. All data are presented as mean $\pm$ SEM.

Further, to investigate possible changes in lipid homeostasis or lipid spillover after adipocyte failure, circulating triglyceride and non-esterified fatty acid contents were measured. Again, there are no significant differences between Ctrl and Hsp60$^{+/-}$ mice (Fig. 3.5 A and B). As mentioned earlier, HSP60 can be secreted by cells and function as an pro-inflammatory agent (Märker *et al.*, 2012, see also section 1.6). Unexpectedly, plasma HSP60 protein levels are not markedly different between groups, despite an expected reduction in expression of 50 % in all tissues of Hsp60$^{+/-}$ mice (Fig. 3.5 C).

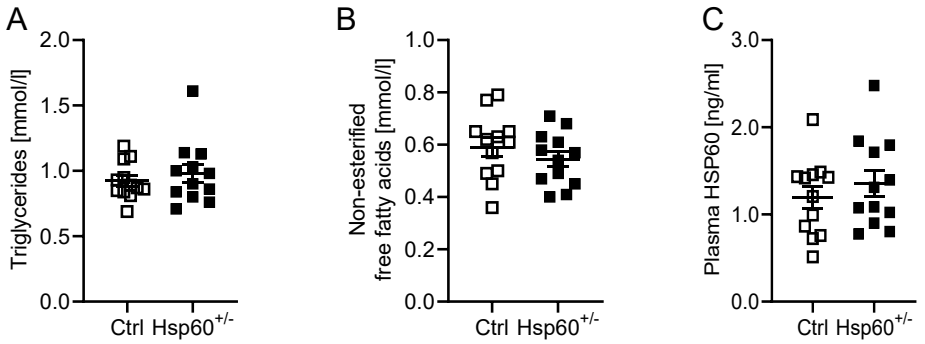

Figure 3.5: No marked changes in circulating lipid metabolites or HSP60 in male Hsp60$^{+/-}$ mice in DIO.
A-C: Plasma content of triglycerides (A), non-esterified fatty acids (B), and HSP60 (C) from mice fed a HFD. All data are presented as mean $\pm$ SEM.

Causative for lower body weight in Hsp60$^{+/-}$ mice could be lower energy intake or storage

capability, higher energy clearance, or increased energy expenditure. To investigate the respective influence of these processes, mice were kept in isolation cages for 48 hours and measured food intake, collected feces for analysis of energy content in a caloric bomb, as well as body temperature. There are no observable differences in either food intake or fecal energy content, as measurements of energy intake and clearance, respectively (Fig. 3.6 A and B). Overall body temperature also shows no differences between groups (Fig. 3.6 C).

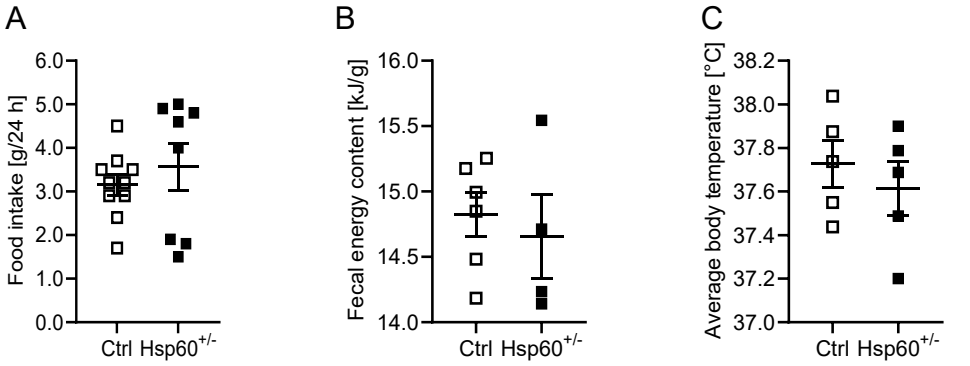

Figure 3.6: No marked changes in energy intake or clearance in male Hsp60$^{+/-}$ mice in DIO.
A: Total food intake over 24 hours. **B:** Fecal energy content from feces collected over 48 hours. **C:** Average body temperature measured over the course of 48 hours. All data are presented as mean $\pm$ SEM.

To assess energy expenditure, I performed indirect calorimetry analysis on Ctrl and Hsp60$^{+/-}$ mice fed a HFD. This revealed an average 17 % increase in energy expenditure relative to body weight measured over 48 hours in Hsp60$^{+/-}$ mice (Fig. 3.7 A). During the light cycle, *i.e.* the resting phase of the mice, there is an almost significant 14 % increase (P = 0.054, Fig. 3.7 B). This effect was increased to a significant 21 % higher energy expenditure in the dark cycle, *i.e.* the active phase, in Hsp60$^{+/-}$ mice (Fig. 3.7 C).

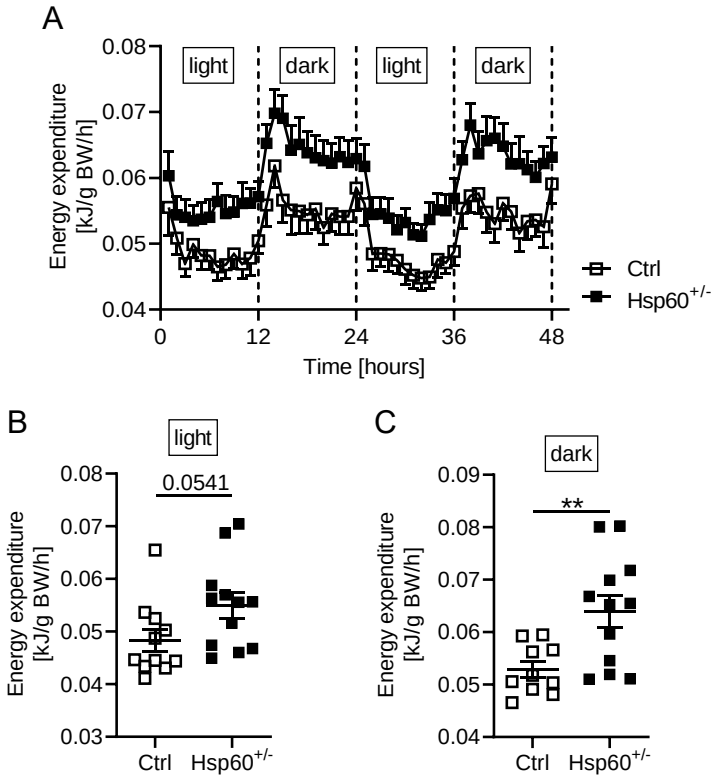

Figure 3.7: HSP60 deficiency in DIO increases energy expenditure of male mice.

A-C: Energy expenditure relative to body weight as a function of time (A) or cumulative in either the light (B) and dark (C) period, respectively, in male Ctrl or Hsp60$^{+/-}$ mice fed a HFD for 14 weeks. ** $P < 0.01$ after 2-tailed Student's *t* test. All data are presented as mean $\pm$ SEM.

The main share of energy expenditure is usually covered by skeletal muscles, and calculating total energy expenditure in relation to lean mass can therefore give valuable insight about the source of differences in energy expenditure between groups. Here, relative to lean mass, there are no significant differences in energy expenditure between groups anymore (Fig. 3.8 A). Indeed, the usually positive correlation of lean mass to energy expenditure is lost specifically in Hsp60$^{+/-}$ mice compared to control (Ctrl: $R^2 = 0.482$, $P = 0.0177$, Hsp60$^{+/-}$: $R^2 = 0.165$, $P = 0.1901$; Fig. 3.8 B). This indicates other sources than the skeletal muscles to be responsible for the increased energy expenditure.

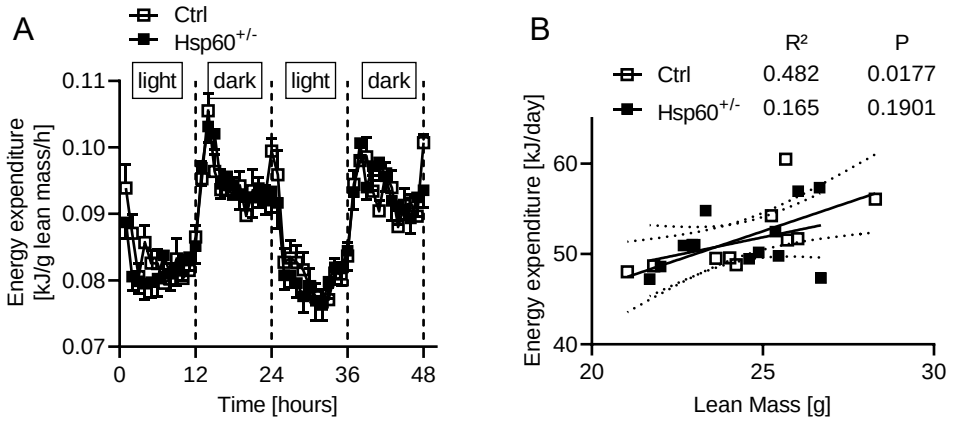

Figure 3.8: Increased energy expenditure of male Hsp60$^{+/-}$ mice is independent of lean mass.
A: Energy expenditure relative to lean mass of male Ctrl or Hsp60$^{+/-}$ mice fed a HFD for 14 weeks mice as a function of time. **B:** Linear regression analysis of lean mass and energy expenditure of the same mice. All data are presented as mean ± SEM.

3.2.1 Brown adipose tissue (BAT) of male Hsp60$^{+/-}$ shows no marked differences

Brown adipose tissue is the main site for non-shivering thermogenesis. Thought to be only a relevant organ for small mammals and humans during infancy, the discovery of functioning BAT in adult humans has since sparked large research interest (Hany *et al.*, 2002; Cypess *et al.*, 2009). The ability to clear excess energy through uncoupling mitochondrial respiration from ATP generation is thought to be a viable target to combat obesity, as white adipose tissue can be induced to show characteristics of brown adipose tissue through a process called "browning" or "beiging". BAT is characterized by multilocular morphology and a high number of mitochondria. The energy clearance process is unique to the BAT and largely due to expression of the uncoupling protein 1 (UCP1), which uses the proton gradient across the inner mitochondrial membrane to generate heat instead of ATP. It could be shown that induction of BAT activity or browning of WAT depots substantially increases energy expenditure in HFD-fed mice (Marinovic *et al.*, 2018). In Hsp60$^{+/-}$ mice, the BAT morphology does indeed show signs of slight alterations towards higher multilocularity (Fig. 3.9 A). However, on a molecular level, BAT of Hsp60$^{+/-}$ mice shows the expected average reduction of *Hsp60* expression of 50 %, but no general differences in known markers of active brown adipocytes (Ussar *et al.*, 2014, Fig. 3.9 B). Only the purinergic receptor ligand-gated ion channel 5

(*P2RX5*) is significantly upregulated in Hsp60$^{+/-}$. The membrane protein P2RX5 belongs to a family of ATP-gated ion channels, predominantly permeable for Na^+ and Ca^{2+} (Garcia-Guzman *et al.*, 1996; North, 2002; Kawate *et al.*, 2011). Interestingly, it has recently been shown that P2RX5 deletion in BAT impaired mitochondrial function and thus BAT functionality (Pramme-Steinwachs, 2019). However, upregulation of P2RX5 alone is insufficient to determine an increase in brown adipocyte presence or brown adipose tissue function.

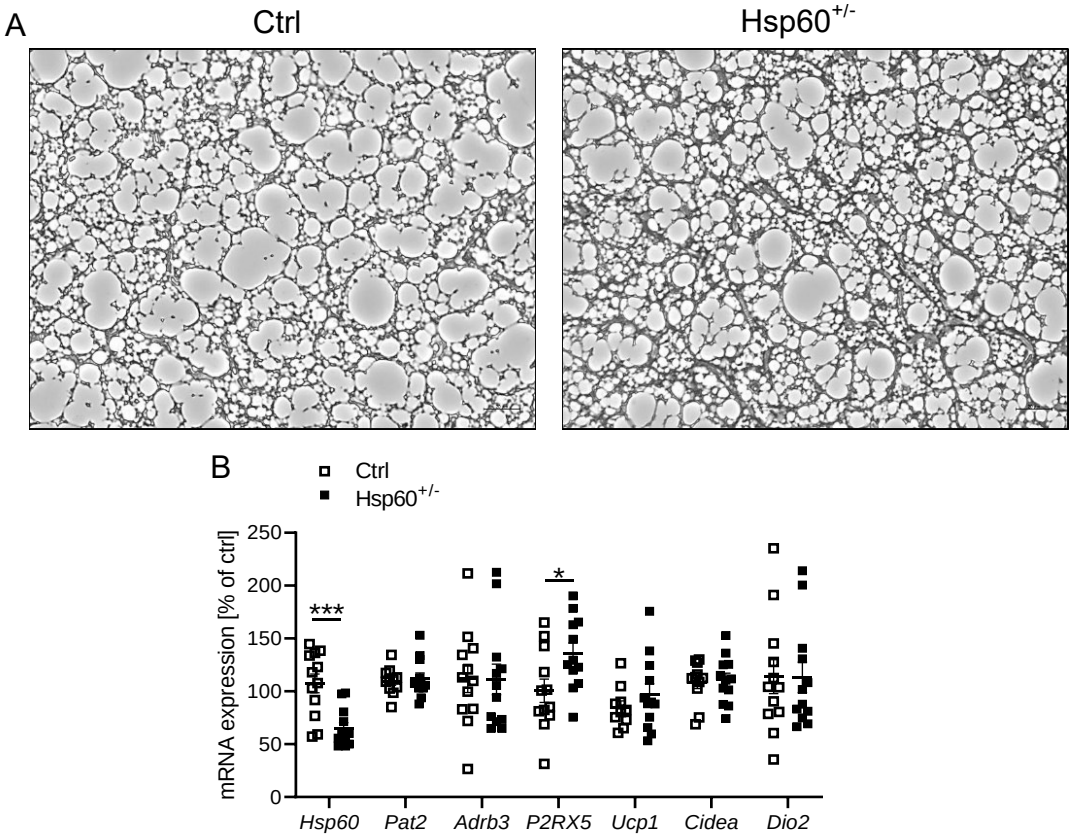

Figure 3.9: No major impact on morphology or browning in BAT of male Hsp60$^{+/-}$ mice fed a HFD.
A: Representative hematoxylin and eosin stain of histological section of the gWAT of Ctrl and Hsp60$^{+/-}$ mice fed a HFD. **B:** mRNA expression of Hsp60 and various brown adipose tissue markers in the BAT of mice fed a HFD. * $P < 0.05$ and *** $P < 0.001$ after 2-tailed Student's *t* test. All data are presented as mean $\pm$ SEM.

To more accurately analyze acute and local insulin sensitivity, an injection of insulin directly into the *vena cava* was performed. This shows no differences in phosphorylation of $AKT1_{S473}$ in the BAT between Ctrl and Hsp60$^{+/-}$ mice (Fig. 3.10 A). In summary, there are no clear indications for altered BAT function in male Hsp60$^{+/-}$ mice fed a HFD.

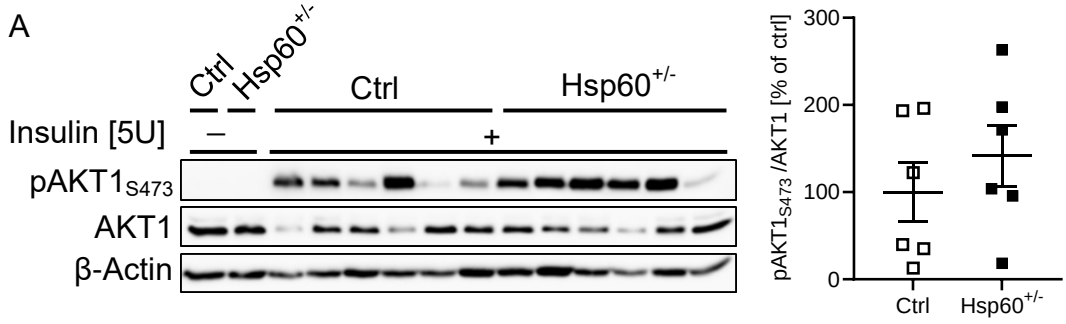

Figure 3.10: No major impact on BAT insulin sensitivity in male Hsp60$^{+/-}$ mice fed a HFD.
A: Western Blot and densitometric analysis of insulin stimulated phosphorylation of $AKT1_{S473}$ in the BAT of mice fed a HFD. All data are presented as mean ± SEM.

3.2.2 White adipose tissue alterations in male Hsp60$^{+/-}$ mice

When challenged with a high-fat diet, male Hsp60$^{+/-}$ mice show a reduction in adipose tissue mass as well as a decrease in energy expenditure that seems to be unrelated to both skeletal muscle and BAT activity. In mice, the gonadal white adipose tissue (gWAT) is most often associated with detrimental changes in terms of insulin sensitivity and inflammation during DIO and was therefore chosen for further analysis (Tran *et al.*, 2008; van Beek *et al.*, 2015; Chusyd *et al.*, 2016). First, expression of HSP60 in the gWAT shows the expected decrease in mRNA and protein expression of around 50 % in Hsp60$^{+/-}$ mice (Fig. 3.11 A and B).

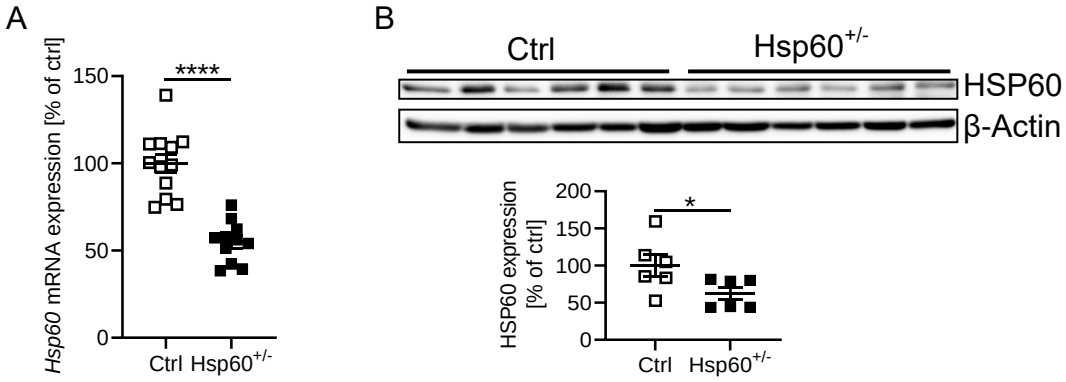

Figure 3.11: Decreased HSP60 expression in the gWAT of male Hsp60$^{+/-}$ mice fed a HFD.
A: Expression of Hsp60 mRNA in the gWAT of Ctrl and Hsp60$^{+/-}$ mice fed a HFD for 16 weeks. **B:** Western Blot and densitometric analysis HSP60 expression of the same mice. * $P < 0.05$ and **** $P < 0.0001$ after 2-tailed Student's *t* test. All data are presented as mean ± SEM.

Morphological analysis of histological sections of gonadal white adipose tissue from mice fed a HFD for 16 weeks using a macro written for ImageJ Fiji (translated and modified by me from Leboucher *et al.*, 2019, see Appendix B) reveals significantly more as well as smaller adipocytes in Hsp60$^{+/-}$ mice (Fig. 3.12 A-C). Here, the overall cell count in Hsp60$^{+/-}$ mice is two-fold increased compared to Ctrl mice, and average adipocyte area is reduced by 22 % in Hsp60$^{+/-}$. Specifically, the violin plot shows that the number of adipocytes in the largest quartile is reduced in Hsp60$^{+/-}$ mice. As hypertrophic adipocytes are prone to show increased inflammation, which can result in insulin resistance, I analyzed the gene expression of the inflammatory markers EGF-like module-containing mucin-like hormone receptor-like 1 (*F4/80*), tumor necrosis factor α (*Tnf-*α), chemokine (C-C motif) ligand 2 (*Ccl2*), and interleukin 4 (*Il-4*). However, there are no differences in the gene expression of these markers (Fig. 3.12 D). Next, to further investigate whether inflammatory processes are involved in the gWAT phenotype, histological sections of gWAT were stained with an antibody for F4/80, which would reveal macrophage infiltration. In confirmation of the gene expression data, there is no difference in F4/80 positive cells (data not shown). Taken together, this suggests that there is no substantial decrease in inflammation in the gWAT of Hsp60$^{+/-}$ mice.

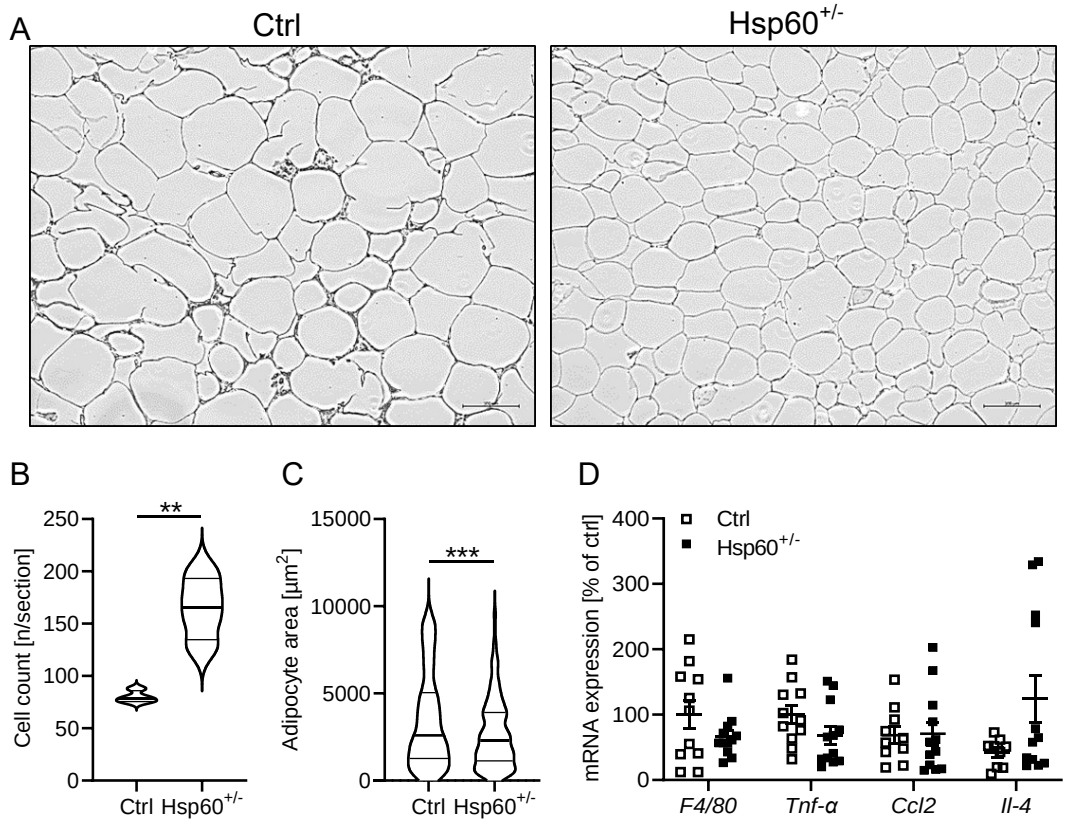

Figure 3.12: Male Hsp60$^{+/-}$ mice fed a HFD display decreased adipocyte hypertrophy in the gonadal white adipose tissue.
A: Representative hematoxylin and eosin stain of histological sections of the gWAT of Ctrl and Hsp60$^{+/-}$ mice fed a HFD for 16 weeks. **B, C:** Cell count (B) and average size (C) of adipocytes in gWAT sections from A. **D:** Gene expression levels of inflammatory markers in the gWAT of Ctrl and Hsp60$^{+/-}$ mice fed a HFD for 16 weeks. ** $P < 0.01$ and *** $P < 0.001$ after 2-tailed Student's *t* test. All data are presented as mean $\pm$ SEM.

Further, the decrease in adipocyte hypertrophy, or increased hyperplasia, as observed here is usually associated with increased insulin sensitivity and overall improved adipocyte function (Blüher *et al.*, 2002; Longo *et al.*, 2019). Therefore, to gain more insight into local insulin sensitivity, both Ctrl and Hsp60$^{+/-}$ mice were fed the 60 % HFD for 16 weeks and afterwards treated with a bolus injection of 5U insulin directly into the *vena cava* (2.3.10). Here, Hsp60$^{+/-}$ mice show a 73 % decrease in insulin-induced AKT_{S473} phosphorylation, indicating a reduced insulin sensitivity specifically in the gonadal adipose tissue, as none of the other tissues analyzed here were affected (Fig. 3.13 A and Appendix Fig. A.4).

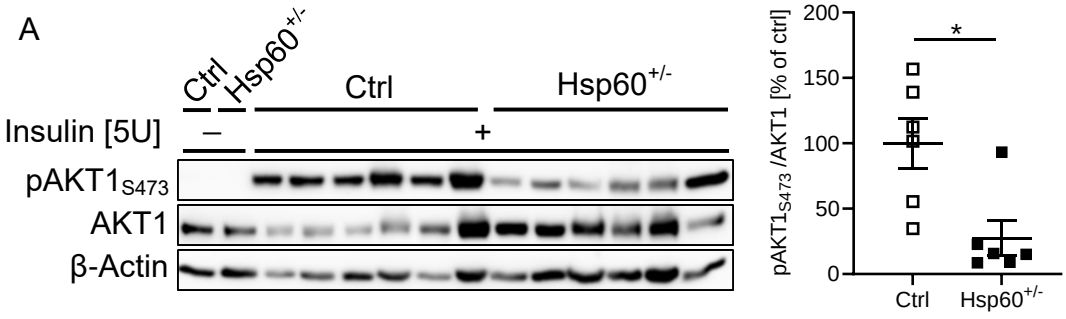

Figure 3.13: The gWAT of male Hsp60$^{+/-}$ shows increased insulin resistance.

A: Western Blot and densitometric analysis of insulin stimulated phosphorylation of $AKT1_{S473}$ in the gWAT after *vena cava* injection of insulin in Ctrl and Hsp60$^{+/-}$ mice fed a HFD for 16 weeks. * $P < 0.05$ after 2-tailed Student's *t* test. All data are presented as mean $\pm$ SEM.

3.3 Phenotypic consequences of an HSP60 reduction in female mice on a high fat diet

Obesity development differs greatly between male and female mice, where females are usually more protected against diet-induced obesity and insulin resistance when compared to males (Kautzky-Willer *et al.*, 2016). Interestingly, feeding female Ctrl and Hsp60$^{+/-}$ mice a HFD for 16 weeks leads to an average increase in final body weight by 20 % in the heterozygous animals (Ctrl = 28.30 g *vs.* Hsp60$^{+/-}$ = 34.05 g Fig. 3.14 A). This however is due to an increase in lean mass rather than fat mass, as the NMR measurement after 14 weeks of HFD shows a 7 % increase in lean mass and no changes in fat mass (Fig. 3.14 B). Further, weighing various muscles during organ harvesting after 16 weeks of DIO reveals an increased weight of some muscle types (Fig. 3.14 C). This narrowly misses significance for the quadriceps (8 % increase, P = 0.06). Interestingly, the heart mass is significantly increased by 15 %. Calculating the combined muscle mass and comparing those reveals an overall increased muscle mass of 10 % in Hsp60$^{+/-}$ mice (Fig. 3.14 D).

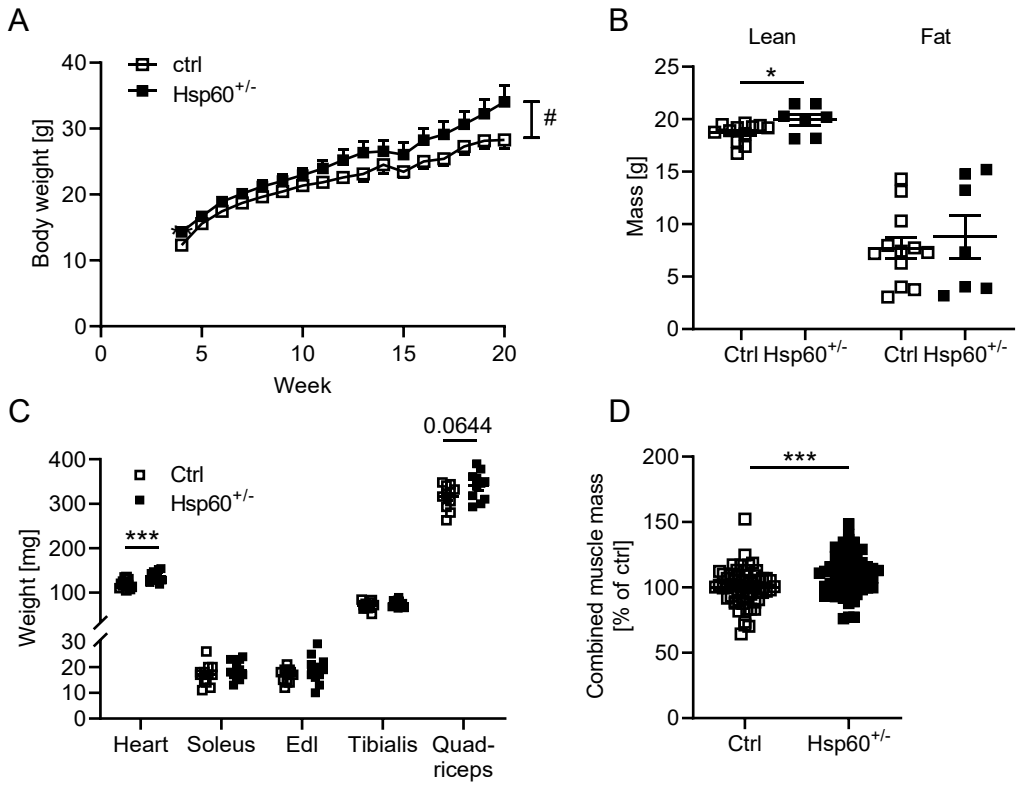

Figure 3.14: HSP60 deficiency in female mice increases lean mass specific weight gain in DIO.

A: Final body weight measurements after 16 week of HFD. **B:** Body composition as measured *via* NMR after 14 weeks of HFD. **C:** Weight of muscle types of female mice fed a HFD for 16 weeks (Edl: *Extensor digitorum longus* muscle). **D:** Comparison of combined muscle mass between groups (data from panel C). * $P < 0.05$ and *** $P < 0.005$ after 2-tailed Student's *t* test, and # $P < 0.05$ after 2-way ANOVA with Šidák's *Post-hoc* test. All data are presented as mean $\pm$ SEM.

These differences in body composition do not influence insulin sensitivity or glucose tolerance, as there are no differences in either the i.p.ITT or oGTT (Fig. 3.15 A and B). Consequently, calculating either HOMA-IR or the Matsuda Index from the data from it oGTT shows no difference between groups (Fig. 3.15 C and D).

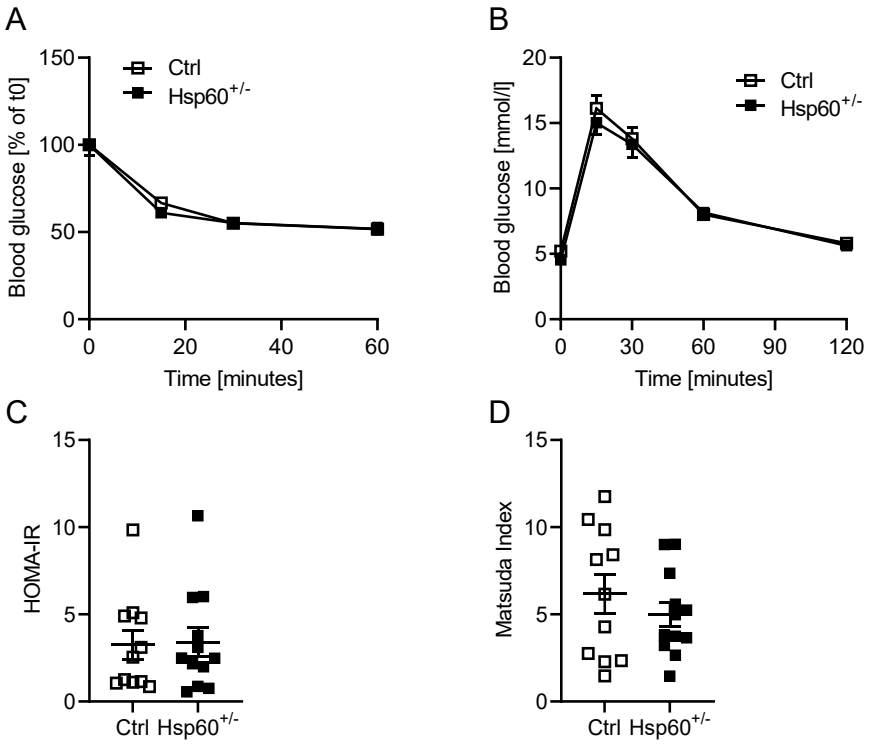

Figure 3.15: HSP60 deficiency in female mice increases weight gain without changes in insulin sensitivity in DIO.

A: Blood glucose values during an i.p.ITT after 10 weeks of HFD. **B:** Blood glucose values during an oGTT after 11 weeks of HFD. **C:** Homeostatic Model Assessment of Insulin Resistance (HOMA-IR) values in female mice fed a HFD. **D:** Matsuda Index of insulin sensitivity values in female mice fed a HFD. All data are presented as mean $\pm$ SEM.

Nevertheless, female Hsp60$^{+/-}$ mice have lower fasted blood glucose levels with a reduction in fasting glycemia by 24 % (Fig. 3.16 A). Interestingly, while there are no differences in fasted insulin values, the pancreatic insulin content is increased by 26 % in Hsp60$^{+/-}$ mice (Fig. 3.16 B and C). It needs to be noted however, that the pancreatic insulin measurement was performed in non-fasted animals.

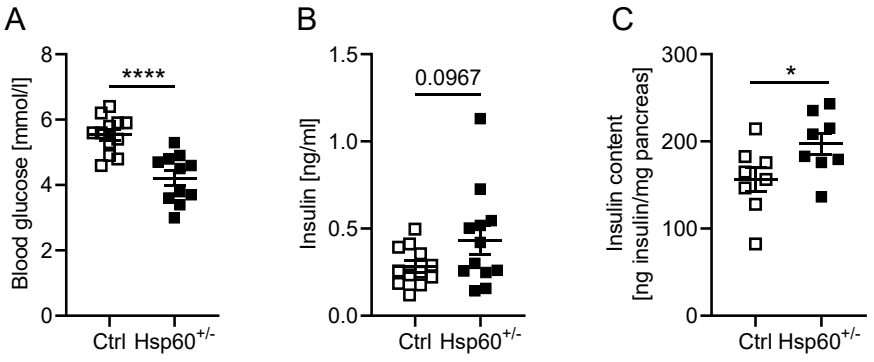

Figure 3.16: HSP60 deficiency in female mice induces fasting hypoglycemia in DIO].

A, B: Fasted content of blood glucose (A) and plasma insulin (B) from female mice fed a HFD. **C:** Pancreatic insulin content in female mice fed a HFD. * $P < 0.05$ and **** $P < 0.0001$ after 2-tailed Student's *t* test. All data are presented as mean $\pm$ SEM.

As opposed to male mice, the energy expenditure relative to total body weight was reduced in female Hsp60$^{+/-}$ mice by an average of 22 % (Fig. 3.17 A). This effect was slightly more pronounced in the light, resting phase, with 23 % ($P < 0.0001$) than in the dark, active phase with a 21 % ($P < 0.0001$) decrease (Fig. 3.17 B and C). Furthermore, female Hsp60$^{+/-}$ mice retain the positive correlation between lean mass and energy expenditure (Ctrl: R^2 = 0.5046, P = 0.0143, Hsp60$^{+/-}$: R^2 = 0.5625, P = 0.0125; Fig. 3.17 D).

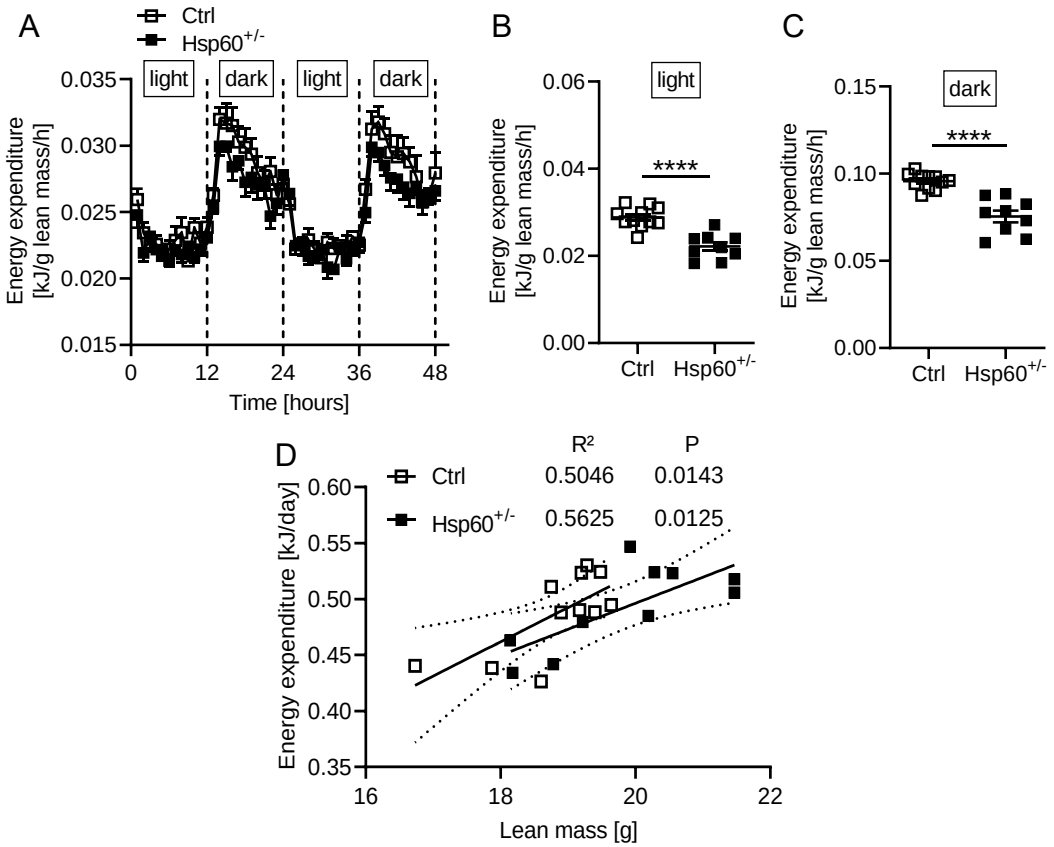

Figure 3.17: HSP60 deficiency in female mice alters energy homeostasis in DIO.

A-C: Energy expenditure relative to lean mass as a function of time (A) or cumulative in either the light (B) and dark (C) period, respectively, in female Ctrl or Hsp60$^{+/-}$ mice fed a HFD for 14 weeks. **** $P < 0.001$ after 2-tailed Student's *t* test. All data are presented as mean $\pm$ SEM.

Interestingly though, the gWAT of female Hsp60$^{+/-}$ also shows decreased hyperplasia with a 48 % increase in adipocyte number and a 24 % decrease in adipocyte size (Fig. 3.18 A-C).

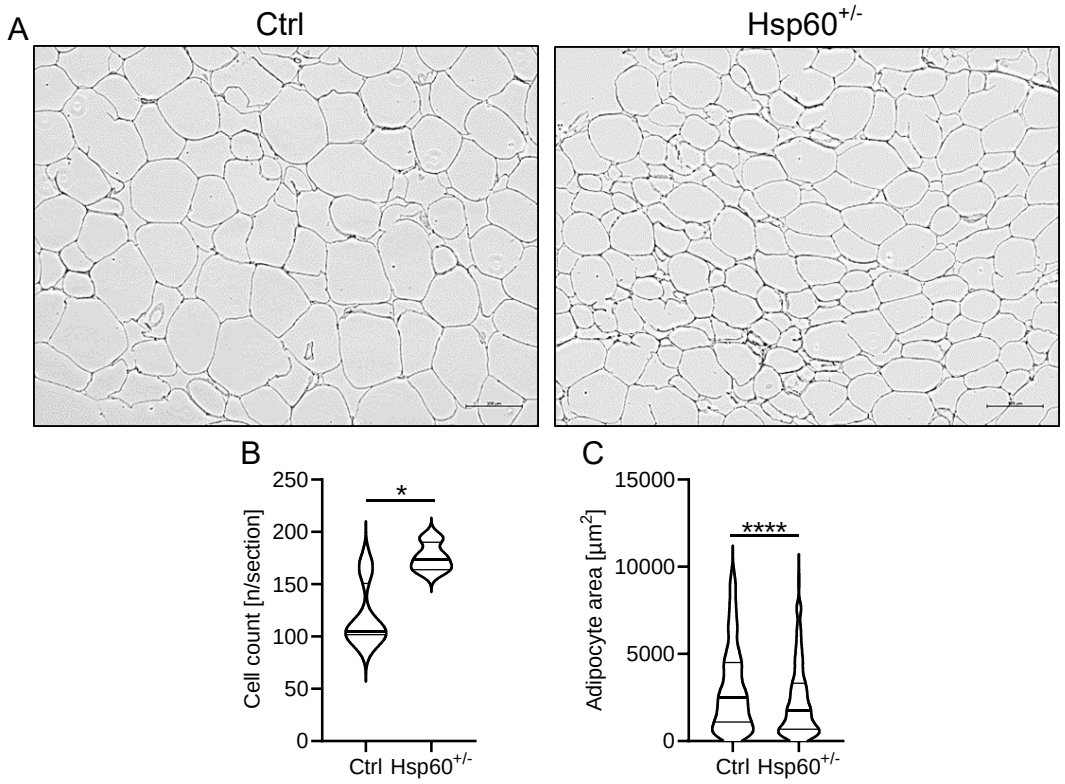

Figure 3.18: HSP60 deficiency in female mice alters white adipose tissue morphology in DIO.
A Representative hematoxylin and eosin stain of histological sections of the gWAT of female Ctrl and Hsp60$^{+/-}$ mice fed a HFD. **B, C:** Count (B) and average size (C) of adipocytes in gWAT sections from A. * $P < 0.05$ and **** $P < 0.001$ after 2-tailed Student's *t* test. All data are presented as mean $\pm$ SEM.

Performing the *vena cava* insulin injection after HFD feeding in female mice and probing for AKT1$_{S473}$ phosphorylation to asses local insulin sensitivity reveals no differences between groups (Fig. 3.19 A).

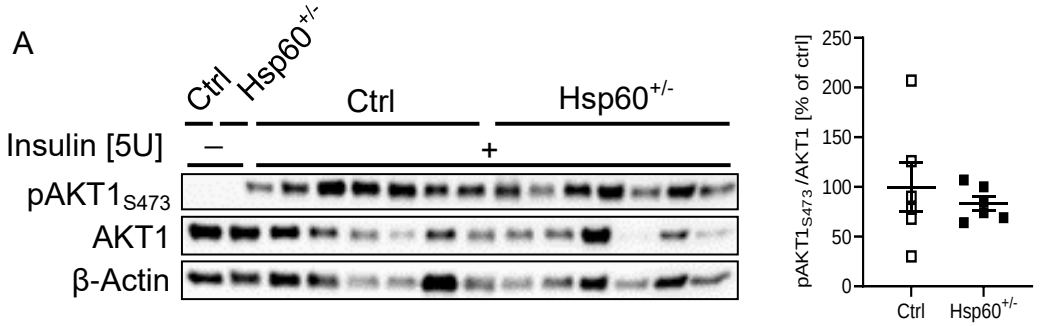

Figure 3.19: HSP60 deficiency in female mice does not impact gWAT insulin sensitivity in DIO.
A: Western Blot and densitometric analysis of insulin stimulated phosphorylation of $AKT1_{S473}$ in gWAT of female mice fed a HFD for 16 weeks. All data are presented as mean ± SEM.

As demonstrated above, female Hsp60$^{+/-}$ mice share the morphological phenotype in the WAT with male Hsp60$^{+/-}$ mice, but display the opposite in body weight development with increased muscle mass as opposed to an decrease in adipose tissue mass. However, only male Hsp60$^{+/-}$ mice exhibited local insulin resistance, therefore further studies focused on the gWAT of the male mice.

3.4 Functional alterations of white adipose tissue in male Hsp60$^{+/-}$ mice

Insulin resistance is closely associated with mitochondrial dysfunction. In male Hsp60$^{+/-}$ mice the gonadal adipose tissue showed a decoupling of apparent healthy adipocyte morphology and insulin sensitivity (see 3.2.2, Figs. 3.12 and 3.13). To further analyze this discrepancy, I excised explants from the gWAT of mice fed a HFD for 16 weeks followed by analysis of mitochondrial function in the Seahorse Flux Analyzer. This revealed a significant reduction in basal and maximal respiration by 68 % and 23 %, respectively (Fig. 3.20 A and B). Further, the expression of the anti-oxidative enzyme glutathione peroxidase 1 (GPx1) is increased 3-fold in Hsp60$^{+/-}$ mice, suggesting a compensatory upregulation in response to the presence of reactive oxygen species (Fig. 3.20 C). Extended oxidative stress can lead to irreversible protein modifications, where reactive oxygen species oxidize carbon atoms of amino acid residues to form carbonylated proteins. Indeed, Hsp60$^{+/-}$ mice display a more

than two-fold increase in cellular protein carbonylation (Fig. 3.20 C), indicating the presence of oxidative stress in the gWAT of male Hsp60$^{+/-}$ mice.

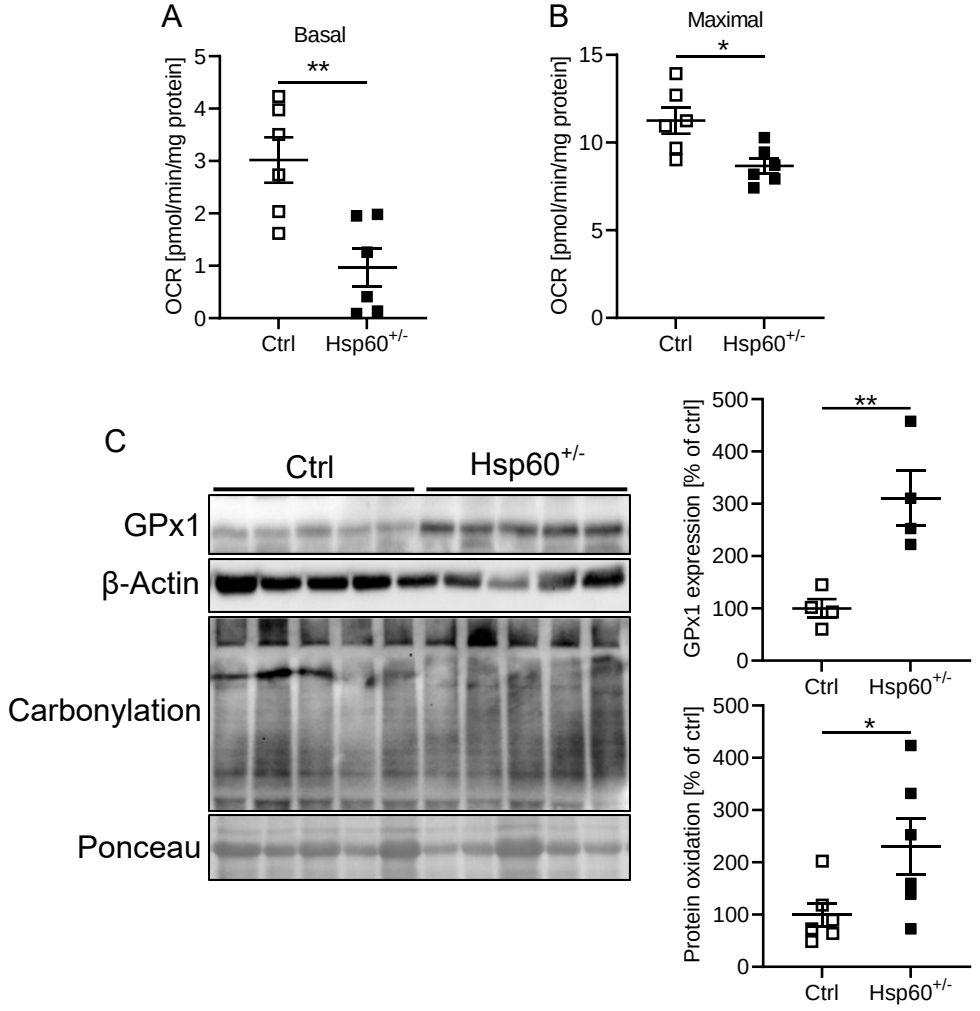

Figure 3.20: Male Hsp60$^{+/-}$ mice fed a HFD display signs of mitochondrial dysfunction and oxidative stress in the gWAT.
A, B: Basal (A) and maximal (B) oxygen consumption rate (OCR) in explants of gWAT from mice fed a HFD measured in the Seahorse Flux Analyzer. **C** Representative Western Blot image and densitometric analysis of GPx1 expression and total protein carbonylation in gWAT of mice fed a HFD. * $P < 0.05$ and ** $P < 0.01$ after 2-tailed Student's *t* test. All data are presented as mean $\pm$ SEM.

Mitochondrial dysfunction and accompanying oxidative stress are strong predictors for insulin resistance, and this seems to be the case in Hsp60$^{+/-}$ mice as well, as shown through the *vena cava* insulin injection in figure 3.13. However, to further investigate consequences

of insulin resistance and mitochondrial function on adipocyte physiology, I analyzed additional aspects of insulin signaling in adipocytes. As alluded to earlier, adipocyte differentiation can be effectively stimulated by insulin. Thus, the stromal vascular fraction (SVF) from the gWAT of mice fed a HFD was isolated and subjected to an *in vitro* adipogenic differentiation protocol. The degree of differentiation can be approximated by treatment of the cells with the lipid stain Oil Red O (Proescher, 1927; Kraus *et al.*, 2016). An increase in differentiation capacity within the same time frame should lead to more Oil Red O accumulation in a given sample. Here, Hsp60$^{+/-}$ samples show significantly lower Oil Red O absorption compared to the control group, indicative of lower overall adipocyte differentiation (Fig. 3.21 A).

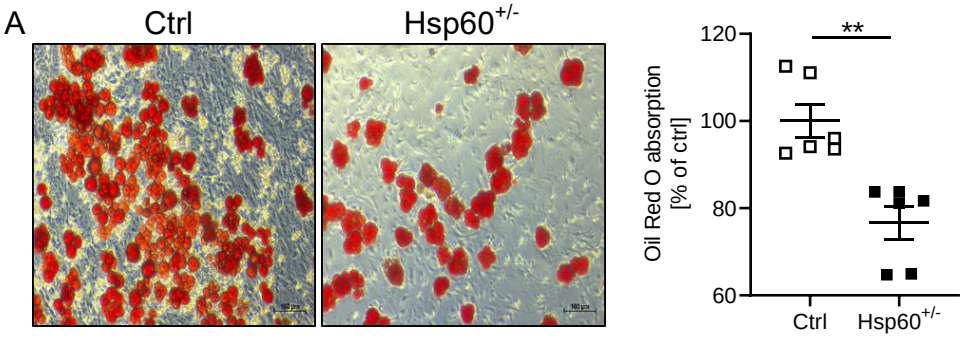

Figure 3.21: Lower differentiation capacity of gWAT derived SVF cells from male Hsp60$^{+/-}$ mice fed a HFD.
A: Representative Oil Red O staining and analysis of absorbance intensity in *in vitro* differentiated SVF cells from gWAT of mice fed a HFD for 16 weeks. ** $P < 0.01$ after 2-tailed Student's *t* test. All data are presented as mean $\pm$ SEM.

One of the most well described insulin-dependent functions of WAT is the uptake of glucose. To gain insight into this metabolic pathway, gWAT explants from HFD-fed mice were incubated with radioactively labeled 2-Deoxy-d-glucose ([^{14}C]-DOG) and stimulated with insulin. Interestingly, both explants from Ctrl and Hsp60$^{+/-}$ mice show insulin resistance, where only Ctrl explants display a trend towards increased glucose uptake after insulin stimulation ($P = 0.08$), whereas Hsp60$^{+/-}$ explants show no increase in glucose uptake after insulin treatment (Fig 3.22 A). Strikingly however, explants from Hsp60$^{+/-}$ gWAT show a significant two-fold higher glucose uptake on a basal level (Fig 3.22 A). Analysis of the gene expression patterns of various glucose transporters described to be present in the adipose tissue (Chadt *et al.*, 2020), reveals increased expression of *Glut2* and *Glut8* in the gWAT of Hsp60$^{+/-}$ mice

(Fig. 3.22 B). Further, this leads to a two-fold increased protein expression of GLUT8 in the gWAT of Hsp60$^{+/-}$ mice (Fig. 3.22 C), suggesting that an increase in GLUT8 expression and surface localization could be responsible to increase basal glucose uptake in Hsp60$^{+/-}$ mice.

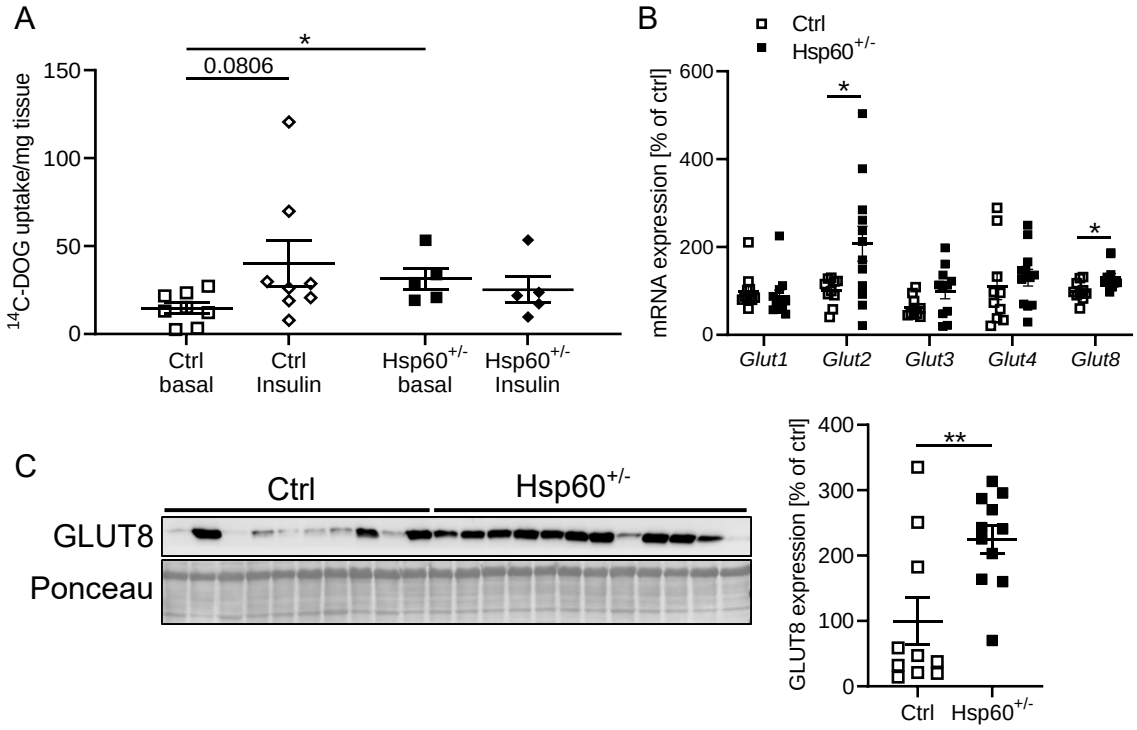

Figure 3.22: Explants from gWAT of male Hsp60$^{+/-}$ mice fed a HFD have increased basal glucose uptake.
A: Basal and insulin stimulated *ex vivo* 2-[^{14}C]-Deoxy-d-glucose [^{14}C-DOG] uptake in explants of gWAT from mice fed a HFD for 16 weeks. **B:** mRNA expression of different glucose transporters in the gWAT of mice fed a HFD for 16 weeks. **C:** Western Blot and densitometric analysis of GLUT8 expression in the gWAT of mice fed a HFD for 16 weeks. * $P < 0.05$ and ** $P < 0.01$ after 2-tailed Student's *t* test. All data are presented as mean $\pm$ SEM.

3.4.1 Transcriptomic analysis of gWAT

To gain further insights into HSP60 induced alterations in adipocyte metabolism, RNA samples from the gWAT of Ctrl and Hsp60$^{+/-}$ mice fed a HFD for 16 weeks were submitted to microarray transcriptomic analysis. The reduction of HSP60 protein levels by 50 % has substantial and diverse effects on gWAT morphology and functionality, with an apparent dissociation of adipocyte hyperplasia and cellular metabolic health. In total, 926 differentially expressed genes were found. Of these, 220 were down, and 706 were upregulated in Hsp60$^{+/-}$ mice (Fig 3.23).

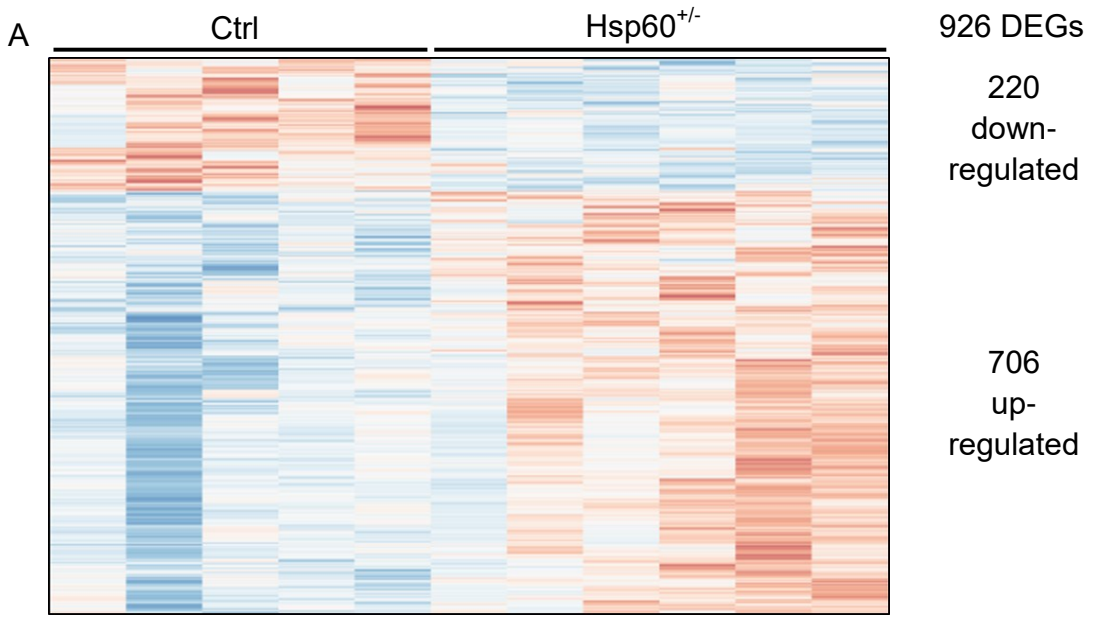

Figure 3.23: Differentially expressed genes in the gWAT of male Ctrl and Hsp60$^{+/-}$ mice fed a HFD.
A: Expression pattern of 926 differentially expressed genes (DEGs) after analysis of the microarray transcriptomic data. Figure was generated with the online tool ClustVis.

For further data analysis, both the proprietary software Ingenuity Pathway Analysis (IPA, QIAGEN), and the Gene Ontology enRIchment anaLysis and visuaLizAtion tool (GOrilla) were used. Here, the downregulated genes show no enrichment in specific pathways or gene ontology terms. In the subset of upregulated genes however, both the IPA and the gene ontology analysis show an enrichment of upregulated genes that are involved in the cellular process of autophagy, including Beclin 1, Ulk2, and a variety of autophagy related proteins (Atg) and phosphoinositide 3-kinases (Fig. 3.24 A and B).

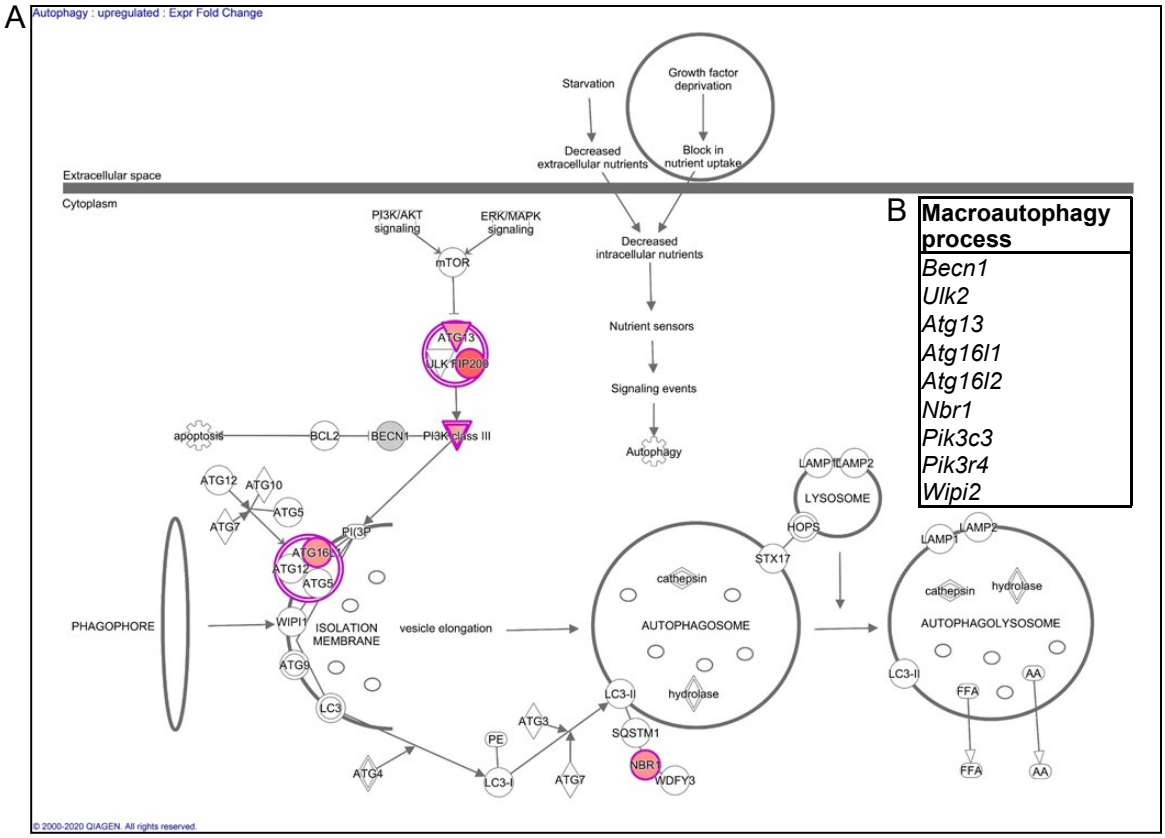

Figure 3.24: Pathway analysis of upregulated genes in the gWAT of male Hsp60$^{+/-}$ mice fed a HFD.
A: Result of the ingenuity pathway analysis of upregulated genes. **B:** Genes belonging to the macroautophagy process, enriched in the subset of upregulated genes. Panel A was generated with the Ingenuity Pathway Analysis (IPA) from QIAGEN, panel B with the Gene Ontology enRIchment anaLysis and visuaLizAtion tool GOrilla.

As mentioned in section 1.6, formation of the autophagosome involves at a central point the recruitment of microtubule-associated protein 1A/1B light chain 3B (LC3), and its subsequent conversion from the cytosolic form LC3-I to LC3-II by conjugation to phosphatidylethanolamine, which is then recruited to autophagosomal membranes. Interestingly, Hsp60$^{+/-}$ mice show a significant two-fold increase in LC3-I and three-fold increase for LC3-II levels in the gWAT, which indicates an increased propensity for autophagosome formation (Fig. 3.25 A). As both LC3-I and LC3-II are increased, the often used ratio of LC3-II/I as an indicator of autophagy shows no difference between groups.

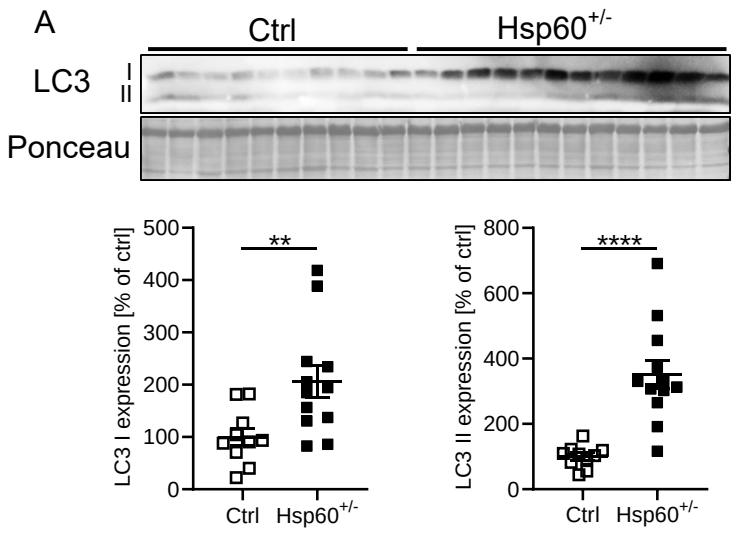

Figure 3.25: The gWAT of male Hsp60$^{+/-}$ mice fed a HFD shows signs of increased autophagy.
A: Western Blot and densitometric analysis of microtubule-associated proteins 1A/1B light chain 3B I and II (LC3-I/II) in the gWAT of mice fed a HFD for 16 weeks. ** $P < 0.01$ and **** $P < 0.0001$ after 2-tailed Student's *t* test. All data are presented as mean $\pm$ SEM.

However, as autophagy is a highly dynamic process during which the involved proteins are constantly degraded and resynthesized, the sole presence of transcripts, proteins or protein ratios (*e.g.* the LCR-II/I ratio), that are involved in autophagy is insufficient to draw conclusion about its induction (Mizushima *et al.*, 2007). As stated above, autophagic processes are dependent on the lysosomes. Traditionally used in cell viability assays, the compound Neutral Red incorporates into active lysosomes. Given equal cell viability, it can therefore be used to gauge differences in lysosome quantities between samples. Infecting 3T3-L1 fibroblasts with either a non-target (NT) siRNA or an siRNA targeted to Hsp60 mRNA (Hsp60KD) leads to a 48 % reduction in Hsp60 mRNA levels (Fig. 3.26 A), but at the same time not to any differences in cell viability, as measured *via* the enzymatic conversion of MTT to formazan during an MTT assay (Fig. 3.26 B). However, Neutral Red absorption in Hsp60KD cells is slightly, but significantly increased by 5 % (Fig. 3.26 C). Finally, to gain further insight into the autophagic activity in the gWAT of Ctrl and Hsp60$^{+/-}$ mice fed a HFD, a protein lysate was prepared under non denaturing conditions and the lysosomal activity was measured by substrate turnover in the presence of ATP and a fluorescent reporter system. Here, the gWAT of Hsp60$^{+/-}$ mice shows 79 % increase in lysosomal activity (Fig. 3.26 D). Therefore, the combined evidence from transcriptomic data, cell culture, and the animal

model strongly suggest a substantial increase in autophagic activity in the gWAT of HFD-fed Hsp60$^{+/-}$ mice.

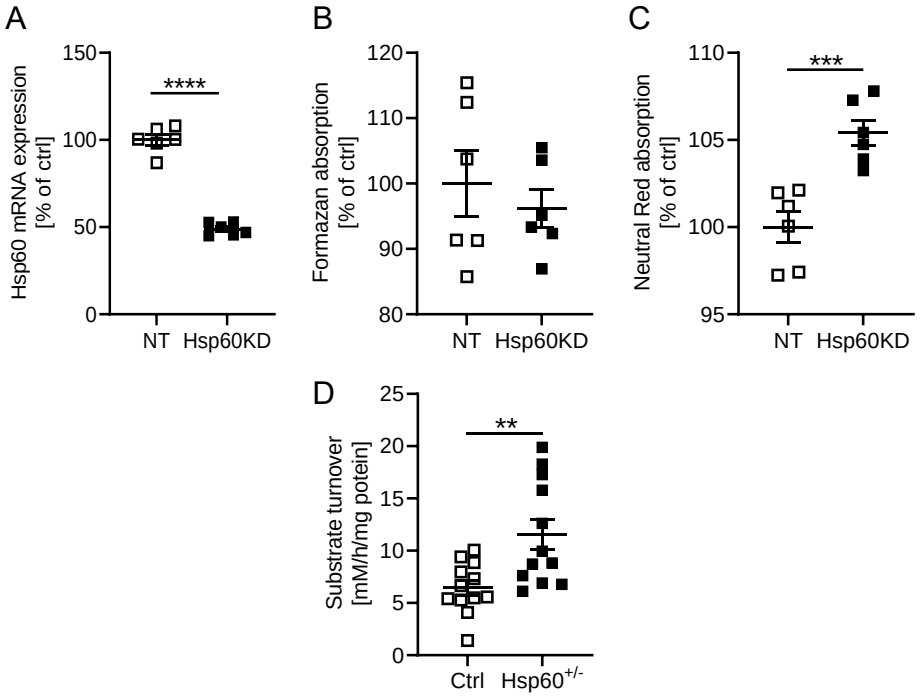

Figure 3.26: Reduction of HSP60 increases autophagy *in vitro* and *in vivo*.

A: Hsp60 mRNA expression in 3T3-L1 fibroblasts infected with siRNA targeting either non-template (NT) or Hsp60 (Hsp60KD). **B:** Light absorption at 560 nm (for Formazan) in NT or Hsp60KD 3T3-L1 cells. **C:** Light absorption at 540 nm (for the lysosomal dye neutral red) in NT or Hsp60KD 3T3-L1 cells. **D:** Lysosomal activity measured in gWAT lysates of male mice fed a HFD for 16 weeks. ** $P < 0.01$, *** $P < 0.001$, and **** $P < 0.0001$ after 2-tailed Student's *t* test. All data are presented as mean $\pm$ SEM.

In summary, the reduction of HSP60 leads to a decrease in diet-induced obesity with a combination of apparent beneficial changes in WAT morphology, but local insulin resistance. Yet, indices of systemic insulin resistance are improved, and basal glucose uptake is increased. On a molecular level, the gWAT shows signs of oxidative stress and an induction of macroautophagy.

Discussion

The development of obesity and its associated comorbidities, such as type 2 diabetes (T2D) is intricately linked to white adipose tissue (WAT) health. WAT health and its ability to dynamically react to changing levels of circulating nutrients and insulin with changes in glucose uptake, lipolysis and lipogenesis activity, and ultimately adipocyte proliferation or expansion, is in turn linked with mitochondrial function. Thus, maintaining mitochondrial function throughout metabolic challenge is crucial for alleviating, or indeed preventing, metabolic deterioration in WAT.

Mitochondrial function and insulin sensitivity are interconnected and represent important signaling nodes for propagation of adipose tissue health and thus overall metabolic health through both storing and releasing excess energy during feeding and starvation, respectively, as well as through control of energy expenditure and feeding behavior *via* adipokines.

4.1 Mitochondrial protein quality control and metabolism

Various mouse models of obesity and T2D, as well as T2D patients, show a reduction in expression of the key component for regulating mitochondrial protein homeostasis and thus maintenance of mitochondrial function, HSP60, of around 50 % (Kleinridders *et al.*, 2013, see also data from the Attie Laboratory Database in Appendix Fig. A.1). Excluding proteins of the citric acid cycle or the oxidative phosphorylation machinery, HSP60 is among the most abundant proteins found in mitochondria (comparing single-cell RNA sequencing data of different mitochondrial genes in 6 months old mice from the *Tabula muris senis*, published in Schaum *et al.*, 2019, (Appendix Fig. A.2). Highlighting its indispensable role is the fact that a complete loss results in apoptosis and early embryonic lethality, and that HSP60 mutations are causal to varieties of hereditary spastic paraplegia, neurodegenerative hypomyelinating leukodystrophy (Cheng *et al.*, 1989; J. J. Hansen *et al.*, 2002; J. Hansen *et al.*, 2007; Bross

et al., 2007; Magen *et al.*, 2008). Therefore, it is interesting to note that the removal of half the HSP60 protein in male and female Hsp60$^{+/-}$ mice does not have more drastic phenotypic consequences. In this context, it is of specific importance, that all existing data on the Hsp60$^{+/}$ mice stem from mice on the C57BL/6J (Jackson Laboratories) background, which differs from the C57BL/6N (National Institute of Health) background in several key aspects. These two strains have been separated in 1951 and have since accumulated genotypic and phenotypic differences (Simon *et al.*, 2013). Especially noteworthy in the context of mitochondrial function, the C57BL/6N mouse bears a deletion of 5 exons in the *Nnt* gene on chromosome 13, coding for the Nicotinamide nucleotide transhydrogenase. This enzyme uses energy from the proton gradient across the inner mitochondrial membrane to replenish the NADPH pool, which in turn is used to detoxify mitochondrial ROS, and upkeep of the reduced glutathione pool, *i.e.* a high GSH/GSSG ratio (Forsmark-Andrée *et al.*, 1996). Thus, it plays a crucial role in maintaining mitochondrial redox status and whole-body metabolism. Consequently, C57BL/6J mice are already glucose intolerant on a normal chow diet, as well as showing decreased energy expenditure (Kulkarni *et al.*, 2003; Rossmeisl *et al.*, 2003; Toye *et al.*, 2005).

During this study, the insulin resistance during an ITT described for Hsp60$^{+/-}$ mice on a C57BL/6J background fed a NCD (Kleinridders *et al.*, 2013 *vs.* Fig. 3.1 E) could not be recapitulated for the Hsp60$^{+/-}$ mice on the C57BL/6N background. In particular, as the insulin resistant phenotype of reduced HSP60 expression was due to elevated oxidative stress levels in C57BL/6J mice (Kleinridders *et al.*, 2013), the absence of systemic insulin resistance in this Hsp60+/- mice on a C57BL/6N background is presumably due to the lack of extensive oxidative stress. Confirmatory, the gWAT of Hsp60+/- mice on a C57BL/6N background display oxidative stress and with this insulin resistance (Fig. 3.20 C and Fig. 3.13 A), but the scWAT without oxidative stress does not (Appendix Fig. A.6 B and C). Further, only a slight increase in energy expenditure was observed when feeding these mice a normal chow diet (Fig. 3.1 H). This begs the question why HSP60 is expressed at such high values when its function is undiminished, or negative consequences due to its reduction are absent on a NCD, respectively.

4.2 HSP60 expression affects fertility in male mice

As *de novo* protein synthesis, including translation, transcription, transport, and folding is a highly energy demanding process, it seems wasteful to produce such a quantity of HSP60, when 50 % is sufficient to retain mitochondrial function and cellular health. It is known that these mice will develop neurodegeneration, specifically a late onset motoneuron disorder, in aging (Magnoni *et al.*, 2013). Beginning at the age of 12 months, motoneuronal function is significantly impaired in Hsp60$^{+/-}$ mice. From a biological standpoint however, this is long past the point of reproduction for mice, and reproductive fitness, *i.e.* the ability to produce viable offspring, is commonly viewed as one of the most potent drivers of selection for or against certain traits (Bennett, 1872). During breeding of the C57BL/6N Hsp60$^{+/-}$ mice, it became apparent, that the genetic distribution of the offspring did not follow Mendelian ratios (Appendix Fig. A.3 A). As mentioned in 1.6, homozygous loss of the *Hspd1* gene, coding for HSP60, is embryonic lethal. Therefore, breeding was performed with one C57BL/6N and one Hsp60$^{+/-}$ parental animal to generate Ctrl and heterozygous mice, respectively. Here, when the male parent carried the heterozygous deletion, Hsp60$^{+/-}$ pups made up only 32 % of the offspring, as opposed to the expected 50 %, when following Mendelian hereditary rules. Interestingly, sorting sperm cells for active mitochondria in a fluorescence activated cell sorting (FACS) using rhodamine 123 dye revealed a 22 % reduction in active mitochondria in sperm cells originating from Hsp60$^{+/-}$ mice (Appendix Fig. A.3 B, experiment performed by Dr. Karin Müller, Leibniz Institute for Zoo and Wildlife Research, Berlin). One unresolved aspect remains if all the mitochondria in sperm from Hsp60$^{+/-}$ mice are pre-damaged or if only those sperm cells carrying the allele with the Hsp60 deletion are affected. It is generally assumed that sperm cells are trancriptionally inactive. Thus, the Hsp60 deletion should not further affect HSP60 protein levels in sperm cells after meiosis. As of now, the observation remains that a reduction of HSP60, while showing no apparent metabolic or neuronal phenotype at the age of 20 weeks, on a normal chow diet induces a fertility deficiency in male mice, potentially explaining why HSP60 is as highly expressed.

4.3 The effect of an HSP60 reduction during metabolic challenge

During sustained metabolic challenge, adipocyte expansion – through hypertrophy or hyperplasia– is an indispensable compensatory mechanism to prevent lipodystrophy, *i.e* the ectopic accumulation of lipids. Prerequisite for healthy WAT expansion by hyperplasia are functional mitochondria, specifically the ability for mitochondrial biogenesis. Thus, limiting mitochondrial biogenesis in adipocytes by knockout of the crucial transcription factor Nuclear factor-erythroid 2-related factor 1 (Nrf1), severely reduces white adipocyte mass, gene expression markers of mature adipocytes, and induces glucose intolerance and insulin resistance (Hou *et al.*, 2018). Mitochondrial biogenesis itself is an energy intensive process and arguably dependent on the influx of *de novo* synthesized mitochondrial proteins. A large percentage of mitochondrial proteins are folded through the HSP10/60 chaperonin system, with currently over 300 known target proteins (Kerner *et al.*, 2005; Hartl *et al.*, 2009; Bie *et al.*, 2020). Reducing the HSP60 amount by 50 % in Hsp60$^{+/-}$ mice was already shown to lead to mitochondrial dysfunction and mild insulin resistance under normal chow diet (NCD) conditions (Kleinridders *et al.*, 2013). Therefore, when these mice were fed a high-fat diet (HFD), they could be expected to develop mitochondrial dysfunction, and subsequently adipose tissue dysfunction, insulin resistance, and obesity.

Interestingly, male Hsp60$^{+/-}$ mice after 16 weeks of HFD are protected from diet-induced obesity, and even display signs of increased whole-body insulin sensitivity after calculating either HOMA-IR or the Matsuda index (Fig. 3.2 A, B, and 3.3 B-D). Further, there were no indications of ectopic lipid accumulation, as assessed by Oil Red O staining of histological section of the liver (data not shown). The apparent increase in insulin sensitivity is driven by decreased insulin content both at a basal level, as well as throughout a glucose challenge. One could argue, that if an organism is able to maintain comparable glucose levels with lower amounts of insulin relative to a control, that this in itself is a sign of increased insulin sensitivity. Main organs for insulin-mediated glucose uptake are the skeletal muscle, liver, and adipose tissue. 16 weeks of HFD is sufficient to induce local insulin resistance in these tissues in C57BL/6 mice (White *et al.*, 2014; Liu *et al.*, 2015; Roberts-Toler *et al.*, 2015). Thus, when assessing local insulin sensitivity with a bolus injection of insulin through the

vena cava, comparable phosphorylation of AKT_{S473} between Ctrl and $Hsp60^{+/-}$ mice would indicate the presence of local insulin resistance. Indeed, here $Hsp60^{+/-}$ mice show indistinguishable AKT phosphorylation in skeletal muscle, liver and brown and subcutaneous WAT (Appendix Fig. A.4). Interestingly, the gonadal WAT even displays increased insulin resistance in male $Hsp60^{+/-}$ mice (Fig. 3.13 A). Taken together, this indicates an insulin-independent mechanism of glucose uptake in $Hsp60^{+/-}$ mice. To gain further insights, I performed *ex vivo* glucose uptake assays with live explants from the gWAT of male Ctrl and $Hsp60^{+/-}$ mice. Confirming insulin resistance in the gWAT of HFD-fed mice, both explants where unresponsive to insulin, although Ctrl mice showed a trend toward elevated glucose uptake after insulin stimulation (P = 0.08, Fig. 3.22 A). Most interestingly however, glucose uptake was increased two-fold on basal level in $Hsp60^{+/-}$ mice (Fig. 3.22 A).

4.4 Insulin independent glucose uptake

Cellular glucose influx is mediated by a family of transporter proteins, the solute carrier family 2, facilitated glucose transporter members (SLC2a, or GLUT), with currently 14 members described. While analyzing the gene expression patterns of various glucose transporters described to be present in the adipose tissue (Chadt *et al.*, 2020), it became apparent, that *Glut2* and *Glut8* are significantly upregulated in the gWAT of HFD-fed $Hsp60^{+/-}$ mice (Fig. 3.22 B). GLUT2 is the major glucose transporter in hepatocytes, as well as in pancreatic β-cells. It has a high Michaelis constant for glucose ($K_m \sim 17$ mM), indicating a low affinity. Thus, GLUT2 covers a wide range of circulating glucose concentrations and can act as a glucose sensor (Thorens, 2015). In pancreatic β-cells, it is indispensable for glucose-stimulated insulin secretion (Guillam *et al.*, 1997). As such, GLUT2 facilitates glucose transport independent of insulin. Analyzing the mRNA expression levels of *Glut2* and *Glut8*, but relative only to the internal control (TATA-box binding protein *Tbp*), shows *Glut8* to be about 8 times higher expressed than *Glut2* (Appendix Fig. A.5). Consequently, only GLUT8 could be detected on a protein level and showed a significant increase in $Hsp60^{+/-}$ gWAT (Fig. 3.22 C). GLUT8 has a higher affinity for glucose than GLUT4, the classical insulin-dependent glucose transporter ($K_M \sim 4.3$ *vs.* $K_M \sim 2$ mM). GLUT8 was independently described simultanously by two separate groups (Ibberson *et al.*, 2000; Doege *et al.*, 2000). Interestingly, the translocation of GLUT8 has been shown to be unresponsive to insulin in mature rat adipocytes, but

co-expressing the dynamin mutant dynamin-K44A, a potent inhibitor of endocytosis (Kao *et al.*, 1998), shows a 5-fold increase in cell-surface GLUT8 compared to unstimulated controls, reaching values of around 50 % of insulin-stimulated GLUT4 surface expression (Lisinski *et al.*, 2001). The authors conclude that GLUT8 seems to be in constant flux between intracellular compartments and the cell surface in a dynamin-dependent manner. Further, GLUT8 shows reconstitutable glucose transport activity similar to that of GLUT4, suggesting that GLUT8 could compensate for glucose transport in mice lacking GLUT4, as these mice show no obvious diabetic phenotype and normal glucose tolerance (Katz *et al.*, 1995; Doege *et al.*, 2000). It needs to be pointed out, however, that whole-body deletion of GLUT8 does not lead to obvious defects in energy or glucose homeostasis (Gawlik *et al.*, 2008). Nevertheless, GLUT8 has a high affinity for glucose, it is present in the gWAT, and – assuming the rat and mouse models have comparable GLUT8 activation and translocation dynamics – is able to translocate to the cell surface independently of insulin, and can, therefore, form the mechanistic basis for higher basal glucose uptake in the gWAT of $Hsp60^{+/-}$ mice. However, if this increase in GLUT8 does indeed lead to higher surface localization and can in this way explain higher baseline glucose uptake remains to be elucidated. To further test this hypothesis, it is necessary to confirm GLUT8 translocation in murine adipocytes. Additionally, the identification of the translocation stimulus for GLUT8 could give insights how, or indeed if, this translocation is related to mitochondrial function.

4.5 White adipose tissue remodeling

During high-fat diet feeding, excess energy is stored in the white adipose tissue as lipids. During sustained metabolic challenge, the adipose tissue will increase its lipid storing capacity through an increase in adipocyte number (hyperplasia) and adipocyte volume (hypertrophy). It could be shown that hypertrophy is the earlier mechanism, while the development of new adipocyte during hyperplasia is a later response during sustained HFD challenge (Jo *et al.*, 2009; Wang *et al.*, 2013). Hypertrophic adipocytes are correlated with decreased insulin sensitivity and increased inflammation (Hotamisligil, 2006; Ghaben *et al.*, 2019; Longo *et al.*, 2019). Smaller adipocytes derived from adipocyte hyperplasia on the other hand retain their capabilities to adequately react to hormone stimuli and to release adipokines (Skurk

et al., 2007). It is believed therefore, that hyperplasia acts as a "recovery mechanism" during overnutrition, where increasing adipocyte hypertrophy and accompanying deterioration of cellular functions leads to an increase in adipogenesis (Spalding *et al.*, 2008; Bambace *et al.*, 2011; Meyer *et al.*, 2013; Eriksson-Hogling *et al.*, 2015).

Adipogenesis, *i.e* the process by which mature adipocytes are derived from adipocyte precursor cells, is an energy-intensive process, dependent on both mitochondrial biogenesis and mitochondrial respiration (Wilson-Fritch *et al.*, 2003; Zhang *et al.*, 2013). These two processes are in turn dependent on a functioning mitochondrial proteostasis, meaning the ability to synthesize, import, and correctly fold mitochondrial proteins, as well as protease mediated disposal of misfolded or damaged proteins (Voos *et al.*, 2002). Central for the maintenance of mitochondrial proteostasis is the molecular chaperone HSP60 (Voos, 2013). One could thus expect that $Hsp60^{+/-}$ mice show impaired adipogenesis and consequently an increase in hypertrophic adipocytes in the WAT. Interestingly however, $Hsp60^{+/-}$ mice have significantly smaller, as well as more adipocytes in gonadal WAT (Fig. 3.12 A-C and Fig. 3.18 A-C). Depleting other factors involved in the mitochondrial proteostasis was shown to yield similar phenotypes. Two separate studies utilizing mice with a whole-body knockout of the mitochondrial protease ClpP ($ClpP^{-/-}$) demonstrated that these mice are protected against DIO and show smaller adipocytes after HFD feeding (Becker *et al.*, 2018; Bhaskaran *et al.*, 2018). Further, the decrease in body weight gain in ClpP deficiency is due to an increase in energy expenditure, mirroring the data presented in this work. Paradoxically, local gWAT insulin sensitivity was increased in $ClpP^{-/-}$ mice, although this particular experiment was only performed in NCD-fed mice. Mitochondrial function in the WAT was generally increased in these animals as well after HFD feeding, as opposed to the apparent mitochondrial dysfunction in $Hsp60^{+/-}$ mice. Although a direct comparison is difficult, as the mice in the aforementioned studies were fed a HFD for a shorter period of time (8 and 10 weeks for $ClpP^{-/-}$ *vs.* 16 weeks for $Hsp60^{+/-}$ mice), as well as having a different genetic background. Nevertheless, it is interesting to note that interfering with the mitochondrial proteostasis from both the folding and the disposal side in a whole-body mouse model yields a similar adipocyte hyperplasia phenotype.

4.6 A role for autophagy in the adipocyte morphology

Smaller adipocytes in the Hsp60$^{+/-}$ model could also lead to an alternative interpretation. The gWAT shows mitochondrial dysfunction and insulin resistance, and there were no obvious indications of an increase in adipogenesis, as markers of mature adipocytes or cell proliferation were not altered (data not shown). Confirmatory, the transcriptomic analysis did not reveal any changes in regards to adipogenesis or proliferation. Therefore, these data indicate that smaller adipocytes could rather be a consequence of reduced hypertrophy instead of increased hyperplasia. There are three main mechanisms which explain a reduced hypertrophy: (i) reduced energy uptake and thus reduced availability of energy to store in adipocytes, (ii) increased energy clearance, or (iii) increased energy usage. In the present work, food intake between groups was unchanged (Fig. 3.6 A). It could be shown previously, that HSP60 deficiency impairs the function of intestinal epithelial cells (Berger *et al.*, 2016). If Hsp60$^{+/-}$ mice are less able to extract energy from the consumed food, this should be reflected in elevated energy content in the fecal matter. As shown in Fig. 3.6 B, fecal energy content is unchanged. Similarly, body temperature is unaltered between groups (Fig. 3.6 C). Thus, it is unlikely that altered energy uptake or clearance is responsible for the body weight phenotype. However, energy expenditure was significantly increased in Hsp60$^{+/-}$ mice both during the active and resting phase, respectively (Fig. 3.7 A-C). Furthermore, this increase is independent of lean mass, as the usual positive correlation between lean mass and energy expenditure is abolished in Hsp60$^{+/-}$ mice (Fig. 3.8 A and B), indicating a role for the adipose tissue in the elevated energy expenditure.

Reducing the folding capacity through a reduction of the mitochondrial chaperone system has been shown to lead to an accumulation of unfolded proteins in yeast (Craig *et al.*, 1987; Ostermann *et al.*, 1989), and arguably in mammals as well, which in turn can lead to mitochondrial dysfunction (Voos, 2013). Taking together the reduction of basal and maximal mitochondrial respiration (Fig. 3.20 A and B), the induction of antioxidant protein GPx1, and elevated protein carbonylation (Fig. 3.20 C) indicates the presence of substantial mitochondrial dysfunction in the gWAT of Hsp60$^{+/-}$ mice. As damaged mitochondria are degraded through macroautophagy, it is possible that these processes are induced in the gWAT of Hsp60$^{+/-}$ mice. To gain more insight into the specific changes in the gWAT of Hsp60$^{+/-}$ mice, a transcriptomic analysis using a microarray format was performed.

Interestingly, analysis of the 706 significantly upregulated genes regarding gene ontology enrichment, the macroautophagy process was shown to be induced in the gWAT of heterozygous mice (Figs. 3.23 and 3.24). Warranting further analysis, probing for activated AMPK or Beclin 1 in a Western Blot of the gWAT of Ctrl and Hsp60$^{+/-}$ mice did not show an increase in either protein's activation (data not shown). Following the autophagy signaling pathway downstream, the gWAT of Hsp60$^{+/-}$ mice displays significant increases in LC3-I and LC3-II protein levels. One complicating factor in accurately assessing autophagic processes is that all proteins that are involved in the activation or formation of the autophagolysosome will be degraded along with the targeted cell components (Mizushima *et al.*, 2007). A siRNA mediated knockdown of *Hsp60* by $\sim$ 50 % in 3T3-L1 fibroblasts (Hsp60KD) and incubation with Neutral Red, a dye that incorporates into active lysosomes (Winckler, 1974), was used as an approximation of lysosomal activity. This showed a two-fold increase in Neutral Red absorption in Hsp60KD cells, indicating an increased presence of active lysosomes. Further, direct measurements of lysosomal activity in non-denatured protein lysates of gWAT samples mice showed an almost two-fold increase in lysosomal activity in Hsp60$^{+/-}$ mice. Taken together, the combination of transcriptomic data, and both indirect and direct indications for increased lysosomal activity, strongly suggests the presence of substantial autophagic processes in the gWAT of HFD-fed Hsp60$^{+/-}$ mice.

There exists an interesting connection of the induction of autophagy and the above mentioned upregulation of GLUT8 in the gWAT of Hsp60$^{+/-}$ mice. The to date available evidence suggests a primarily intracellular localization of GLUT8 at lysosomal compartments (Augustin *et al.*, 2005; Schmidt *et al.*, 2009). This is supported by both the presence of a targeting motif in the GLUT8 sequence, as well as co-localization and subcellular fractionation experiments. Following this, GLUT8 might play a role in shuttling glucose from the lysosome to other intracellular compartments. However, recent findings in hepatocytes suggest a role for GLUT8 in the induction of autophagy as well. (Mayer *et al.*, 2016). Here, knockdown of GLUT8 leads to resistance against AMPK-activated autophagy and also decreased basal [^{14}C]-DOG uptake. This latter point specifically supports the possibility of GLUT8 compensating the glucose uptake for the decrease in insulin-dependent GLUT4 translocation in Hsp60$^{+/-}$ mice. It needs to be pointed out, that GLUT8 translocation – if indeed present in Hsp60$^{+/-}$ – could be consequence of the induction of autophagy as mentioned above. Following this, the increase in basal glucose uptake in Hsp60$^{+/-}$ mice is then a by-product of the

requirements of the autophagic process, rather than a compensatory mechanism of GLUT4 translocation failure due to insulin resistance.

4.7 Phenotypic specificity in the gWAT

One remaining question is why the here presented changes in adipose tissue function are specific to the gonadal WAT, as for example the adiponectin-controlled TFAM knockout and the whole-body Clpp knockout showed the same phenotype in both gWAT and scWAT (Vernochet *et al.*, 2014; Becker *et al.*, 2018). On the other hand, over expression of CDGSH iron sulfur domain 1 protein (mitoNEET) in ob/ob mice led to adipocyte hyperplasia specifically in the scWAT (Kusminski *et al.*, 2012). Analyzing the scWAT of Hsp60$^{+/-}$ reveals the same morphological changes as found in the gWAT, *i.e.* smaller and more numerous adipocytes, as the gWAT (Appendix Fig. A.6 A). However, the scWAT does not show increased oxidative damage, and consequently no decrease in insulin sensitivity compared to Ctrl (Appendix Fig. A.6 B and C). As these parameters were only altered in gWAT, none of the further experiments (transcriptomics, mitochondrial function, glucose uptake, or lysosomal activity) were performed in the scWAT, precluding definitive statements about possible changes of these characteristics. It has been suggested that gWAT possesses more plasticity than scWAT, and could therefore be more susceptible to detrimental changes in adipogenic potential (Wang *et al.*, 2013; S. M. Kim *et al.*, 2014). The authors demonstrate how reduced adipogenic capacity is correlated with insulin resistance, and that this effect is more pronounced in gWAT than scWAT. Following this, the substantial defects in mitochondrial function in Hsp60$^{+/-}$ mice could lead to reduced adipogenic potential and thus rendering the gWAT more susceptible to insulin resistance. Mitochondrial dysfunction connects to local insulin resistance though a chronic increase in reactive oxygen species leading to oxidative stress (Frohnert *et al.*, 2013; Fedorova *et al.*, 2014). ROS derived from dysfunctional mitochondria has been shown to induce local insulin resistance *via* a mechanism involving IKKβ, PKCθ and JNK to suppress IRS activation (Tiganis, 2011). Thus, increased oxidative stress in the gWAT can help explain the presence of local insulin resistance. Oxidative stress is often linked to inflammation, by integration of the aforementioned signaling pathways into inflammatory responses (Hotamisligil, 2010). However, there are no indications of increased inflammation in the gWAT of Hsp60$^{+/-}$ mice. Simultaneously, neither induction in activity of

JNK or IKK, nor immunohistological evidence of inflammation are present in Hsp60$^{+/-}$ mice (data not shown). Autophagy has been shown to suppress inflammatory responses by inhibiting cytokine production (*e.g.* IL1β, IFN1), by IL1β degradation in the autophagosome, as well as through direct inhibition of the inflammasome (Jansen *et al.*, 2012; Shibutani *et al.*, 2015; Matsuzawa-Ishimoto *et al.*, 2018; Clemente-Postigo *et al.*, 2020). Additionally, inhibition of autophagy leads to adipocyte hypertrophy and WAT inflammation (Saitoh *et al.*, 2008; Müller *et al.*, 2013). Therefore, the enhanced autophagy in Hsp60$^{+/-}$ mice could act protective against a further increase in diet-and oxidative stress-induced WAT inflammation.

4.8 Sex specific effects of a HSP60 reduction

A reduction in HSP60 affects metabolism in a sex-specific manner. In opposition to males, female Hsp60$^{+/-}$ mice show an increase in body weight after HFD feeding, due to an increase in lean mass, specifically muscle mass (Fig. 3.14 A-D). This is accompanied by a decrease in energy expenditure, and the positive correlation between energy expenditure and lean mass is indeed still significant (Fig. 3.17 A-D), again as opposed to male Hsp60$^{+/-}$ mice. Although not explicitly analyzed during this work, one can speculate about the presence of some degree of mitochondrial dysfunction in the skeletal muscle of female Hsp60$^{+/-}$ mice. Inducible deletion of HSP60 in cardiomyocytes (targeted *via* a Myosin heavy chain, α isoform (MHCα-*Cre*)) led to substantial mitochondrial dysfunction, oxidative stress and subsequent heart failure in mice (Fan *et al.*, 2020). Interestingly, mirroring the results for female Hsp60$^{+/-}$ mice presented here, the authors demonstrate a dose-dependent heart hypertrophy, where heart morphology deteriorated with the progressive depletion of HSP60.

For the skeletal muscle it seems counter intuitive that a HSP60 reduction should lead to muscle growth, as mitochondrial dysfunction is usually associated with skeletal muscle atrophy (Schiaffino *et al.*, 2013; Romanello *et al.*, 2016; Sartori *et al.*, 2021). On the other hand, a low-grade mitochondrial dysfunction could lead to constitutively increased generation of reactive oxygen species (ROS). Low-grade ROS signaling has been shown to induce muscle adaptation and hypertrophy *in vitro* through hydrogen peroxide treatment and in humans through endurance and resistance training. Further, this effect can be abolished by anti-oxidant application (Powers *et al.*, 2010). It is interesting to speculate whether the reduction of HSP60 leads to a switch in fiber types in the skeletal muscle through a decrease

of functional mitochondria. Type I slow twitch, oxidative muscle fibers are crucially dependent on functioning mitochondria (Schiaffino *et al.*, 2011). Further, experimental induction of mitochondrial dysfunction through depletion of mitochondrial DNA leads to an increase of glycolytic type II fibers (Venhoff *et al.*, 2012). Coincidentally, glycolytic type II fibers store more glycogen, leading to an increase in stored water, which is the main driver of skeletal muscle hypertrophy in high resistance training (B. Egan *et al.*, 2013; Hawley *et al.*, 2014). Therefore type II fibers are generally heavier than type I fibers, which could explain increased muscle mass in female Hsp60$^{+/-}$ mice.

Interestingly, the white adipose tissue recapitulates the phenotype of male Hsp60$^{+/-}$ mice, with smaller and more numerous adipocytes (Fig. 3.18 A-C). Opposed to the male Hsp60$^{+/-}$ mice, this did not lead to alterations in insulin sensitivity in female $^{+/-}$ mice, although they did have lower fasting glycemia, but no alterations in other determinants of insulin sensitivity (*e.g.* ITT, GTT, HOMA-IR, Matsuda index). Further, why this is selectively increased in female mice remains to be elucidated. It is however recognized that a strong sex-dependent effect of insulin resistance and diabetes prevalence exists, where in both humans and animal models females are generally more protected from diet-induced obesity and accompanying pathologies (Kautzky-Willer *et al.*, 2016). The Non-Communicable Disease (NCD) Risk Factor Collaboration showed in an age-standardized analysis of 751 population based studies, that the diabetes prevalence between 1980 and 2014 increased more markedly in men (4 % to 9 %) than in women (5 % to 8 %) (NCD Risk Factor Collaboration (NCD-RisC), 2016). Similarly, the International Diabetes Federation published their global estimates for 2019 and the results indicate a sex difference for diabetes prevalence (9.1 % in women *vs.* 9.6 % in men). Worldwide, this suggests that as of 2019, around 38.5 million more men than women are living with diabetes (Saeedi *et al.*, 2019). Female sex hormones have been shown in clinical and experimental research to influence this disparity. Thus, loss of endogenous estrogen after menopause negatively impacts both body composition and glucose homeostasis (Mauvais-Jarvis *et al.*, 2013). Further, estrogen therapy compared to placebo in post-menopausal women shows an up to 35 % reduction in diabetes incidence (Kanaya *et al.*, 2003; Margolis *et al.*, 2004). In mice, lack of the estrogen receptor α (ERα) renders females prone to DIO (Handgraaf *et al.*, 2013). Similarly, estrogen depletion by ovariectomy abolishes the usual protection from DIO and hyperglycemia, which can be reverted by estrogen treatment (Vogel *et al.*, 2013; Riant *et al.*, 2009).

In the work presented here, although female Hsp60$^{+/-}$ mice have increased body weight after HFD feeding, they do not show an increase in adiposity, as this increase is due to increased muscle mass. Accordingly, the lack of decreased insulin sensitivity in WAT of female Hsp60$^{+/-}$ mice could be due to a lack of adiposity in female mice generally. The fact that the protection of diet-induced WAT hypertrophy is the same in female and male mice suggests that this specific phenotype might be independent of estrogen signaling. Importantly however, while ovariectomy of Hsp60$^{+/-}$ mice did lead to a loss of the increased body weight phenotype (average final weight: OVX Ctrl = 40.3 g *vs.* OVX Hsp60$^{+/-}$ = 40.2 g), it did not recapitulate the male phenotype of a decrease in fat mass (Appendix Fig. A.7 A and B). Therefore, estrogen regulation is probably not the exclusive determinant of the sex-specific phenotype in regards to body weight and body composition described here.

4.9 Summary and Conclusion

This *in vitro* and *in vivo* study presents a comprehensive metabolic phenotyping of both female and male Hsp60$^{+/-}$ mice as a model of impaired mitochondrial proteostasis on both lean and DIO conditions, as well as providing insights on the influence of a reduction of HSP60 on organ-specific and systemic metabolism. While lean Hsp60$^{+/-}$ mice did only show a slightly elevated energy expenditure, and an interesting fertility deficiency in males, subjecting these mice to high-fat diet feeding resulted in a variety of sex-independent, as well as sex-specific effects.

Female Hsp60$^{+/-}$ mice after 16 weeks of HFD have higher body weight through increased skeletal muscle mass and decreased energy expenditure. Although the adipose tissue also shows decreased adipocyte hypertrophy, they do not display alterations in either local or whole-body insulin sensitivity.

Male Hsp60$^{+/-}$ mice, on the other hand, are protected from DIO through increased energy expenditure and reduced fat mass. They also show reduced gWAT adipocyte hypertrophy, but improved systemic insulin sensitivity by calculation of insulin resistance and sensitivity indices. Simultaneously however, the presence of mitochondrial dysfunction and local insulin resistance indicates functional impairment of the gWAT. Indeed, insulin-stimulated glucose uptake and differentiation capacity is decreased in Hsp60$^{+/-}$ mice. This coincides with an increase in basal glucose uptake, possibly involving GLUT8, a decrease in mitochondrial respiration, and a compensatory upregulation of macroautophagy.

The work presented here shows the importance of HSP60 as a regulator of mitochondrial proteostasis that curiously has the largest impact on adipocyte function. It highlights that apparently beneficial seeming changes in tissue morphology do not need to coincide with positive tissue functions but can still lead to the improvement of commonly used indicators of obesity and insulin resistance. Thus, careful interpretation of results as well as vigilant testing of working hypotheses derived from them through use of *in vitro* and *in vivo* methods is needed to approach an understanding of the interplay between mitochondrial, tissue-specific, and whole-body metabolism.

One further difficulty lies partially in the fact that mitochondrial dysfunctions as a general term seems ever more inappropriate. Mouse models of mitochondrial dysfunction, even

within the same target tissue, show a large variety of phenotypes, depending on the specific site of disturbance, such as the ETC complexes, protein quality control, mitochondrial dynamics, or detoxification capacity. This is further complicated by a lack of data or reporting regarding sex-specific effects in the literature, which have been shown here to have a major impact on the interaction of mitochondrial function and metabolism, even leading to opposing phenotypes.

In conclusion, impairment of HSP60 expression, as it is found in obesity and diabetes in mice and humans, leads to adipose tissue specific deterioration of mitochondrial metabolism and an unexpected protection against diet-induced obesity in males, with indications of improved whole-body insulin sensitivity in female and male mice. Nevertheless, HSP60 reduction will lead to neurodegeneration in mouse and humans, and, as shown here, reduced fertility. WAT specific HSP60 reduction might thus be a short-term beneficial adaptation to diet-induced adipocyte failure through upregulation of autophagy and insulin-independent glucose uptake (Fig. 4.1).

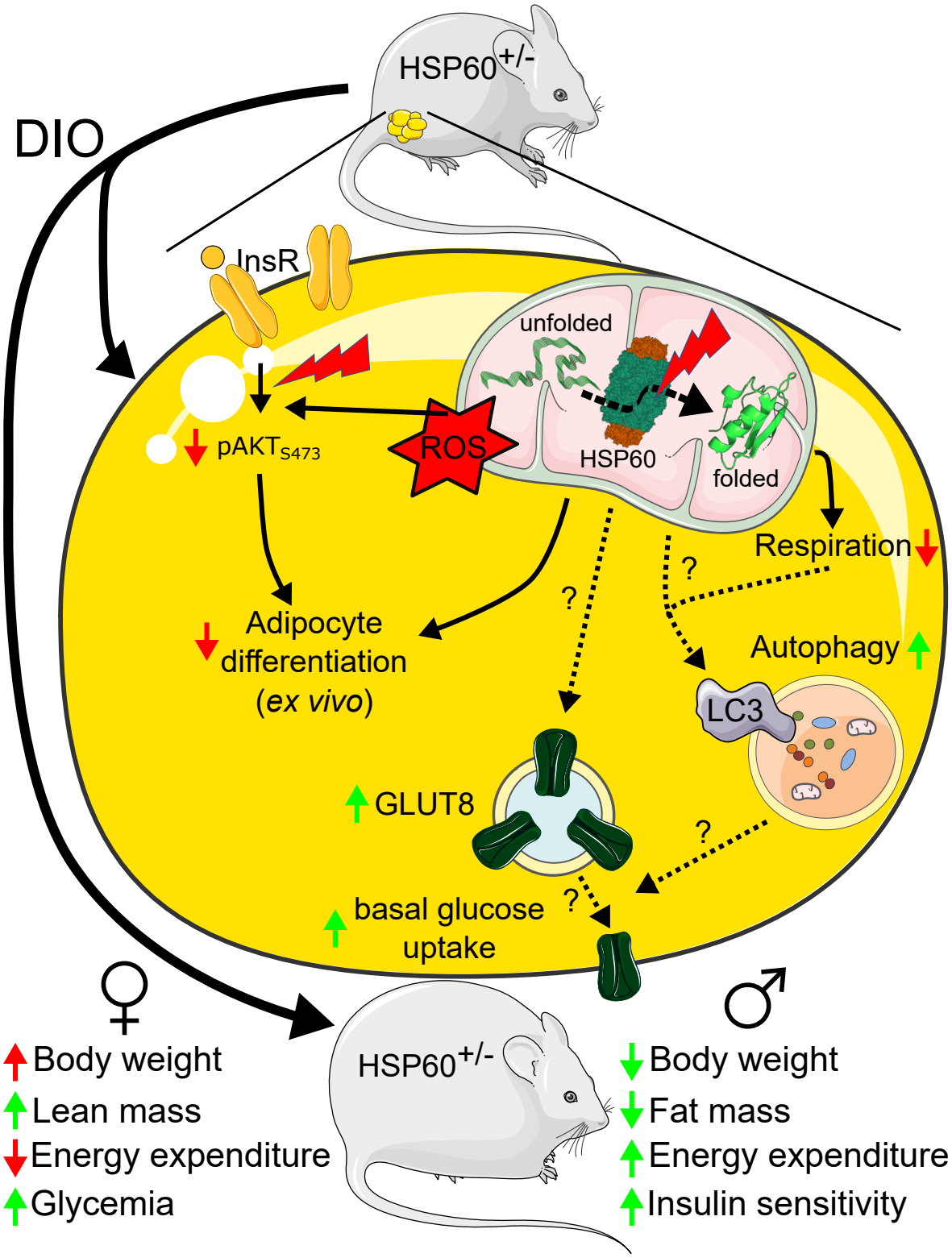

Figure 4.1: Proposed model of the impact of an HSP60 reduction adipocyte function and sex-specific metabolic phenotype in DIO.
In Hsp60$^{+/-}$ WAT, mitochondrial respiration is reduced and ROS production increased. Following, insulin stimulated AKT phosphorylation, as well as adipocyte differentiation (*ex vivo* are impaired, autophagy is increased. Basal glucose uptake is elevated, possibly *via* action of GLUT8. Overall, HSP60 reduction leads to an opposing impact on body weight, body composition, and energy expenditure, while both female and male Hsp60$^{+/-}$ mice show signs of protection from diet-induced insulin resistance. **---** hypothetical interaction, **—** interaction supported by data presented in this thesis.

Additional figures

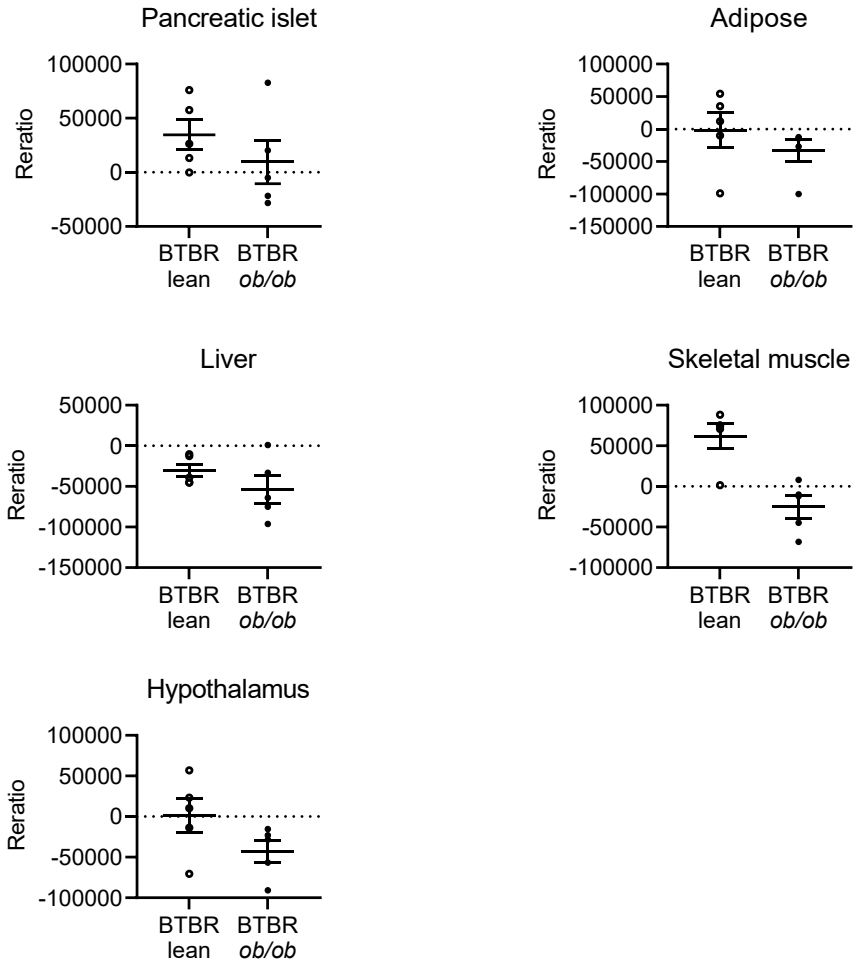

Figure A.1: Reduction of *Hsp60* gene expression in a variety of tissues in obese and diabetic mice.

Comparison of Hsp60 gene expression between lean BTBR and obese and diabetic *ob/ob* BTBR mice. Data extracted from the Attie Lab database

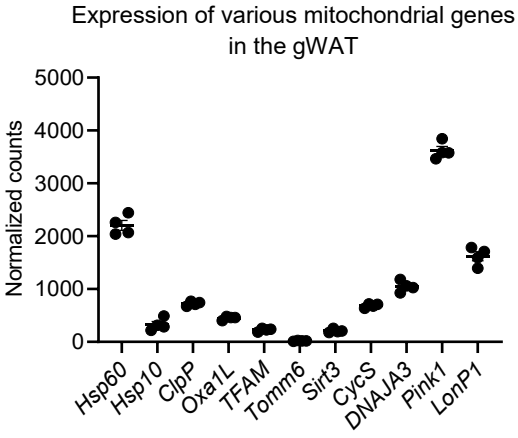

Figure A.2: Expression of various mitochondrial genes in the gWAT of 6 months old mice.
Data are extracted from the publicly available *Tabula muris senis*. All data are presented as mean ± SEM.

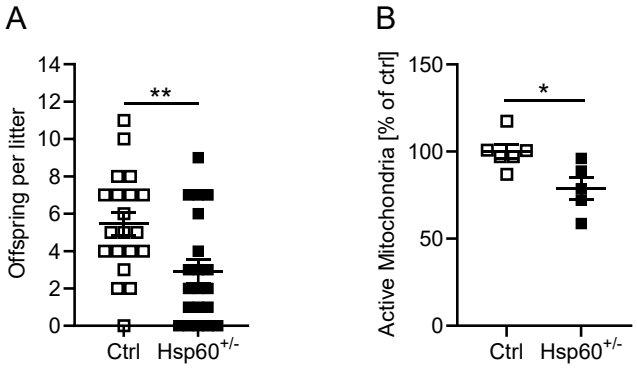

Figure A.3: Impaired fertility of male Hsp60$^{+/-}$ mice.
A: Offspring distribution in litters from C57Bl/6N females and Hsp60$^{+/-}$ males. **B:** Percentage of active mitochondria after FACS in sperm cells of Hsp60$^{+/-}$ males. * $P < 0.05$, and ** $P < 0.01$ after 2-tailed Student's *t* test. All data are presented as mean ± SEM.

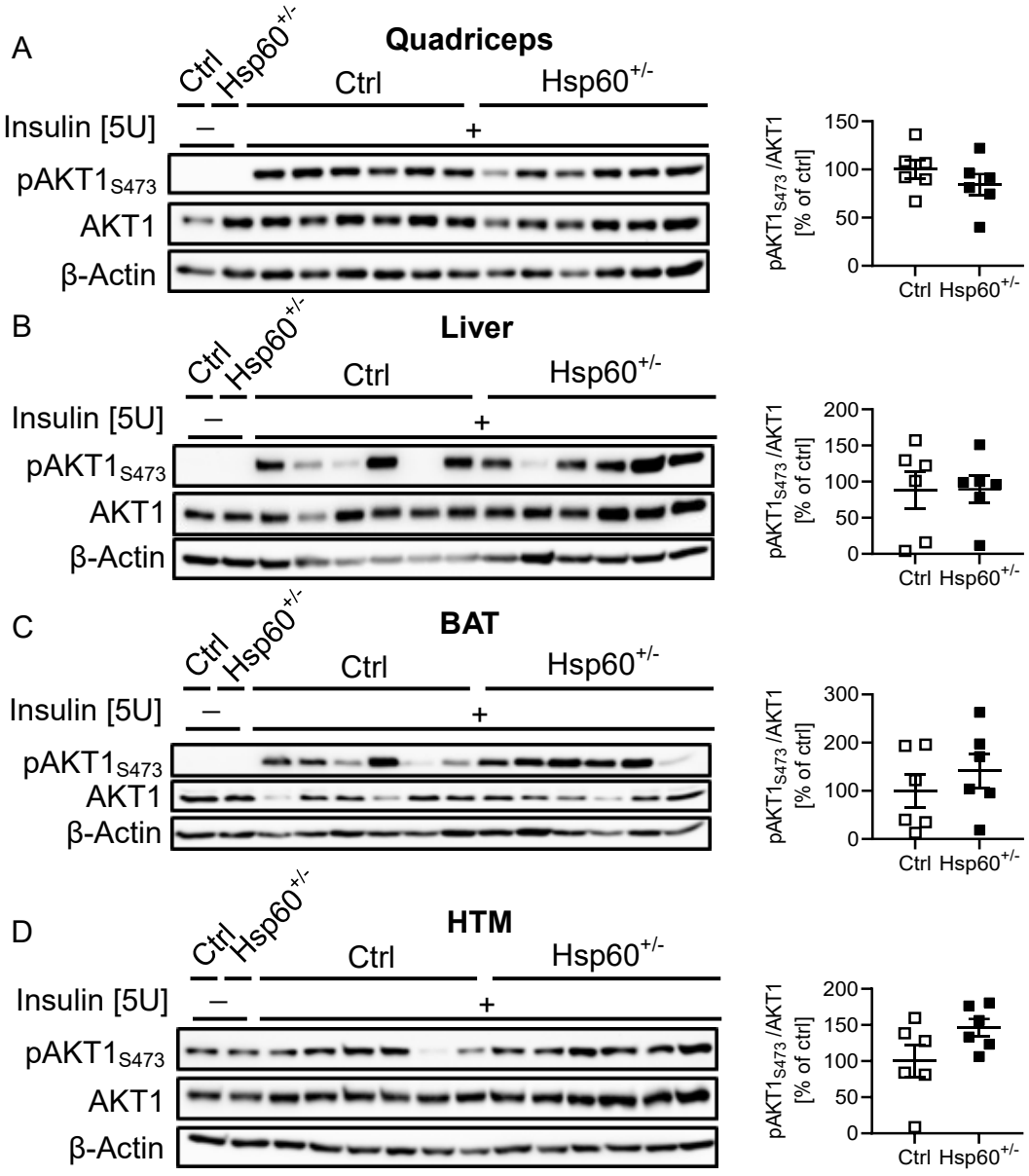

Figure A.4: No differences in local insulin sensitivity in male Ctrl and Hsp60$^{+/-}$ mice fed a HFD.

A-D: Western Blot and densitometric analysis of insulin stimulated phosphorylation of AKT1$_{S473}$ in quadriceps (A), liver (B), brown adipose tissue (BAT, C), and hypothalamus (HTM, D). All data are presented as mean ± SEM.

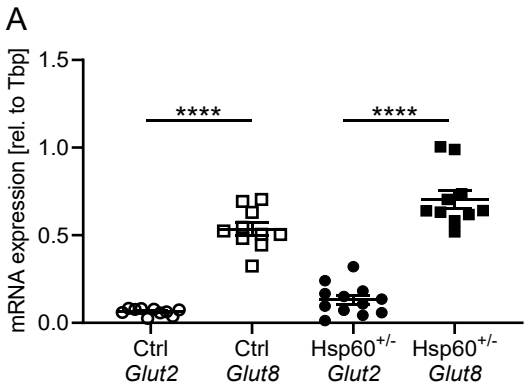

Figure A.5: Comparing *Glut2* and *Glut8* expression in the gWAT of HFD-fed male mice.

A: Relative mRNA expression of *Glut2* and *Glut8* in the gWAT of male mice after 16 weeks of HFD. **** $P < 0.0001$ after 2-tailed Student's *t* test. All data are presented as mean $\pm$ SEM.

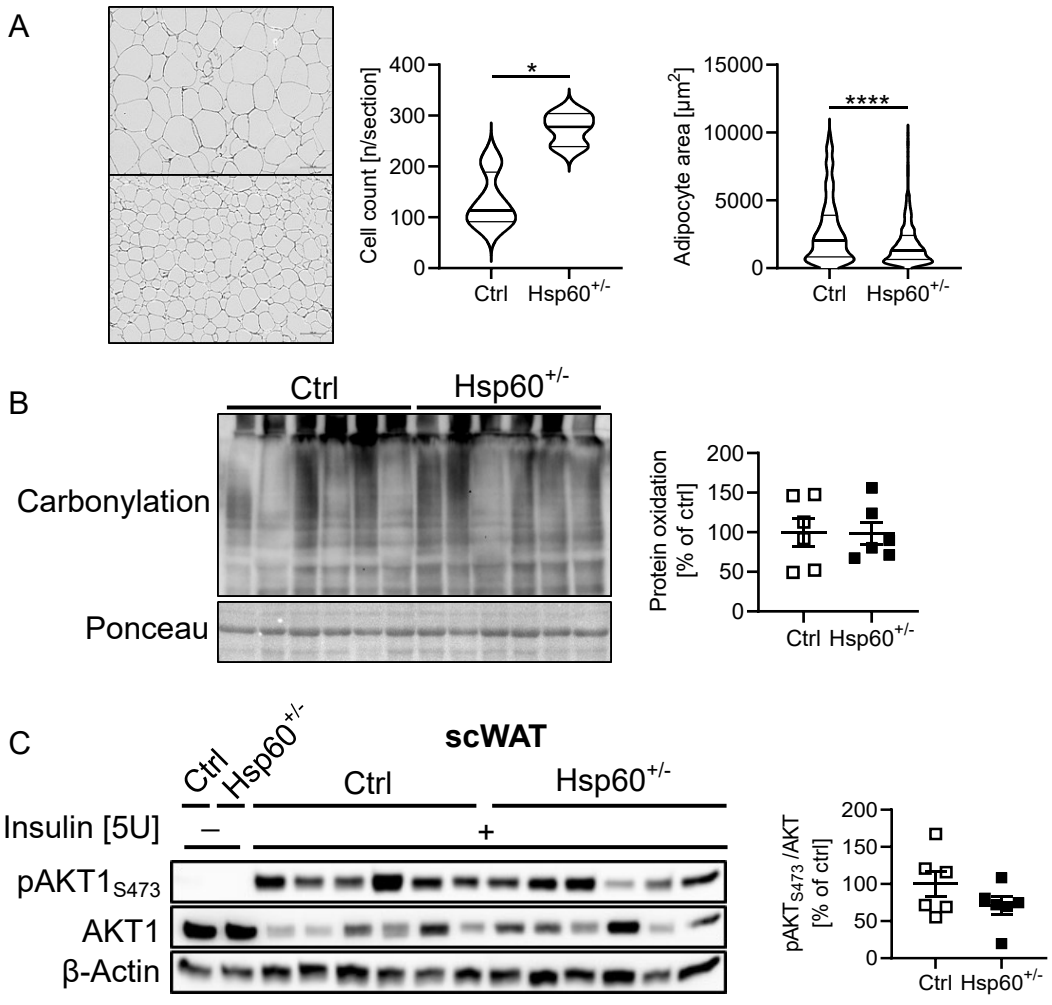

Figure A.6: Subcutaneous white adipose tissue shows comparable morphology without impaired insulin sensitivity in male mice fed a HFD.
A: Representative hematoxylin and eosin stain of histological section of the gWAT of Ctrl and Hsp60$^{+/-}$, as well as cell count and average size of adipocytes in scWAT sections of mice after 16 weeks of HFD. **C:** Western Blot and densitometric analysis of insulin stimulated phosphorylation of AKT1$_{S473}$ in the scWAT after *vena cava* injection of insulin. All data are presented as mean ± SEM.

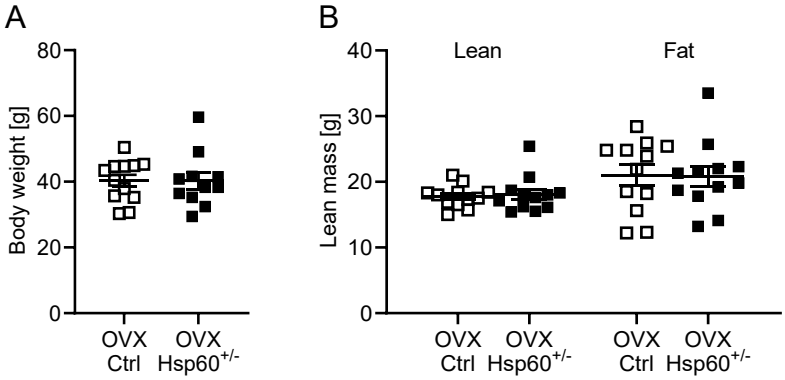

Figure A.7: Ovariectomized Hsp60$^{+/-}$ mice partially lose their metabolic phenotype.

A: Final body weight of ovariectomized (OVX) Ctrl and Hsp60$^{+/-}$ after 16 weeks of HFD. **B:** Body composition of ovariectomized (OVX) Ctrl and Hsp60$^{+/-}$ as measured *via* NMR after 14 weeks of HFD. All data are presented as mean $\pm$ SEM.

ImageJ Fiji macro for adipocyte analysis

```
// Macro for the characterisation of adipocytes
// Input : histological RGB tif
// Output : Result image + cell number + cell areas + % of total surface area
// Antoine Leboucher Equipe Bardoni Février 2015 IJ v1.49o
// modified and translated by Robert Hauffe April 2017 IJ v1.51k

// General initialisation-----------------------------------------------

run("Set Measurements...", "area area_fraction redirect=None decimal=2");
run("Colors...", "foreground=white background=black selection=yellow");
run("Options...", "iterations=1 count=1 edm=Overwrite");

Dialog.create("Analyse Adipocytes");
Dialog.addNumber("Size of a pixel (µm):",0.35);
Dialog.addNumber("Exclusion threshold for objects (µm2):",100);
Dialog.addNumber("Threshold for roundness of objects :",0);
Dialog.show();
scale=Dialog.getNumber();
threshold=Dialog.getNumber();
circ=Dialog.getNumber();

do {
dir=getDirectory("Folder containing original tif images");
dires=getDirectory("Folder to store results");
if (dires==dir) showMessage("Try again","Choose different folder");
}
while (dires==dir);
list = getFileList(dir);

for (f=0; f<list.length; f++) {
run("Clear Results");
setKeyDown("none");
```

```
open(dir+list[f]);
file=getTitle();
i=indexOf(file, ".tif");
file_trunc=substring(file, 0, i);
run("Split Channels");
waitForUser("Delete images with lowest contrasts and click OK");
run("Properties...", "channels=1 slices=1 frames=1 unit=microns



 pixel_width="+scale+" pixel_height="+scale+" voxel_depth=1");
rename("image");
run("Duplicate...", "title="+file_trunc);
run("Subtract Background...", "rolling=20 light");
run("Find Edges");
//run("Threshold...");
setAutoThreshold("Triangle");
waitForUser("Choose threshold of cytoplasm and click OK");
run("Convert to Mask");
run("Fill Holes");
run("Analyze Particles...", "size="+threshold+"-Infinity circularity=



 "+circ+"-1.00 show=Outlines display clear summarize");
run("Invert");
rename("Result");
selectWindow(file_trunc);close();
selectWindow("image");
run("Invert");
imageCalculator("Add", "image","Result");
saveAs("Tiff", ""+dires+"Res_"+file_trunc);
selectWindow("Results");
saveAs("Results", ""+dires+file_trunc+".xls");
run("Close All");
}
name=getString("Name of the file of all the results : ","Analyses_Adipocytes");
selectWindow("Summary");
saveAs("Results", ""+dires+name+".xls");
```

Bibliography

Agsteribbe, E., A. Huckriede, M. Veenhuis, M. H. J. Ruiters, K. E. Niezenkoning, O. H. Skjeldal, K. Skullerud, R. S. Gupta, R. Hallberg, O. P. Vandiggelen, and H. R. Scholte (1993). "A Fatal, Systemic Mitochondrial Disease with Decreased Mitochondrial Enzyme Activities, Abnormal Ultrastructure of the Mitochondria and Deficiency of Heat Shock Protein 60". en. In: *Biochemical and Biophysical Research Communications* 193.1, pp. 146–154. issn: 0006-291X. doi: 10.1006/bbrc.1993.1602.

Ahmadian, M., J. M. Suh, N. Hah, C. Liddle, A. R. Atkins, M. Downes, and R. M. Evans (2013). "PPARγ Signaling and Metabolism: The Good, the Bad and the Future". en. In: *Nature Medicine* 19.5, pp. 557–566. issn: 1546-170X. doi: 10.1038/nm.3159.

Ajluni, N., R. Meral, A. H. Neidert, G. F. Brady, E. Buras, B. McKenna, F. DiPaola, T. L. Chenevert, J. F. Horowitz, C. Buggs-Saxton, A. R. Rupani, P. E. Thomas, M. K. Tayeh, J. W. Innis, M. B. Omary, H. Conjeevaram, and E. A. Oral (2017). "Spectrum of Disease Associated with Partial Lipodystrophy: Lessons from a Trial Cohort". en. In: *Clinical Endocrinology* 86.5, pp. 698–707. issn: 1365-2265. doi: 10.1111/cen.13311.

Albers, D. S. and M. Flint Beal (2000). "Mitochondrial Dysfunction and Oxidative Stress in Aging and Neurodegenerative Disease". In: *Advances in Dementia Research*. Ed. by K. Jellinger, R. Schmidt, and M. Windisch. Vienna: Springer Vienna, pp. 133–154. isbn: 978-3-7091-6781-6.

Alessi, D. R., M. Andjelkovic, B. Caudwell, P. Cron, N. Morrice, P. Cohen, and B. A. Hemmings (1996). "Mechanism of Activation of Protein Kinase B by Insulin and IGF-1." In: *The EMBO Journal* 15.23, pp. 6541–6551. issn: 0261-4189. doi: 10.1002/j.1460-2075.1996.tb01045.x.

Alzheimer's-Association (2018). "2018 Alzheimer's Disease Facts and Figures". en. In: *Alzheimer's & Dementia* 14.3, pp. 367–429. issn: 1552-5260. doi: 10.1016/j.jalz.2018.02.001.

Augustin, R., J. Riley, and K. H. Moley (2005). "GLUT8 Contains a [DE]XXXL[LI] Sorting Motif and Localizes to a Late Endosomal/Lysosomal Compartment". en. In: *Traffic* 6.12, pp. 1196–1212. issn: 1600-0854. doi: 10.1111/j.1600-0854.2005.00354.x.

Badman, M. K. and J. S. Flier (2007). "The Adipocyte as an Active Participant in Energy Balance and Metabolism". English. In: *Gastroenterology* 132.6, pp. 2103–2115. issn: 0016-5085, 1528-0012. doi: 10.1053/j.gastro.2007.03.058.

Baerga, R., Y. Zhang, P.-H. Chen, S. Goldman, and S. V. Jin (2009). "Targeted Deletion of Autophagy-Related 5 (Atg5) Impairs Adipogenesis in a Cellular Model and in Mice". In: *Autophagy* 5.8, pp. 1118–1130. issn: 1554-8627. doi: 10.4161/auto.5.8.9991.

Bambace, C., M. Telesca, E. Zoico, A. Sepe, D. Olioso, A. Rossi, F. Corzato, V. Di Francesco, A. Mazzucco, F. Santini, and M. Zamboni (2011). "Adiponectin Gene Expression and Adipocyte Diameter: A Comparison between Epicardial and Subcutaneous Adipose Tissue in Men". en. In: *Cardiovascular Pathology* 20.5, e153–e156. issn: 1054-8807. doi: 10.1016/j.carpath.2010.07.005.

Becker, C., A. Kukat, K. Szczepanowska, S. Hermans, K. Senft, C. P. Brandscheid, P. Maiti, and A. Trifunovic (2018). "CLPP Deficiency Protects against Metabolic Syndrome but

Hinders Adaptive Thermogenesis". In: *EMBO reports* 19.5, e45126. issn: 1469-221X. doi: 10.15252/embr.201745126.

Bennett, A. W. (1872). "The Origin of Species by Means of Natural Selection; or the Preservation of Favoured Races in the Struggle for Life". en. In: *Nature* 5.121, pp. 318–319. issn: 1476-4687. doi: 10.1038/005318a0.

Berger, E., E. Rath, D. Yuan, N. Waldschmitt, S. Khaloian, M. Allgäuer, O. Staszewski, E. M. Lobner, T. Schöttl, P. Giesbertz, O. I. Coleman, M. Prinz, A. Weber, M. Gerhard, M. Klingenspor, K.-P. Janssen, M. Heikenwalder, and D. Haller (2016). "Mitochondrial Function Controls Intestinal Epithelial Stemness and Proliferation". In: *Nature Communications* 7, p. 13171. issn: 2041-1723. doi: 10.1038/ncomms13171.

Berridge, M. V. and A. S. Tan (1993). "Characterization of the Cellular Reduction of 3-(4,5-Dimethylthiazol-2-Yl)-2,5-Diphenyltetrazolium Bromide (MTT): Subcellular Localization, Substrate Dependence, and Involvement of Mitochondrial Electron Transport in MTT Reduction". en. In: *Archives of Biochemistry and Biophysics* 303.2, pp. 474–482. issn: 0003-9861. doi: 10.1006/abbi.1993.1311.

Bhaskaran, S., G. Pharaoh, R. Ranjit, A. Murphy, S. Matsuzaki, B. C. Nair, B. Forbes, S. Gispert, G. Auburger, K. M. Humphries, M. Kinter, T. M. Griffin, and S. S. Deepa (2018). "Loss of Mitochondrial Protease ClpP Protects Mice from Diet-Induced Obesity and Insulin Resistance". In: *EMBO reports* 19.3, e45009. issn: 1469-221X. doi: 10.15252/embr.201745009.

Bie, A. S., P. Fernandez-Guerra, R. I. D. Birkler, S. Nisemblat, D. Pelnena, X. Lu, J. L. Deignan, H. Lee, N. Dorrani, T. J. Corydon, J. Palmfeldt, L. Bivina, A. Azem, K. Herman, and P. Bross (2016). "Effects of a Mutation in the HSPE1 Gene Encoding the Mitochondrial Co-Chaperonin HSP10 and Its Potential Association with a Neurological and Developmental Disorder". English. In: *Frontiers in Molecular Biosciences* 3. issn: 2296-889X. doi: 10.3389/fmolb.2016.00065.

Bie, A. S., C. Cömert, R. Körner, T. J. Corydon, J. Palmfeldt, M. S. Hipp, F. U. Hartl, and P. Bross (2020). "An Inventory of Interactors of the Human HSP60/HSP10 Chaperonin in the Mitochondrial Matrix Space". en. In: *Cell Stress and Chaperones* 25.3, pp. 407–416. issn: 1466-1268. doi: 10.1007/s12192-020-01080-6.

Blüher, M., M. Michael, O. D. Peroni, K. Ueki, N. Carter, B. B. Kahn, and C. Kahn (2002). "Adipose Tissue Selective Insulin Receptor Knockout Protects against Obesity and Obesity-Related Glucose Intolerance". In: *Developmental Cell* 3.1, pp. 25–38. issn: 15345807. doi: 10.1016/S1534-5807(02)00199-5.

Borenfreund, E. and J. A. Puerner (1985). "Toxicity Determined in Vitro by Morphological Alterations and Neutral Red Absorption". en. In: *Toxicology Letters* 24.2, pp. 119–124. issn: 0378-4274. doi: 10.1016/0378-4274(85)90046-3.

Boucher, J., S. Softic, A. El Ouaamari, M. T. Krumpoch, A. Kleinridders, R. N. Kulkarni, B. T. O'Neill, and C. R. Kahn (2016). "Differential Roles of Insulin and IGF-1 Receptors in Adipose Tissue Development and Function". eng. In: *Diabetes* 65.8, pp. 2201–2213. issn: 1939-327X. doi: 10.2337/db16-0212.

Briones, P., M. A. Vilaseca, A. Ribes, A. Vernet, M. Lluch, V. Cusi, A. Huckriede, and E. Agsteribbe (1997). "A New Case of Multiple Mitochondrial Enzyme Deficiencies with Decreased Amount of Heat Shock Protein 60". en. In: *Journal of Inherited Metabolic Disease* 20.4, pp. 569–577. issn: 1573-2665. doi: 10.1023/A:1005303008439.

Bross, P., Z. Li, J. Hansen, J. J. Hansen, M. N. Nielsen, T. J. Corydon, C. Georgopoulos, D. Ang, J. B. Lundemose, K. Niezen-Koning, H. Eiberg, H. Yang, S. Kølvraa, L. Bolund, and N. Gregersen (2007). "Single-Nucleotide Variations in the Genes Encoding the Mitochondrial Hsp60/Hsp10 Chaperone System and Their Disease-Causing Potential." In: *Journal of human genetics* 52.1, pp. 56–65. issn: 1434-5161. doi: 10.1007/s10038-006-0080-7.

Bruder-Nascimento, T., T. C. Kress, and E. J. Belin de Chantemele (2019). “Recent Advances in Understanding Lipodystrophy: A Focus on Lipodystrophy-Associated Cardiovascular Disease and Potential Effects of Leptin Therapy on Cardiovascular Function”. en. In: *F1000Research* 8, p. 1756. issn: 2046-1402. doi: 10.12688/f1000research.20150.1.

Brüning, J. C., D. Gautam, D. J. Burks, J. Gillette, M. Schubert, P. C. Orban, R. Klein, W. Krone, D. Müller-Wieland, and C. R. Kahn (2000). “Role of Brain Insulin Receptor in Control of Body Weight and Reproduction”. en. In: *Science* 289.5487, pp. 2122–2125. issn: 0036-8075, 1095-9203. doi: 10.1126/science.289.5487.2122.

Calzadilla, P., D. Sapochnik, S. Cosentino, V. Diz, L. Dicelio, J. C. Calvo, and L. N. Guerra (2011). “N-Acetylcysteine Reduces Markers of Differentiation in 3T3-L1 Adipocytes”. en. In: *International Journal of Molecular Sciences* 12.10, pp. 6936–6951. doi: 10.3390/ijms12106936.

Chadt, A. and H. Al-Hasani (2020). “Glucose Transporters in Adipose Tissue, Liver, and Skeletal Muscle in Metabolic Health and Disease”. en. In: *Pflügers Archiv - European Journal of Physiology* 472.9, pp. 1273–1298. issn: 1432-2013. doi: 10.1007/s00424-020-02417-x.

Cheng, M. Y., F.-U. Hartl, J. Martin, R. A. Pollock, F. Kalousek, W. Neuper, E. M. Hallberg, R. L. Hallberg, and A. L. Horwich (1989). “Mitochondrial Heat-Shock Protein Hsp60 Is Essential for Assembly of Proteins Imported into Yeast Mitochondria”. en. In: *Nature* 337.6208, pp. 620–625. issn: 1476-4687. doi: 10.1038/337620a0.

Chomczynski, P. and N. Sacchi (1987). “Single-Step Method of RNA Isolation by Acid Guanidinium Thiocyanate-Phenol-Chloroform Extraction”. eng. In: *Analytical Biochemistry* 162.1, pp. 156–159. issn: 0003-2697. doi: 10.1006/abio.1987.9999.

Christensen, J. H., M. N. Nielsen, J. Hansen, A. Füchtbauer, E.-M. Füchtbauer, M. West, T. J. Corydon, N. Gregersen, and P. Bross (2010). “Inactivation of the Hereditary Spastic Paraplegia-Associated Hspd1 Gene Encoding the Hsp60 Chaperone Results in Early Embryonic Lethality in Mice.” In: *Cell stress & chaperones* 15.6, pp. 851–63. issn: 1466-1268. doi: 10.1007/s12192-010-0194-x.

Chusyd, D. E., D. Wang, D. M. Huffman, and T. R. Nagy (2016). “Relationships between Rodent White Adipose Fat Pads and Human White Adipose Fat Depots”. English. In: *Frontiers in Nutrition* 3. issn: 2296-861X. doi: 10.3389/fnut.2016.00010.

Clemente-Postigo, M., A. Tinahones, R. El Bekay, M. M. Malagón, and F. J. Tinahones (2020). “The Role of Autophagy in White Adipose Tissue Function: Implications for Metabolic Health”. en. In: *Metabolites* 10.5, p. 179. doi: 10.3390/metabo10050179.

Craig, E. A., J. Kramer, and J. Kosic-Smithers (1987). “SSC1, a Member of the 70-kDa Heat Shock Protein Multigene Family of Saccharomyces Cerevisiae, Is Essential for Growth”. en. In: *Proceedings of the National Academy of Sciences* 84.12, pp. 4156–4160. issn: 0027-8424, 1091-6490. doi: 10.1073/pnas.84.12.4156.

Cypess, A. M., S. Lehman, G. Williams, I. Tal, D. Rodman, A. B. Goldfine, F. C. Kuo, E. L. Palmer, Y.-H. Tseng, A. Doria, G. M. Kolodny, and C. R. Kahn (2009). “Identification and Importance of Brown Adipose Tissue in Adult Humans”. In: *New England Journal of Medicine* 360.15, pp. 1509–1517. issn: 0028-4793. doi: 10.1056/NEJMoa0810780.

Delgado, C. L. (2003). “Rising Consumption of Meat and Milk in Developing Countries Has Created a New Food Revolution”. In: *The Journal of Nutrition* 133.11, 3907S–3910S. issn: 0022-3166. doi: 10.1093/jn/133.11.3907S.

Doege, H., A. Schürmann, G. Bahrenberg, A. Brauers, and H.-G. Joost (2000). “GLUT8, a Novel Member of the Sugar Transport Facilitator Family with Glucose Transport Activity”. en. In: *Journal of Biological Chemistry* 275.21, pp. 16275–16280. issn: 0021-9258, 1083-351X. doi: 10.1074/jbc.275.21.16275.

Dorn, G. W. (2019). “Evolving Concepts of Mitochondrial Dynamics”. In: *Annual Review of Physiology* 81.1, pp. 1–17. doi: 10.1146/annurev-physiol-020518-114358.

Egan, B. and J. R. Zierath (2013). “Exercise Metabolism and the Molecular Regulation of Skeletal Muscle Adaptation”. en. In: *Cell Metabolism* 17.2, pp. 162–184. issn: 1550-4131. doi: 10.1016/j.cmet.2012.12.012.

Egan, D. F., D. B. Shackelford, M. M. Mihaylova, S. Gelino, R. A. Kohnz, W. Mair, D. S. Vasquez, A. Joshi, D. M. Gwinn, R. Taylor, J. M. Asara, J. Fitzpatrick, A. Dillin, B. Viollet, M. Kundu, M. Hansen, and R. J. Shaw (2011). “Phosphorylation of ULK1 (hATG1) by AMP-Activated Protein Kinase Connects Energy Sensing to Mitophagy”. en. In: *Science* 331.6016, pp. 456–461. issn: 0036-8075, 1095-9203. doi: 10.1126/science.1196371.

Eriksson-Hogling, D., D. P. Andersson, J. Bäckdahl, J. Hoffstedt, S. Rössner, A. Thorell, E. Arner, P. Arner, and M. Rydén (2015). “Adipose Tissue Morphology Predicts Improved Insulin Sensitivity Following Moderate or Pronounced Weight Loss”. en. In: *International Journal of Obesity* 39.6, pp. 893–898. issn: 1476-5497. doi: 10.1038/ijo.2015.18.

Færch, K., D. Vistisen, G. Pacini, S. S. Torekov, N. B. Johansen, D. R. Witte, A. Jonsson, O. Pedersen, T. Hansen, T. Lauritzen, M. E. Jørgensen, B. Ahrén, and J. J. Holst (2016). “Insulin Resistance Is Accompanied by Increased Fasting Glucagon and Delayed Glucagon Suppression in Individuals With Normal and Impaired Glucose Regulation”. en. In: *Diabetes* 65.11, pp. 3473–3481. issn: 0012-1797, 1939-327X. doi: 10.2337/db16-0240.

Fagone, P. and S. Jackowski (Jan. 2009). “Membrane Phospholipid Synthesis and Endoplasmic Reticulum Function”. English. In: *Journal of Lipid Research* 50, S311–S316. issn: 0022-2275, 1539-7262. doi: 10.1194/jlr.R800049-JLR200.

Fan, F., Y. Duan, F. Yang, C. Trexler, H. Wang, L. Huang, Y. Li, H. Tang, G. Wang, X. Fang, J. Liu, N. Jia, J. Chen, and K. Ouyang (2020). “Deletion of Heat Shock Protein 60 in Adult Mouse Cardiomyocytes Perturbs Mitochondrial Protein Homeostasis and Causes Heart Failure”. en. In: *Cell Death & Differentiation* 27.2, pp. 587–600. issn: 1476-5403. doi: 10.1038/s41418-019-0374-x.

Fearnley, G. R., C. T. Vincent, and R. Chakrabarti (1959). “Reduction of Blood Fibrinolytic Activity in Diabetes Mellitus by Insulin”. English. In: *The Lancet* 274.7111, p. 1067. issn: 0140-6736, 1474-547X. doi: 10.1016/S0140-6736(59)91534-X.

Fedorova, M., R. C. Bollineni, and R. Hoffmann (2014). “Protein Carbonylation as a Major Hallmark of Oxidative Damage: Update of Analytical Strategies”. en. In: *Mass Spectrometry Reviews* 33.2, pp. 79–97. issn: 1098-2787. doi: 10.1002/mas.21381.

Fernando, R., K. Wardelmann, S. Deubel, R. Kehm, T. Jung, M. Mariotti, A. Vasilaki, V. N. Gladyshev, A. Kleinridders, T. Grune, and J. P. Castro (2020). “Low Steady-State Oxidative Stress Inhibits Adipogenesis by Altering Mitochondrial Dynamics and Decreasing Cellular Respiration”. en. In: *Redox Biology* 32, p. 101507. issn: 2213-2317. doi: 10.1016/j.redox.2020.101507.

Finkel, T. (2011). “Signal Transduction by Reactive Oxygen Species”. In: *Journal of Cell Biology* 194.1, pp. 7–15. issn: 0021-9525. doi: 10.1083/jcb.201102095.

Finkel Toren, Menazza Sara, Holmström Kira M., Parks Randi J., Liu Julia, Sun Junhui, Liu Jie, Pan Xin, and Murphy Elizabeth (2015). “The Ins and Outs of Mitochondrial Calcium”. In: *Circulation Research* 116.11, pp. 1810–1819. doi: 10.1161/CIRCRESAHA.116.305484.

Foretz, M., C. Guichard, P. Ferré, and F. Foufelle (1999). “Sterol Regulatory Element Binding Protein-1c Is a Major Mediator of Insulin Action on the Hepatic Expression of Glucokinase and Lipogenesis-Related Genes”. en. In: *Proceedings of the National Academy of Sciences* 96.22, pp. 12737–12742. issn: 0027-8424, 1091-6490. doi: 10.1073/pnas.96.22.12737.

Forsmark-Andrée, P., B. Persson, R. Radi, G. Dallner, and L. Ernster (1996). “Oxidative Modification of Nicotinamide Nucleotide Transhydrogenase in Submitochondrial Particles: Effect of Endogenous Ubiquinol”. en. In: *Archives of Biochemistry and Biophysics* 336.1, pp. 113–120. issn: 0003-9861. doi: 10.1006/abbi.1996.0538.

Freychet, P., M. H. Laudat, P. Laudat, G. Rosselin, C. R. Kahn, P. Gorden, and J. Roth (1972). “Impairment of Insulin Binding to the Fat Cell Plasma Membrane in the Obese Hyperglycemic Mouse”. en. In: *FEBS Letters* 25.2, pp. 339–342. issn: 1873-3468. doi: 10.1016/0014-5793(72)80519-2.

Frohnert, B. I. and D. A. Bernlohr (2013). “Protein Carbonylation, Mitochondrial Dysfunction, and Insulin Resistance”. In: *Advances in Nutrition* 4.2, pp. 157–163. issn: 2161-8313. doi: 10.3945/an.112.003319.

Garcia-Guzman, M., F. Soto, B. Laube, and W. Stühmer (1996). “Molecular Cloning and Functional Expression of a Novel Rat Heart P2X Purinoceptor”. en. In: *FEBS Letters* 388.2-3, pp. 123–127. issn: 1873-3468. doi: 10.1016/0014-5793(96)00499-1.

Gawlik, V., S. Schmidt, A. Scheepers, G. Wennemuth, R. Augustin, G. Aumüller, M. Moser, H. Al-Hasani, R. Kluge, H.-G. Joost, and D. A. Schürmann (2008). “Targeted Disruption of Slc2a8 (GLUT8) Reduces Motility and Mitochondrial Potential of Spermatozoa”. In: *Molecular Membrane Biology* 25.3, pp. 224–235. issn: 0968-7688. doi: 10.1080/09687680701855405.

Ghaben, A. L. and P. E. Scherer (Apr. 2019). “Adipogenesis and Metabolic Health”. en. In: *Nature Reviews Molecular Cell Biology* 20.4, pp. 242–258. issn: 1471-0080. doi: 10.1038/s41580-018-0093-z.

Giorgi, C., S. Marchi, and P. Pinton (Nov. 2018). “The Machineries, Regulation and Cellular Functions of Mitochondrial Calcium”. en. In: *Nature Reviews Molecular Cell Biology* 19.11, pp. 713–730. issn: 1471-0080. doi: 10.1038/s41580-018-0052-8.

Goldman, S. J., Y. Zhang, and S. Jin (2010). “Autophagic Degradation of Mitochondria in White Adipose Tissue Differentiation”. In: *Antioxidants & Redox Signaling* 14.10, pp. 1971–1978. issn: 1523-0864. doi: 10.1089/ars.2010.3777.

Green, H. and O. Kehinde (1975). “An Established Preadipose Cell Line and Its Differentiation in Culture II. Factors Affecting the Adipose Conversion”. en. In: *Cell* 5.1, pp. 19–27. issn: 0092-8674. doi: 10.1016/0092-8674(75)90087-2.

Guillam, M.-T., E. Huemmler, E. Schaerer, J.-Y. Wu, M. J. Birnbaum, F. Beermann, A. Schmidt, N. Dériaz, and B. Thorens (1997). “Early Diabetes and Abnormal Postnatal Pancreatic Islet Development in Mice Lacking Glut-2”. en. In: *Nature Genetics* 17.3, pp. 327–330. issn: 1546-1718. doi: 10.1038/ng1197-327.

Han, Y. H., M. Buffolo, K. M. Pires, S. Pei, P. E. Scherer, and S. Boudina (2016). “Adipocyte-Specific Deletion of Manganese Superoxide Dismutase Protects From Diet-Induced Obesity Through Increased Mitochondrial Uncoupling and Biogenesis”. en. In: *Diabetes* 65.9, pp. 2639–2651. issn: 0012-1797, 1939-327X. doi: 10.2337/db16-0283.

Handgraaf, S., E. Riant, A. Fabre, A. Waget, R. Burcelin, P. Lière, A. Krust, P. Chambon, J.-F. Arnal, and P. Gourdy (2013). “Prevention of Obesity and Insulin Resistance by Estrogens Requires ERα Activation Function-2 (ERαAF-2), Whereas ERαAF-1 Is Dispensable”. en. In: *Diabetes* 62.12, pp. 4098–4108. issn: 0012-1797, 1939-327X. doi: 10.2337/db13-0282.

Hansen, J., K. Svenstrup, D. Ang, M. N. Nielsen, J. H. Christensen, N. Gregersen, J. E. Nielsen, C. Georgopoulos, and P. Bross (2007). “A Novel Mutation in the HSPD1 Gene in a Patient with Hereditary Spastic Paraplegia”. en. In: *Journal of Neurology* 254.7, p. 897. issn: 1432-1459. doi: 10.1007/s00415-006-0470-y.

Hansen, J., P. Bross, M. Westergaard, M. Nielsen, H. Eiberg, A. Børglum, J. Mogensen, K. Kristiansen, L. Bolund, and N. Gregersen (2003). “Genomic Structure of the Human Mitochondrial Chaperonin Genes: HSP60 and HSP10 Are Localised Head to Head on Chromosome 2 Separated by a Bidirectional Promoter”. In: *Human Genetics* 112.1, pp. 71–77. issn: 0340-6717. doi: 10.1007/s00439-002-0837-9.

Hansen, J. J., A. Dürr, I. Cournu-Rebeix, C. Georgopoulos, D. Ang, M. N. Nielsen, C.-S. Davoine, A. Brice, B. Fontaine, N. Gregersen, and P. Bross (2002). “Hereditary Spastic Paraplegia SPG13 Is Associated with a Mutation in the Gene Encoding the Mitochondrial Chaperonin Hsp60”. English. In: *The American Journal of Human Genetics* 70.5, pp. 1328–1332. issn: 0002-9297, 1537-6605. doi: 10.1086/339935.

Hany, T. F., E. Gharehpapagh, E. M. Kamel, A. Buck, J. Himms-Hagen, and G. K. von Schulthess (2002). “Brown Adipose Tissue: A Factor to Consider in Symmetrical Tracer Uptake in the Neck and Upper Chest Region”. en. In: *European Journal of Nuclear Medicine and Molecular Imaging* 29.10, pp. 1393–1398. issn: 1619-7089. doi: 10.1007/s00259-002-0902-6.

Hartl, F. U. and M. Hayer-Hartl (2009). “Converging Concepts of Protein Folding in Vitro and in Vivo”. en. In: *Nature Structural & Molecular Biology* 16.6, pp. 574–581. issn: 1545-9985. doi: 10.1038/nsmb.1591.

Hauffe, R., V. Stein, C. Chudoba, T. Flore, M. Rath, K. Ritter, M. Schell, K. Wardelmann, S. Deubel, J. F. Kopp, M. Schwarz, K. Kappert, M. Blüher, T. Schwerdtle, A. P. Kipp, and A. Kleinridders (2020). “GPx3 Dysregulation Impacts Adipose Tissue Insulin Receptor Expression and Sensitivity”. en. In: *JCI Insight* 5.11. issn: 0021-9738. doi: 10.1172/jci.insight.136283.

Hawley, J. A., M. Hargreaves, M. J. Joyner, and J. R. Zierath (2014). “Integrative Biology of Exercise”. English. In: *Cell* 159.4, pp. 738–749. issn: 0092-8674, 1097-4172. doi: 10.1016/j.cell.2014.10.029.

Hotamisligil, G. S. (2006). “Inflammation and Metabolic Disorders”. In: *Nature* 444.1476-4687 (Electronic), pp. 860–867. issn: 1476-4687. doi: 10.1038/nature05485.

Hotamisligil, G. S., P. Arner, J. F. Caro, R. L. Atkinson, and B. M. Spiegelman (1995). “Increased Adipose Tissue Expression of Tumor Necrosis Factor-Alpha in Human Obesity and Insulin Resistance.” en. In: *The Journal of Clinical Investigation* 95.5, pp. 2409–2415. issn: 0021-9738. doi: 10.1172/JCI117936.

Hotamisligil, G. S., D. L. Murray, L. N. Choy, and B. M. Spiegelman (1994). “Tumor Necrosis Factor Alpha Inhibits Signaling from the Insulin Receptor”. en. In: *Proceedings of the National Academy of Sciences* 91.11, pp. 4854–4858. issn: 0027-8424, 1091-6490. doi: 10.1073/pnas.91.11.4854.

Hotamisligil, G. S., N. S. Shargill, and B. M. Spiegelman (1993). “Adipose Expression of Tumor Necrosis Factor-Alpha: Direct Role in Obesity-Linked Insulin Resistance”. en. In: *Science* 259.5091, pp. 87–91. issn: 0036-8075, 1095-9203. doi: 10.1126/science.7678183.

Hotamisligil, G. S. (2010). “Endoplasmic Reticulum Stress and the Inflammatory Basis of Metabolic Disease”. English. In: *Cell* 140.6, pp. 900–917. issn: 0092-8674, 1097-4172. doi: 10.1016/j.cell.2010.02.034.

Hotamisligil, G. S., P. Peraldi, A. Budavari, R. Ellis, M. F. White, and B. M. Spiegelman (1996). “IRS-1-Mediated Inhibition of Insulin Receptor Tyrosine Kinase Activity in TNF-α- and Obesity-Induced Insulin Resistance”. en. In: *Science* 271.5249, pp. 665–670. issn: 0036-8075, 1095-9203. doi: 10.1126/science.271.5249.665.

Hou, Y., Z. Liu, Z. Zuo, T. Gao, J. Fu, H. Wang, Y. Xu, D. Liu, M. Yamamoto, B. Zhu, Y. Zhang, M. E. Andersen, Q. Zhang, and J. Pi (2018). “Adipocyte-Specific Deficiency of Nfe2l1 Disrupts Plasticity of White Adipose Tissues and Metabolic Homeostasis in Mice”. en. In: *Biochemical and Biophysical Research Communications* 503.1, pp. 264–270. issn: 0006-291X. doi: 10.1016/j.bbrc.2018.06.013.

Hsu, C.-C., L.-M. Tseng, and H.-C. Lee (2016). “Role of Mitochondrial Dysfunction in Cancer Progression”. en. In: *Experimental Biology and Medicine* 241.12, pp. 1281–1295. issn: 1535-3702. doi: 10.1177/1535370216641787.

Ibberson, M., M. Uldry, and B. Thorens (2000). “GLUTX1, a Novel Mammalian Glucose Transporter Expressed in the Central Nervous System and Insulin-Sensitive Tissues”. en. In: *Journal of Biological Chemistry* 275.7, pp. 4607–4612. issn: 0021-9258, 1083-351X. doi: 10.1074/jbc.275.7.4607.

Ingalls, A. M., M. M. Dickie, and G. D. Snell (1950). “Obese, a New Mutation in the House Mouse”. In: *Journal of Heredity* 41.12, pp. 317–318. issn: 0022-1503. doi: 10.1093/oxfordjournals.jhered.a106073.

Jansen, H. J., P. van Essen, T. Koenen, L. A. B. Joosten, M. G. Netea, C. J. Tack, and R. Stienstra (Dec. 2012). “Autophagy Activity Is Up-Regulated in Adipose Tissue of Obese Individuals and Modulates Proinflammatory Cytokine Expression”. In: *Endocrinology* 153.12, pp. 5866–5874. issn: 0013-7227. doi: 10.1210/en.2012-1625.

Jo, J., O. Gavrilova, S. Pack, W. Jou, S. Mullen, A. E. Sumner, S. W. Cushman, and V. Periwal (2009). “Hypertrophy and/or Hyperplasia: Dynamics of Adipose Tissue Growth”. en. In: *PLOS Computational Biology* 5.3, e1000324. issn: 1553-7358. doi: 10.1371/journal.pcbi.1000324.

Kanaya, A. M., D. Herrington, E. Vittinghoff, F. Lin, D. Grady, V. Bittner, J. A. Cauley, and E. Barrett-Connor (2003). “Glycemic Effects of Postmenopausal Hormone Therapy: The Heart and Estrogen/Progestin Replacement Study: A Randomized, Double-Blind, Placebo-Controlled Trial”. In: *Annals of Internal Medicine* 138.1, pp. 1–9. issn: 0003-4819. doi: 10.7326/0003-4819-138-1-200301070-00005.

Kao, A. W., B. P. Ceresa, S. R. Santeler, and J. E. Pessin (1998). “Expression of a Dominant Interfering Dynamin Mutant in 3T3L1 Adipocytes Inhibits GLUT4 Endocytosis without Affecting Insulin Signaling*”. en. In: *Journal of Biological Chemistry* 273.39, pp. 25450–25457. issn: 0021-9258. doi: 10.1074/jbc.273.39.25450.

Katz, E. B., A. E. Stenbit, K. Hatton, R. DePinhot, and M. J. Charron (1995). “Cardiac and Adipose Tissue Abnormalities but Not Diabetes in Mice Deficient in GLUT4”. en. In: *Nature* 377.6545, pp. 151–155. issn: 1476-4687. doi: 10.1038/377151a0.

Kautzky-Willer, A., J. Harreiter, and G. Pacini (2016). “Sex and Gender Differences in Risk, Pathophysiology and Complications of Type 2 Diabetes Mellitus”. In: *Endocrine Reviews* 37.3, pp. 278–316. issn: 0163-769X. doi: 10.1210/er.2015-1137.

Kawate, T., J. L. Robertson, M. Li, S. D. Silberberg, and K. J. Swartz (May 2011). “Ion Access Pathway to the Transmembrane Pore in P2X Receptor Channels”. In: *Journal of General Physiology* 137.6, pp. 579–590. issn: 0022-1295. doi: 10.1085/jgp.201010593.

Kerner, M. J., D. J. Naylor, Y. Ishihama, T. Maier, H.-C. Chang, A. P. Stines, C. Georgopoulos, D. Frishman, M. Hayer-Hartl, M. Mann, and F. U. Hartl (2005). “Proteome-Wide Analysis of Chaperonin-Dependent Protein Folding in Escherichia Coli”. In: *Cell* 122.2, pp. 209–220. issn: 0092-8674. doi: 10.1016/j.cell.2005.05.028.

Kersten, S. (2001). “Mechanisms of Nutritional and Hormonal Regulation of Lipogenesis”. In: *EMBO reports* 2.4, pp. 282–286. issn: 1469-221X. doi: 10.1093/embo-reports/kve071.

Kim, J., M. Kundu, B. Viollet, and K.-L. Guan (2011). “AMPK and mTOR Regulate Autophagy through Direct Phosphorylation of Ulk1”. en. In: *Nature Cell Biology* 13.2, pp. 132–141. issn: 1476-4679. doi: 10.1038/ncb2152.

Kim, S. M., M. Lun, M. Wang, S. E. Senyo, C. Guillermier, P. Patwari, and M. L. Steinhauser (2014). “Loss of White Adipose Hyperplastic Potential Is Associated with Enhanced Susceptibility to Insulin Resistance”. English. In: *Cell Metabolism* 20.6, pp. 1049–1058. issn: 1550-4131. doi: 10.1016/j.cmet.2014.10.010.

Kissová, I., M. Deffieu, S. Manon, and N. Camougrand (Sept. 2004). “Uth1p Is Involved in the Autophagic Degradation of Mitochondria*”. en. In: *Journal of Biological Chemistry* 279.37, pp. 39068–39074. issn: 0021-9258. doi: 10.1074/jbc.M406960200.

Kleiner, S., R. J. Mepani, D. Laznik, L. Ye, M. J. Jurczak, F. R. Jornayvaz, J. L. Estall, D. C. Bhowmick, G. I. Shulman, and B. M. Spiegelman (2012). “Development of Insulin Resistance in Mice Lacking PGC-1α in Adipose Tissues”. en. In: *Proceedings of the National Academy of Sciences* 109.24, pp. 9635–9640. issn: 0027-8424, 1091-6490. doi: 10.1073/pnas.1207287109.

Kleinridders, A., H. Ferris, W. Cai, and R. C. Kahn (2014). “Insulin Action in Brain Regulates Systemic Metabolism and Brain Function”. In: *Diabetes* 63.7, pp. 2232–2243. issn: 0012-1797. doi: 10.2337/db14-0568.

Kleinridders, A., H. P. M. M. Lauritzen, S. Ussar, J. H. Christensen, M. A. Mori, P. Bross, and R. C. Kahn (2013). “Leptin Regulation of Hsp60 Impacts Hypothalamic Insulin Signaling”. In: *The Journal of clinical investigation* 123.11, pp. 4667–80. issn: 1558-8238. doi: 10.1172/JCI67615.

Knoll, A. H. (2015). *Life on a Young Planet*. en. isbn: 978-0-691-16553-0.

Kovsan, J., M. Blüher, T. Tarnovscki, N. Klöting, B. Kirshtein, L. Madar, I. Shai, R. Golan, I. Harman-Boehm, M. R. Schön, A. S. Greenberg, Z. Elazar, N. Bashan, and A. Rudich (2011). “Altered Autophagy in Human Adipose Tissues in Obesity”. In: *The Journal of Clinical Endocrinology & Metabolism* 96.2, E268–E277. issn: 0021-972X. doi: 10.1210/jc.2010-1681.

Kraus, N. A., F. Ehebauer, B. Zapp, B. Rudolphi, B. J. Kraus, and D. Kraus (2016). “Quantitative Assessment of Adipocyte Differentiation in Cell Culture”. In: *Adipocyte* 5.4, pp. 351–358. issn: 2162-3945. doi: 10.1080/21623945.2016.1240137.

Kulkarni, R. N., K. Almind, H. J. Goren, J. N. Winnay, K. Ueki, T. Okada, and C. R. Kahn (2003). “Impact of Genetic Background on Development of Hyperinsulinemia and Diabetes in Insulin Receptor/Insulin Receptor Substrate-1 Double Heterozygous Mice”. en. In: *Diabetes* 52.6, pp. 1528–1534. issn: 0012-1797, 1939-327X. doi: 10.2337/diabetes.52.6.1528.

Kusminski, C. M., W. L. Holland, K. Sun, J. Park, S. B. Spurgin, Y. Lin, G. R. Askew, J. A. Simcox, D. A. McClain, C. Li, and P. E. Scherer (2012). “MitoNEET-Driven Alterations in Adipocyte Mitochondrial Activity Reveal a Crucial Adaptive Process That Preserves Insulin Sensitivity in Obesity”. en. In: *Nature Medicine* 18.10, pp. 1539–1549. issn: 1546-170X. doi: 10.1038/nm.2899.

Laemmli, U. K. (1970). “Cleavage of Structural Proteins during the Assembly of the Head of Bacteriophage T4”. en. In: *Nature* 227.5259, pp. 680–685. issn: 1476-4687. doi: 10.1038/227680a0.

Lass, A., R. Zimmermann, M. Oberer, and R. Zechner (2011). “Lipolysis – A Highly Regulated Multi-Enzyme Complex Mediates the Catabolism of Cellular Fat Stores”. en. In: *Progress in Lipid Research* 50.1, pp. 14–27. issn: 0163-7827. doi: 10.1016/j.plipres.2010.10.004.

Leboucher, A., D. F. Pisani, L. Martinez-Gili, J. Chilloux, P. Bermudez-Martin, A. Van Dijck, T. Ganief, B. Macek, J. A. J. Becker, J. Le Merrer, R. F. Kooy, E.-Z. Amri, E. W. Khandjian, M.-E. Dumas, and L. Davidovic (2019). “The Translational Regulator FMRP Controls Lipid and Glucose Metabolism in Mice and Humans”. en. In: *Molecular Metabolism* 21, pp. 22–35. issn: 2212-8778. doi: 10.1016/j.molmet.2019.01.002.

Lee, H., Y. J. Lee, H. Choi, E. H. Ko, and J.-w. Kim (2009). “Reactive Oxygen Species Facilitate Adipocyte Differentiation by Accelerating Mitotic Clonal Expansion”. en. In: *Journal of Biological Chemistry* 284.16, pp. 10601–10609. issn: 0021-9258, 1083-351X. doi: 10.1074/jbc.M808742200.

Lee, J. W., S. Park, Y. Takahashi, and H.-G. Wang (2010). “The Association of AMPK with ULK1 Regulates Autophagy”. en. In: *PLOS ONE* 5.11, e15394. issn: 1932-6203. doi: 10.1371/journal.pone.0015394.

Lehner, R. and A. D. Quiroga (2016). “Chapter 5 - Fatty Acid Handling in Mammalian Cells”. en. In: *Biochemistry of Lipids, Lipoproteins and Membranes (Sixth Edition)*. Ed. by N. D. Ridgway and R. S. McLeod. Boston: Elsevier, pp. 149–184. isbn: 978-0-444-63438-2. doi: 10.1016/B978-0-444-63438-2.00005-5.

Leto, D. and A. R. Saltiel (2012). “Regulation of Glucose Transport by Insulin: Traffic Control of GLUT4”. en. In: *Nature Reviews Molecular Cell Biology* 13.6, pp. 383–396. issn: 1471-0080. doi: 10.1038/nrm3351.

Lindström, P. (2006). “The Physiology of Obese-Hyperglycemic Mice [Ob/Ob Mice]”. In: *The Scientific World JOURNAL* 7. Ed. by L. A. Frohman, p. 804524. issn: 2356-6140. doi: 10.1100/tsw.2007.117.

Lisinski, I., A. Schürmann, H.-G. Joost, S. W. Cushman, and H. Al-Hasani (2001). “Targeting of GLUT6 (Formerly GLUT9) and GLUT8 in Rat Adipose Cells”. en. In: *Biochemical Journal* 358.2, pp. 517–522. issn: 0264-6021. doi: 10.1042/bj3580517.

Liu, Z., I. Y. Patil, T. Jiang, H. Sancheti, J. P. Walsh, B. L. Stiles, F. Yin, and E. Cadenas (2015). “High-Fat Diet Induces Hepatic Insulin Resistance and Impairment of Synaptic Plasticity”. en. In: *PLOS ONE* 10.5, e0128274. issn: 1932-6203. doi: 10.1371/journal.pone.0128274.

Longo, M., F. Zatterale, J. Naderi, L. Parrillo, P. Formisano, G. A. Raciti, F. Beguinot, and C. Miele (2019). “Adipose Tissue Dysfunction as Determinant of Obesity-Associated Metabolic Complications”. en. In: *International Journal of Molecular Sciences* 20.9, p. 2358. doi: 10.3390/ijms20092358.

Luppino, F. S., L. M. de Wit, P. F. Bouvy, T. Stijnen, P. Cuijpers, B. W. J. H. Penninx, and F. G. Zitman (2010). “Overweight, Obesity, and Depression: A Systematic Review and Meta-Analysis of Longitudinal Studies”. eng. In: *Archives of General Psychiatry* 67.3, pp. 220–229. issn: 1538-3636. doi: 10.1001/archgenpsychiatry.2010.2.

Ma, Z. A., Z. Zhao, and J. Turk (2011). *Mitochondrial Dysfunction and β-Cell Failure in Type 2 Diabetes Mellitus*. en. https://www.hindawi.com/journals/jdr/2012/703538/. Review Article. doi: 10.1155/2012/703538.

Magen, D., C. Georgopoulos, P. Bross, D. Ang, Y. Segev, D. Goldsher, A. Nemirovski, E. Shahar, S. Ravid, A. Luder, B. Heno, R. Gershoni-Baruch, K. Skorecki, and H. Mandel (2008). “Mitochondrial Hsp60 Chaperonopathy Causes an Autosomal-Recessive Neurodegenerative Disorder Linked to Brain Hypomyelination and Leukodystrophy”. English. In: *The American Journal of Human Genetics* 83.1, pp. 30–42. issn: 0002-9297, 1537-6605. doi: 10.1016/j.ajhg.2008.05.016.

Magnoni, R., J. Palmfeldt, J. H. Christensen, M. Sand, F. Maltecca, T. J. Corydon, M. West, G. Casari, and P. Bross (2013). “Late Onset Motoneuron Disorder Caused by Mitochondrial Hsp60 Chaperone Deficiency in Mice”. In: *Neurobiology of Disease* 54, pp. 12–23. issn: 09699961. doi: 10.1016/j.nbd.2013.02.012.

Margolis, K. L., D. E. Bonds, R. J. Rodabough, L. Tinker, L. S. Phillips, C. Allen, T. Bassford, G. Burke, J. Torrens, B. V. Howard, and for the Women’s Health Initiative Investigators (2004). “Effect of Oestrogen plus Progestin on the Incidence of Diabetes in Postmenopausal Women: Results from the Women’s Health Initiative Hormone Trial”. en. In: *Diabetologia* 47.7, pp. 1175–1187. issn: 1432-0428. doi: 10.1007/s00125-004-1448-x.

Marinovic, M. P., J. D. Campeiro, S. C. Lima, A. L. Rocha, M. B. Nering, E. B. Oliveira, M. A. Mori, and M. A. F. Hayashi (Mar. 2018). “Crotamine Induces Browning of Adipose Tissue and Increases Energy Expenditure in Mice”. en. In: *Scientific Reports* 8.1, p. 5057. issn: 2045-2322. doi: 10.1038/s41598-018-22988-1.

Märker, T., H. Sell, P. Zillessen, A. Glode, J. Kriebel, D. M. Ouwens, P. Pattyn, J. Ruige, S. Famulla, M. Roden, J. Eckel, and C. Habich (Mar. 2012). "Heat Shock Protein 60 as a Mediator of Adipose Tissue Inflammation and Insulin Resistance". In: *Diabetes* 61.3, pp. 615–625. issn: 0012-1797. doi: 10.2337/db10-1574.

Martin, W., C. Rotte, M. Hoffmeister, U. Theissen, G. Gelius-Dietrich, S. Ahr, and K. Henze (2003). "Early Cell Evolution, Eukaryotes, Anoxia, Sulfide, Oxygen, Fungi First (?), And a Tree of Genomes Revisited". eng. In: *IUBMB life* 55.4-5, pp. 193–204. issn: 1521-6543. doi: 10.1080/1521654031000141231.

Matsuda, M. and R. A. DeFronzo (1999). "Insulin Sensitivity Indices Obtained from Oral Glucose Tolerance Testing: Comparison with the Euglycemic Insulin Clamp." en. In: *Diabetes Care* 22.9, pp. 1462–1470. issn: 0149-5992, 1935-5548. doi: 10.2337/diacare.22.9.1462.

Matsuzawa-Ishimoto, Y., S. Hwang, and K. Cadwell (2018). "Autophagy and Inflammation". In: *Annual Review of Immunology* 36.1, pp. 73–101. issn: 0732-0582. doi: 10.1146/annurev-immunol-042617-053253.

Matthews, D. R., J. P. Hosker, A. S. Rudenski, B. A. Naylor, D. F. Treacher, and R. C. Turner (July 1985). "Homeostasis Model Assessment: Insulin Resistance and β-Cell Function from Fasting Plasma Glucose and Insulin Concentrations in Man". en. In: *Diabetologia* 28.7, pp. 412–419. issn: 1432-0428. doi: 10.1007/BF00280883.

Mauvais-Jarvis, F., D. J. Clegg, and A. L. Hevener (2013). "The Role of Estrogens in Control of Energy Balance and Glucose Homeostasis". In: *Endocrine Reviews* 34.3, pp. 309–338. issn: 0163-769X. doi: 10.1210/er.2012-1055.

Mayer, A. L., C. B. Higgins, M. R. Heitmeier, T. E. Kraft, X. Qian, J. R. Crowley, K. L. Hyrc, W. L. Beatty, K. E. Yarasheski, P. W. Hruz, and B. J. DeBosch (2016). "SLC2A8 (GLUT8) Is a Mammalian Trehalose Transporter Required for Trehalose-Induced Autophagy". en. In: *Scientific Reports* 6.1, p. 38586. issn: 2045-2322. doi: 10.1038/srep38586.

McClung, J. P., C. A. Roneker, W. Mu, D. J. Lisk, P. Langlais, F. Liu, and X. G. Lei (2004). "Development of Insulin Resistance and Obesity in Mice Overexpressing Cellular Glutathione Peroxidase". en. In: *Proceedings of the National Academy of Sciences* 101.24, pp. 8852–8857. issn: 0027-8424, 1091-6490. doi: 10.1073/pnas.0308096101.

Meyer, L. K., T. P. Ciaraldi, R. R. Henry, A. C. Wittgrove, and S. A. Phillips (2013). "Adipose Tissue Depot and Cell Size Dependency of Adiponectin Synthesis and Secretion in Human Obesity". In: *Adipocyte* 2.4, pp. 217–226. issn: 2162-3945. doi: 10.4161/adip.24953.

Mizushima, N., B. Levine, A. M. Cuervo, and D. J. Klionsky (2008). "Autophagy Fights Disease through Cellular Self-Digestion". en. In: *Nature* 451.7182, pp. 1069–1075. issn: 1476-4687. doi: 10.1038/nature06639.

Mizushima, N. and T. Yoshimori (2007). "How to Interpret LC3 Immunoblotting". In: *Autophagy* 3.6, pp. 542–545. issn: 1554-8627. doi: 10.4161/auto.4600.

Mosmann, T. (1983). "Rapid Colorimetric Assay for Cellular Growth and Survival: Application to Proliferation and Cytotoxicity Assays". en. In: *Journal of Immunological Methods* 65.1, pp. 55–63. issn: 0022-1759. doi: 10.1016/0022-1759(83)90303-4.

Müller, T. D. *et al.* (2013). "P62 Links β-Adrenergic Input to Mitochondrial Function and Thermogenesis". en. In: *The Journal of Clinical Investigation* 123.1, pp. 469–478. issn: 0021-9738. doi: 10.1172/JCI64209.

NCD Risk Factor Collaboration (NCD-RisC), B. (2016). "Worldwide Trends in Diabetes since 1980: A Pooled Analysis of 751 Population-Based Studies with 4·4 Million Participants". English. In: *The Lancet* 387.10027, pp. 1513–1530. issn: 0140-6736, 1474-547X. doi: 10.1016/S0140-6736(16)00618-8.

Nielsen, K. L., N. McLennan, M. Masters, and N. J. Cowan (Sept. 1999). "A Single-Ring Mitochondrial Chaperonin (Hsp60-Hsp10) Can Substitute for GroEL-GroES In Vivo". en. In: *Journal of Bacteriology* 181.18, pp. 5871–5875. issn: 0021-9193, 1098-5530. doi: 10.1128/JB.181.18.5871-5875.1999.

Nisemblat, S., O. Yaniv, A. Parnas, F. Frolow, and A. Azem (2015). “Crystal Structure of the Human Mitochondrial Chaperonin Symmetrical Football Complex”. en. In: *Proceedings of the National Academy of Sciences* 112.19, pp. 6044–6049. issn: 0027-8424, 1091-6490. doi: 10.1073/pnas.1411718112.

North, R. A. (Jan. 2002). “Molecular Physiology of P2X Receptors”. In: *Physiological Reviews* 82.4, pp. 1013–1067. issn: 0031-9333. doi: 10.1152/physrev.00015.2002.

O’Neill, S. and L. O’Driscoll (2015). “Metabolic Syndrome: A Closer Look at the Growing Epidemic and Its Associated Pathologies”. en. In: *Obesity Reviews* 16.1, pp. 1–12. issn: 1467-789X. doi: 10.1111/obr.12229.

Ogston, D. and G. M. Mcandrew (1964). “Fibrinolysis in Obesity”. English. In: *The Lancet* 284.7371, pp. 1205–1207. issn: 0140-6736, 1474-547X. doi: 10.1016/S0140-6736(64)91042-6.

Oh, S. S., K. A. Sullivan, J. E. Wilkinson, C. Backus, J. M. Hayes, S. A. Sakowski, and E. L. Feldman (2012). “Neurodegeneration and Early Lethality in Superoxide Dismutase 2-Deficient Mice: A Comprehensive Analysis of the Central and Peripheral Nervous Systems”. en. In: *Neuroscience* 212, pp. 201–213. issn: 0306-4522. doi: 10.1016/j.neuroscience.2012.03.026.

Olefsky, J. M. (1976). “Decreased Insulin Binding to Adipocytes and Circulating Monocytes from Obese Subjects.” en. In: *The Journal of Clinical Investigation* 57.5, pp. 1165–1172. issn: 0021-9738. doi: 10.1172/JCI108384.

Omura, T. (1998). “Mitochondria-Targeting Sequence, a Multi-Role Sorting Sequence Recognized at All Steps of Protein Import into Mitochondria”. In: *The Journal of Biochemistry* 123.6, pp. 1010–1016. issn: 0021-924X. doi: 10.1093/oxfordjournals.jbchem.a022036.

Ostermann, J., A. L. Horwich, W. Neupert, and F.-U. Hartl (1989). “Protein Folding in Mitochondria Requires Complex Formation with Hsp60 and ATP Hydrolysis”. en. In: *Nature* 341.6238, pp. 125–130. issn: 1476-4687. doi: 10.1038/341125a0.

Pellegrino, M. W., A. M. Nargund, and C. M. Haynes (2013). “Signaling the Mitochondrial Unfolded Protein Response”. In: *Biochimica et Biophysica Acta (BBA) - Molecular Cell Research* 1833.2, pp. 410–416. issn: 01674889. doi: 10.1016/j.bbamcr.2012.02.019.

Phan, J. and K. Reue (2005). “Lipin, a Lipodystrophy and Obesity Gene”. English. In: *Cell Metabolism* 1.1, pp. 73–83. issn: 1550-4131. doi: 10.1016/j.cmet.2004.12.002.

Polyzos, S. A., N. Perakakis, and C. S. Mantzoros (2019). “Fatty Liver in Lipodystrophy: A Review with a Focus on Therapeutic Perspectives of Adiponectin and/or Leptin Replacement”. English. In: *Metabolism - Clinical and Experimental* 96, pp. 66–82. issn: 0026-0495, 1532-8600. doi: 10.1016/j.metabol.2019.05.001.

Popkin, B. M., L. S. Adair, and S. W. Ng (2012). “Global Nutrition Transition and the Pandemic of Obesity in Developing Countries”. In: *Nutrition Reviews* 70.1, pp. 3–21. issn: 0029-6643. doi: 10.1111/j.1753-4887.2011.00456.x.

Porter, R. K. and M. D. Brand (1995). “Mitochondrial Proton Conductance and H+/0 Ratio Are Independent of Electron Transport Rate in Isolated Hepatocytes”. In: *Biochemical Journal* 310.2, pp. 379–382. issn: 0264-6021. doi: 10.1042/bj3100379.

Powers, S. K., J. Duarte, A. N. Kavazis, and E. E. Talbert (2010). “Reactive Oxygen Species Are Signalling Molecules for Skeletal Muscle Adaptation”. en. In: *Experimental Physiology* 95.1, pp. 1–9. issn: 1469-445X. doi: 10.1113/expphysiol.2009.050526.

Pramme-Steinwachs, I. (2019). “The Role of Calcium and Its Transporter P2RX5 in Brown Adipocyte Function”. Dissertation. München: Technische Universität München.

Proescher, F. (1927). “Oil Red O Pyridin, A Rapid Fat Stain”. In: *Stain Technology* 2.2, pp. 60–61. issn: 0038-9153. doi: 10.3109/10520292709115655.

Riant, E., A. Waget, H. Cogo, J.-F. Arnal, R. Burcelin, and P. Gourdy (May 2009). “Estrogens Protect against High-Fat Diet-Induced Insulin Resistance and Glucose Intolerance

in Mice". In: *Endocrinology* 150.5, pp. 2109–2117. issn: 0013-7227. doi: 10.1210/en.2008-0971.

Rich, P. (2003). "The Molecular Machinery of Keilin's Respiratory Chain". In: *Biochemical Society Transactions* 31.6, pp. 1095–1105. issn: 0300-5127. doi: 10.1042/bst0311095.

Rieusset, J., F. Andreelli, D. Auboeuf, M. Roques, P. Vallier, J. P. Riou, J. Auwerx, M. Laville, and H. Vidal (1999). "Insulin Acutely Regulates the Expression of the Peroxisome Proliferator-Activated Receptor-Gamma in Human Adipocytes." en. In: *Diabetes* 48.4, pp. 699–705. issn: 0012-1797, 1939-327X. doi: 10.2337/diabetes.48.4.699.

Ristow, M., K. Zarse, A. Oberbach, N. Klöting, M. Birringer, M. Kiehntopf, M. Stumvoll, C. R. Kahn, and M. Blüher (2009). "Antioxidants Prevent Health-Promoting Effects of Physical Exercise in Humans". en. In: *Proceedings of the National Academy of Sciences* 106.21, pp. 8665–8670. issn: 0027-8424, 1091-6490. doi: 10.1073/pnas.0903485106.

Roberts-Toler, C., B. T. O'Neill, and A. M. Cypess (2015). "Diet-Induced Obesity Causes Insulin Resistance in Mouse Brown Adipose Tissue". en. In: *Obesity* 23.9, pp. 1765–1770. issn: 1930-739X. doi: 10.1002/oby.21134.

Rohan de Silva, H., N. L. Khan, and N. W. Wood (2000). "The Genetics of Parkinson's Disease". en. In: *Current Opinion in Genetics & Development* 10.3, pp. 292–298. issn: 0959-437X. doi: 10.1016/S0959-437X(00)00082-4.

Romanello, V. and M. Sandri (2016). "Mitochondrial Quality Control and Muscle Mass Maintenance". English. In: *Frontiers in Physiology* 6. issn: 1664-042X. doi: 10.3389/fphys.2015.00422.

Rossmeisl, M., J. S. Rim, R. A. Koza, and L. P. Kozak (2003). "Variation in Type 2 Diabetes-Related Traits in Mouse Strains Susceptible to Diet-Induced Obesity". en. In: *Diabetes* 52.8, pp. 1958–1966. issn: 0012-1797, 1939-327X. doi: 10.2337/diabetes.52.8.1958.

Rudenski, A. S., D. R. Matthews, J. C. Levy, and R. C. Turner (1991). "Understanding "Insulin Resistance": Both Glucose Resistance and Insulin Resistance Are Required to Model Human Diabetes". English. In: *Metabolism - Clinical and Experimental* 40.9, pp. 908–917. issn: 0026-0495, 1532-8600. doi: 10.1016/0026-0495(91)90065-5.

Ryabova, N. A., V. V. Marchenkov, S. Y. Marchenkova, N. V. Kotova, and G. V. Semisotnov (2013). "Molecular Chaperone GroEL/ES: Unfolding and Refolding Processes". en. In: *Biochemistry (Moscow)* 78.13, pp. 1405–1414. issn: 1608-3040. doi: 10.1134/S0006297913130038.

Saeedi, P., I. Petersohn, P. Salpea, B. Malanda, S. Karuranga, N. Unwin, S. Colagiuri, L. Guariguata, A. A. Motala, K. Ogurtsova, J. E. Shaw, D. Bright, and R. Williams (2019). "Global and Regional Diabetes Prevalence Estimates for 2019 and Projections for 2030 and 2045: Results from the International Diabetes Federation Diabetes Atlas, 9th Edition". English. In: *Diabetes Research and Clinical Practice* 157. issn: 0168-8227, 1872-8227. doi: 10.1016/j.diabres.2019.107843.

Saibil, H. R., W. A. Fenton, D. K. Clare, and A. L. Horwich (2013). "Structure and Allostery of the Chaperonin GroEL". en. In: *Journal of Molecular Biology*. Allosteric Interactions and Biological Regulation (Part I) 425.9, pp. 1476–1487. issn: 0022-2836. doi: 10.1016/j.jmb.2012.11.028.

Saitoh, T., N. Fujita, M. H. Jang, S. Uematsu, B.-G. Yang, T. Satoh, H. Omori, T. Noda, N. Yamamoto, M. Komatsu, K. Tanaka, T. Kawai, T. Tsujimura, O. Takeuchi, T. Yoshimori, and S. Akira (2008). "Loss of the Autophagy Protein Atg16L1 Enhances Endotoxin-Induced IL-1β Production". en. In: *Nature* 456.7219, pp. 264–268. issn: 1476-4687. doi: 10.1038/nature07383.

Saltiel, A. R. and C. R. Kahn (2001). "Insulin Signalling and the Regulation of Glucose and Lipid Metabolism". en. In: *Nature* 414.6865, pp. 799–806. issn: 1476-4687. doi: 10.1038/414799a.

Sarbassov, D. D., D. A. Guertin, S. M. Ali, and D. M. Sabatini (2005). “Phosphorylation and Regulation of Akt/PKB by the Rictor-mTOR Complex”. en. In: *Science* 307.5712, pp. 1098–1101. issn: 0036-8075, 1095-9203. doi: 10.1126/science.1106148.

Sartori, R., V. Romanello, and M. Sandri (2021). “Mechanisms of Muscle Atrophy and Hypertrophy: Implications in Health and Disease”. en. In: *Nature Communications* 12.1, p. 330. issn: 2041-1723. doi: 10.1038/s41467-020-20123-1.

Schaum, N. *et al.* (2019). “The Murine Transcriptome Reveals Global Aging Nodes with Organ-Specific Phase and Amplitude”. en. In: *bioRxiv*, p. 662254. doi: 10.1101/662254.

Schiaffino, S., K. A. Dyar, S. Ciciliot, B. Blaauw, and M. Sandri (2013). “Mechanisms Regulating Skeletal Muscle Growth and Atrophy”. en. In: *The FEBS Journal* 280.17, pp. 4294–4314. issn: 1742-4658. doi: 10.1111/febs.12253.

Schiaffino, S. and C. Reggiani (2011). “Fiber Types in Mammalian Skeletal Muscles”. In: *Physiological Reviews* 91.4, pp. 1447–1531. issn: 0031-9333. doi: 10.1152/physrev.00031.2010.

Schmidt, S., H.-G. Joost, and A. Schürmann (2009). “GLUT8, the Enigmatic Intracellular Hexose Transporter”. In: *American Journal of Physiology-Endocrinology and Metabolism* 296.4, E614–E618. issn: 0193-1849. doi: 10.1152/ajpendo.91019.2008.

Sehnal, D., A. S. Rose, J. Koča, S. K. Burley, and S. Velankar (2018). “Mol*: Towards a Common Library and Tools for Web Molecular Graphics”. In: *Proceedings of the Workshop on Molecular Graphics and Visual Analysis of Molecular Data*. MolVA ’18. Goslar, DEU: Eurographics Association, pp. 29–33.

Shang, L., S. Chen, F. Du, S. Li, L. Zhao, and X. Wang (2011). “Nutrient Starvation Elicits an Acute Autophagic Response Mediated by Ulk1 Dephosphorylation and Its Subsequent Dissociation from AMPK”. en. In: *Proceedings of the National Academy of Sciences* 108.12, pp. 4788–4793. issn: 0027-8424, 1091-6490. doi: 10.1073/pnas.1100844108.

Shibutani, S. T., T. Saitoh, H. Nowag, C. Münz, and T. Yoshimori (2015). “Autophagy and Autophagy-Related Proteins in the Immune System”. en. In: *Nature Immunology* 16.10, pp. 1014–1024. issn: 1529-2916. doi: 10.1038/ni.3273.

Sies, H., C. Berndt, and D. P. Jones (2017). “Oxidative Stress”. In: *Annual Review of Biochemistry* 86.1, pp. 715–748. issn: 0066-4154. doi: 10.1146/annurev-biochem-061516-045037.

Simon, M. M. *et al.* (2013). “A Comparative Phenotypic and Genomic Analysis of C57BL/6J and C57BL/6N Mouse Strains”. En. In: *Genome biology* 14.7, R82. issn: 1474-760X. doi: 10.1186/gb-2013-14-7-r82.

Singh, R. and A. M. Cuervo (2011). “Autophagy in the Cellular Energetic Balance”. en. In: *Cell Metabolism* 13.5, pp. 495–504. issn: 1550-4131. doi: 10.1016/j.cmet.2011.04.004.

Singh, R., Y. Xiang, Y. Wang, K. Baikati, A. M. Cuervo, Y. K. Luu, Y. Tang, J. E. Pessin, G. J. Schwartz, and M. J. Czaja (2009). “Autophagy Regulates Adipose Mass and Differentiation in Mice”. en. In: *The Journal of Clinical Investigation* 119.11, pp. 3329–3339. issn: 0021-9738. doi: 10.1172/JCI39228.

Skurk, T., C. Alberti-Huber, C. Herder, and H. Hauner (2007). “Relationship between Adipocyte Size and Adipokine Expression and Secretion”. In: *The Journal of Clinical Endocrinology & Metabolism* 92.3, pp. 1023–1033. issn: 0021-972X. doi: 10.1210/jc.2006-1055.

Song, J., J. M. Herrmann, and T. Becker (2021). “Quality Control of the Mitochondrial Proteome”. en. In: *Nature Reviews Molecular Cell Biology* 22.1, pp. 54–70. issn: 1471-0080. doi: 10.1038/s41580-020-00300-2.

Song, Z., A. M. Xiaoli, and F. Yang (2018). “Regulation and Metabolic Significance of De Novo Lipogenesis in Adipose Tissues”. en. In: *Nutrients* 10.10, p. 1383. doi: 10.3390/nu10101383.

Spalding, K. L., E. Arner, P. O. Westermark, S. Bernard, B. A. Buchholz, O. Bergmann, L. Blomqvist, J. Hoffstedt, E. Näslund, T. Britton, H. Concha, M. Hassan, M. Rydén, J. Frisén, and P. Arner (2008). "Dynamics of Fat Cell Turnover in Humans". en. In: *Nature* 453.7196, pp. 783–787. issn: 1476-4687. doi: 10.1038/nature06902.

Taguchi, H. (2015). "Reaction Cycle of Chaperonin GroEL via Symmetric "Football" Intermediate". en. In: *Journal of Molecular Biology*. Molecular Chaperones and Protein Quality Control (Part II) 427.18, pp. 2912–2918. issn: 0022-2836. doi: 10.1016/j.jmb.2015.04.007.

Tait, S. W. G. and D. R. Green (Sept. 2013). "Mitochondrial Regulation of Cell Death". en. In: *Cold Spring Harbor Perspectives in Biology* 5.9, a008706. issn: , 1943-0264. doi: 10.1101/cshperspect.a008706.

Taniguchi, C. M., B. Emanuelli, and C. R. Kahn (2006). "Critical Nodes in Signalling Pathways: Insights into Insulin Action". en. In: *Nature Reviews Molecular Cell Biology* 7.2, pp. 85–96. issn: 1471-0080. doi: 10.1038/nrm1837.

Thorens, B. (2015). "GLUT2, Glucose Sensing and Glucose Homeostasis". en. In: *Diabetologia* 58.2, pp. 221–232. issn: 1432-0428. doi: 10.1007/s00125-014-3451-1.

Tiganis, T. (2011). "Reactive Oxygen Species and Insulin Resistance: The Good, the Bad and the Ugly". en. In: *Trends in Pharmacological Sciences* 32.2, pp. 82–89. issn: 0165-6147. doi: 10.1016/j.tips.2010.11.006.

Tokita, Y., Y. Maejima, K. Shimomura, S. Takenoshita, N. Ishiyama, M. Akuzawa, Y. Shimomura, and K. Nakajima (2017). "Non-Alcoholic Fatty Liver Disease Is a Risk Factor for Type 2 Diabetes in Middle-Aged Japanese Men and Women". In: *Internal Medicine* 56.7, pp. 763–771. doi: 10.2169/internalmedicine.56.7115.

Toye, A. A., J. D. Lippiat, P. Proks, K. Shimomura, L. Bentley, A. Hugill, V. Mijat, M. Goldsworthy, L. Moir, A. Haynes, J. Quarterman, H. C. Freeman, F. M. Ashcroft, and R. D. Cox (2005). "A Genetic and Physiological Study of Impaired Glucose Homeostasis Control in C57BL/6J Mice". en. In: *Diabetologia* 48.4, pp. 675–686. issn: 1432-0428. doi: 10.1007/s00125-005-1680-z.

Tran, T. T., Y. Yamamoto, S. Gesta, and C. R. Kahn (2008). "Beneficial Effects of Subcutaneous Fat Transplantation on Metabolism". English. In: *Cell Metabolism* 7.5, pp. 410–420. issn: 1550-4131. doi: 10.1016/j.cmet.2008.04.004.

Turner, R. C., R. R. Holman, D. Matthews, T. D. R. Hockaday, and J. Peto (1979). "Insulin Deficiency and Insulin Resistance Interaction in Diabetes: Estimation of Their Relative Contribution by Feedback Analysis from Basal Plasma Insulin and Glucose Concentrations". English. In: *Metabolism - Clinical and Experimental* 28.11, pp. 1086–1096. issn: 0026-0495, 1532-8600. doi: 10.1016/0026-0495(79)90146-X.

Ussar, S., K. Y. Lee, S. N. Dankel, J. Boucher, M.-F. Haering, A. Kleinridders, T. Thomou, R. Xue, Y. Macotela, A. M. Cypess, Y.-H. Tseng, G. Mellgren, and C. R. Kahn (2014). "ASC-1, PAT2, and P2RX5 Are Cell Surface Markers for White, Beige, and Brown Adipocytes". en. In: *Science Translational Medicine* 6.247, 247ra103–247ra103. issn: 1946-6234, 1946-6242. doi: 10.1126/scitranslmed.3008490.

Uysal, K. T., S. M. Wiesbrock, M. W. Marino, and G. S. Hotamisligil (1997). "Protection from Obesity-Induced Insulin Resistance in Mice Lacking TNF-α Function". en. In: *Nature* 389.6651, pp. 610–614. issn: 1476-4687. doi: 10.1038/39335.

van Beek, L., J. B. van Klinken, A. C. M. Pronk, A. D. van Dam, E. Dirven, P. C. N. Rensen, F. Koning, K. Willems van Dijk, and V. van Harmelen (2015). "The Limited Storage Capacity of Gonadal Adipose Tissue Directs the Development of Metabolic Disorders in Male C57Bl/6J Mice". en. In: *Diabetologia* 58.7, pp. 1601–1609. issn: 1432-0428. doi: 10.1007/s00125-015-3594-8.

Van Remmen, H., M. D. Williams, Z. Guo, L. Estlack, H. Yang, E. J. Carlson, C. J. Epstein, T. T. Huang, and A. Richardson (2001). "Knockout Mice Heterozygous for Sod2

Show Alterations in Cardiac Mitochondrial Function and Apoptosis". In: *American Journal of Physiology-Heart and Circulatory Physiology* 281.3, H1422–H1432. issn: 0363-6135. doi: 10.1152/ajpheart.2001.281.3.H1422.

Venhoff, N., D. Lebrecht, D. Pfeifer, A. C. Venhoff, E. Bissé, J. Kirschner, and U. A. Walker (2012). "Muscle-Fiber Transdifferentiation in an Experimental Model of Respiratory Chain Myopathy". In: *Arthritis Research & Therapy* 14.5, R233. issn: 1478-6354. doi: 10.1186/ar4076.

Vernochet, C., F. Damilano, A. Mourier, O. Bezy, M. A. Mori, G. Smyth, A. Rosenzweig, N.-G. Larsson, and C. R. Kahn (2014). "Adipose Tissue Mitochondrial Dysfunction Triggers a Lipodystrophic Syndrome with Insulin Resistance, Hepatosteatosis, and Cardiovascular Complications". en. In: *The FASEB Journal* 28.10, pp. 4408–4419. issn: 1530-6860. doi: 10.1096/fj.14-253971.

Vernochet, C., A. Mourier, O. Bezy, Y. Macotela, J. Boucher, M. J. Rardin, D. An, K. Y. Lee, O. R. Ilkayeva, C. M. Zingaretti, B. Emanuelli, G. Smyth, S. Cinti, C. B. Newgard, B. W. Gibson, N.-G. Larsson, and C. R. Kahn (2012). "Adipose-Specific Deletion of TFAM Increases Mitochondrial Oxidation and Protects Mice against Obesity and Insulin Resistance". In: *Cell Metabolism* 16.6, pp. 765–776. issn: 1550-4131. doi: 10.1016/j.cmet.2012.10.016.

Vlahopoulos, S. and V. C. Zoumpourlis (2004). "JNK: A Key Modulator of Intracellular Signaling". en. In: *Biochemistry (Moscow)* 69.8, pp. 844–854. issn: 1608-3040. doi: 10.1023/B:BIRY.0000040215.02460.45.

Vogel, H., F. Mirhashemi, B. Liehl, F. Taugner, O. Kluth, R. Kluge, H.-G. Joost, and A. Schürmann (2013). "Estrogen Deficiency Aggravates Insulin Resistance and Induces β-Cell Loss and Diabetes in Female New Zealand Obese Mice". en. In: *Hormone and Metabolic Research* 45.06, pp. 430–435. issn: 0018-5043, 1439-4286. doi: 10.1055/s-0032-1331700.

Voos, W. (2013). "Chaperone–Protease Networks in Mitochondrial Protein Homeostasis". en. In: *Biochimica et Biophysica Acta (BBA) - Molecular Cell Research*. Protein Import and Quality Control in Mitochondria and Plastids 1833.2, pp. 388–399. issn: 0167-4889. doi: 10.1016/j.bbamcr.2012.06.005.

Voos, W. and K. Röttgers (2002). "Molecular Chaperones as Essential Mediators of Mitochondrial Biogenesis". en. In: *Biochimica et Biophysica Acta (BBA) - Molecular Cell Research*. Protein Transport into Mitochondria and Chloroplasts Part II 1592.1, pp. 51–62. issn: 0167-4889. doi: 10.1016/S0167-4889(02)00264-1.

Wang, Q. A., C. Tao, R. K. Gupta, and P. E. Scherer (Oct. 2013). "Tracking Adipogenesis during White Adipose Tissue Development, Expansion and Regeneration". en. In: *Nature Medicine* 19.10, pp. 1338–1344. issn: 1546-170X. doi: 10.1038/nm.3324.

Wardelmann, K., S. Blümel, M. Rath, E. Alfine, C. Chudoba, M. Schell, W. Cai, R. Hauffe, K. Warnke, T. Flore, K. Ritter, J. Weiß, C. R. Kahn, and A. Kleinridders (2019). "Insulin Action in the Brain Regulates Mitochondrial Stress Responses and Reduces Diet-Induced Weight Gain". en. In: *Molecular Metabolism* 21, pp. 68–81. issn: 2212-8778. doi: 10.1016/j.molmet.2019.01.001.

White, A. T., A. Philp, H. N. Fridolfsson, J. M. Schilling, A. N. Murphy, D. L. Hamilton, C. E. McCurdy, H. H. Patel, and S. Schenk (2014). "High-Fat Diet-Induced Impairment of Skeletal Muscle Insulin Sensitivity Is Not Prevented by SIRT1 Overexpression". In: *American Journal of Physiology-Endocrinology and Metabolism* 307.9, E764–E772. issn: 0193-1849. doi: 10.1152/ajpendo.00001.2014.

WHO (2017). *The Double Burden of Malnutrition: Policy Brief*. Policy Brief WHO/NMH/NHD/17.3. World Health Organization, p. 10.

Wick, A. N., D. R. Drury, H. I. Nakada, J. B. Wolfe, and W. t. t. a. o. B. B. a. R. Grabowski (1957). “Localization of the Primary Metabolic Block Produced by 2-Deoxyglucose”. en. In: *Journal of Biological Chemistry* 224.2, pp. 963–969. issn: 0021-9258, 1083-351X.

Wigand, J. P. and W. G. Blackard (1979). “Downregulation of Insulin Receptors in Obese Man”. en. In: *Diabetes* 28.4, pp. 287–291. issn: 0012-1797, 1939-327X. doi: 10.2337/diab.28.4.287.

Wilson-Fritch, L., A. Burkart, G. Bell, K. Mendelson, J. Leszyk, S. Nicoloro, M. Czech, and S. Corvera (2003). “Mitochondrial Biogenesis and Remodeling during Adipogenesis and in Response to the Insulin Sensitizer Rosiglitazone”. In: *Molecular and cellular biology* 23.3, pp. 1085–94. issn: 0270-7306. doi: 10.1128/MCB.23.3.1085-1094.2003.

Winckler, J. (1974). “Vitalfärbung von Lysosomen und anderen Zellorganellen der Ratte mit Neutralrot Vital Staining of Lysosomes and Other Cell Organelles of the Rat with Neutral Red”. de. In: *Progress in Histochemistry and Cytochemistry* 6.3, pp. III–89. issn: 0079-6336. doi: 10.1016/S0079-6336(74)80001-X.

Xia, J. Y., K. Sun, C. Hepler, A. L. Ghaben, R. K. Gupta, Y. A. An, W. L. Holland, T. S. Morley, A. C. Adams, R. Gordillo, C. M. Kusminski, and P. E. Scherer (2018). “Acute Loss of Adipose Tissue-Derived Adiponectin Triggers Immediate Metabolic Deterioration in Mice”. en. In: *Diabetologia* 61.4, pp. 932–941. issn: 1432-0428. doi: 10.1007/s00125-017-4516-8.

Youle, R. J. and A. M. van der Bliek (Aug. 2012). “Mitochondrial Fission, Fusion, and Stress”. en. In: *Science* 337.6098, pp. 1062–1065. issn: 0036-8075, 1095-9203. doi: 10.1126/science.1219855.

Zebisch, K., V. Voigt, M. Wabitsch, and M. Brandsch (2012). “Protocol for Effective Differentiation of 3T3-L1 Cells to Adipocytes”. en. In: *Analytical Biochemistry* 425.1, pp. 88–90. issn: 0003-2697. doi: 10.1016/j.ab.2012.03.005.

Zhang, Y., G. Marsboom, P. T. Toth, and J. Rehman (2013). “Mitochondrial Respiration Regulates Adipogenic Differentiation of Human Mesenchymal Stem Cells”. en. In: *PLOS ONE* 8.10, e77077. issn: 1932-6203. doi: 10.1371/journal.pone.0077077.

Zhang, Y., R. Proenca, M. Maffei, M. Barone, L. Leopold, and J. M. Friedman (1994). “Positional Cloning of the Mouse Obese Gene and Its Human Homologue”. en. In: *Nature* 372.6505, pp. 425–432. issn: 1476-4687. doi: 10.1038/372425a0.

Zhang, Y., S. Goldman, R. Baerga, Y. Zhao, M. Komatsu, and S. Jin (2009). “Adipose-Specific Deletion of Autophagy-Related Gene 7 (Atg7) in Mice Reveals a Role in Adipogenesis”. en. In: *Proceedings of the National Academy of Sciences* 106.47, pp. 19860–19865. issn: 0027-8424, 1091-6490. doi: 10.1073/pnas.0906048106.

Publikationen und wissenschaftlicher Beiträge

Publikationen

Hauffe, R., V. Stein, C. Chudoba, T. Flore, M. Rath, K. Ritter, M. Schell, K. Wardelmann, S. Deubel, J. F. Kopp, M. Schwarz, K. Kappert, M. Blüher, T. Schwerdtle, A. P. Kipp, and A. Kleinridders (2020). “GPx3 Dysregulation Impacts Adipose Tissue Insulin Receptor Expression and Sensitivity”. en. In: JCI Insight 5.11. issn: 0021-9738. doi: 10.1172/jci.insight.136283.

Wardelmann, K., S. Blümel, M. Rath, E. Alfine, C. Chudoba, M. Schell, W. Cai, **R. Hauffe**, K. Warnke, T. Flore, K. Ritter, J. Weiß, C. R. Kahn, and A. Kleinridders (2019). “Insulin Action in the Brain Regulates Mitochondrial Stress Responses and Reduces Diet-Induced Weight Gain”. en. In: Molecular Metabolism 21, pp. 68–81. issn: 2212-8778. doi: 10.1016/j.molmet.2019.01.001.

Manuskripte in Vorbereitung

Hauffe, R., M. Rath, M. Schell, K. Wardelmann, K. Ritter, S. Deubel, C. Ott, K. Kappert, M. Jähnert, A. Schürmann, and A. Kleinridders (2021). “HSP60 reduction protects against obesity-induced insulin resistance by modulating energy metabolism in adipose tissue” (Manuscript in submission).

Wardelmann K., M. Rath, J.P. Castro, S. Blümel, M. Schell, **R. Hauffe**, C. Chudoba, F. Schumacher, M. Jähnert, K. Warnke, T. Flore, K. Ritter, A. Wernitz, T. Hosoi, K. Ozawa, B. Kleuser, J. Weiß, A. Schürmann, and A. Kleinridders: "Central acting Hsp10 regulates mitochondrial function, insulin sensitivity and impacts liver metabolism" (Manuscript in submission)

Hauffe, R., M. Rath, K Müller, and A. Kleinridders (2021). “HSP60 reduction impairs fertility through a reduction of sperm activity” (Manuscript in preparation).

Wissenschaftliche Beiträge

Selenite supplementation alleviates diet-induced insulin resistance in C57BL/6N mice
Jahrestagung Federation of European Societies on Trace Elements and Minerals (FESTEM), Potsdam 2019
Postervortrag

Eine selenreiche Hochfettdiät verbessert die Adipositas-induzierte Insulinresistenz in C57BL/6N Mäusen
Jahrestagung Deutsche Gesellschaft für Ernährung (DGE), Gießen 2019
Postervortrag

Metabolic consequences of impaired mitochondrial protein homeostasis during diet-induced obesity Jahrestagung Deutsche Diabetes Gesellschaft (DDG), Berlin 2018
Vortrag

Metabolic consequences of mitochondrial dysfunction during diet-induced obesity
Jahrestagung Deutsche Adipositas Gesellschaft (DAG), Potsdam 2017
Vortrag